To the Graduate Council:

I am submitting herewith a dissertation written by DONG ZHANG entitled "FUNDAMENTAL INVESTIGATION OF THE SPUNBONDING PROCESS". I have examined the final copy of this dissertation for form and content and recommend that it be accepted in partial fulfillment of the requirements for the degree of Doctor of Philosophy, with a major in Human Ecology.

Gajanan Bhat, Co-Chair

Larry C. Wadsworth, Co-Chair

I have read this dissertation and recommend its acceptance:

Kermit E. Duckett

Roberto S. Benson

Accepted for the Council:

Associate Vice Chancellor
and Dean of The Graduate School

FUNDAMENTAL INVESTIGATION OF THE SPUNBONDING PROCESS

A Dissertation

Presented for the

Doctor of Philosophy

Degree

The University of Tennessee, Knoxville

Dong Zhang

December 1995

ACKNOWLEDGMENTS

The author expresses his sincere thanks to his major professors, Dr. Gajanan Bhat, Assistant Professor of Textile Science, and Dr. Larry C. Wadsworth, Director and Professor of Textiles and Nonwovens Development Center, for their advice, guidance and encouragement throughout the course of this work. Appreciation is also extended to other committee members, Dr. Kermit E. Duckett, Professor of Textile Science, Dr. Roberto S. Benson, Associate Professor of Materials Science and Engineering for their guidance and suggestions.

Grateful acknowledgment is extended to Dr. Sanjiv Malkan, Research Assistant Professor for sample preparation and many interesting discussions, and Exxon Chemical Company and TANDEC for financial support on this research. Appreciation is acknowledged to all my colleagues and friends who helped in various ways.

DEDICATION

The author would like to dedicate the paper to his parents in Tianjin CHINA, Mr. and Mrs. Binyue Zhang for their continuous support, and his niece, Nancy Roh Zhang for many good and fun time.

ABSTRACT

The spunbonding process involves extrusion, followed by non-isothermal extensional flow of the melt, and crystallization, accompanied by molecular orientation. The kinematics and development of morphology in the filaments are governed to a large extent by a combination of elongational deformation and stress-induced crystallization. Understanding the influence of the spinline dynamics on the structure of the filament can help in manipulating the process conditions to achieve the desired properties in the filaments.

The inherent properties of the filaments are of utmost importance in spunbonded webs. A good understanding of the structure of individual filaments will be helpful in comprehending the whole process better. Two kinds of polymers, a polypropylene homopolymer and a copolymer of polypropylene containing less than 5 percent polyethylene, were processed using the Reicofil® spunbonding line at the Textiles and Nonwovens Development Center, The University of Tennessee, Knoxville. The filament samples were collected before thermal-bonding. The important filament properties were determined through a variety of experimental techniques, such as molecular orientation in filaments through birefringence, filament and web crystallinity through differential scanning calorimetry and density measurement, x-ray diffraction, scanning electron microscopy, and single filament mechanical properties. In addition, thermo-rheological properties, such as Thermal Mechanical Analysis (TMA), and Thermal Deformation Analysis (TDA) of the collected filament, and the nonwoven samples were evaluated under different temperature and stress.

The filaments were annealed at both constant and free length conditions. The effect of annealing time and temperature was also studied. The structure and properties such as crystalline orientation by x-ray diffraction, crystallinity by DSC, mechanical properties, filament diameter and birefringence of the fibers, before and after annealing, were investigated. In order to understand the effects of various process variables on the final web properties, the related nonwovens were taken after thermal-bonding and characterized for strength (tensile, burst, and tear), tensile elongation, isotropy, air permeability, stiffness, fiber diameter, and bond appearance through microscopy. The results were analyzed through a statistical design. The effect of temperature, throughput, and their interaction were evaluated through statistical means. A mathematical model was developed to evaluate the quality of nonwovens objectively and comprehensively and to optimize the processing conditions.

TABLE OF CONTENTS

LIST OF FIGURES

LIST OF TABLES

CHAPTER I

INTRODUCTION

The spunbonding process is based on the spinning technique and bears many similarities [1]. In the system, the molten polymer is forced by melting pumps through special spinnerets having a large number of holes. The primary blow ducts, located immediately below the spinneret block continuously cool the filaments with conditioned air. Secondary blow ducts, located below the primary blow ducts, supply auxiliary air at room temperature. A blower at the bottom of the enclosed spinline creates a suction for the filaments mixed with air. The continuous filaments are sucked through a venturi (high velocity low pressure zone) and a distributing chamber, which ensures entangling of the filaments. The entangled filaments are deposited as a random web on a moving porous belt for thermal calendering.

The spunbonding process involves extrusion, followed by non-isothermal extensional flow of the melt, and crystallization, accompanied by molecular orientation. The kinematics and development of morphology in the filaments are governed to a large extent by the combination of elongational deformation and the stress-induced crystallization. Understanding the influence of the spinline dynamics on the structure of the filaments can help in manipulating the process conditions to achieve the desired properties in the filaments.

The effect of stress induced crystallization in melt spinning has been studied [2].

The effect of stress on oriented crystallization was demonstrated by deformation of uniaxially loaded fibers exposed to temperatures in the processing range. The response of the filaments in subsequent thermo-mechanical processing (such as calendering) is greatly influenced by the structure of the filaments. This response can range from severe embrittlement of initially very ductile material to enhancement of ductility. New regimes of post-spinning deformation can be inferred from these studies to produce fabrics with superior properties.

The inherent properties of the filaments are of utmost importance in spunbonded webs. Therefore, the necessarity to study the structure of individual filaments. The important filament properties were determined through a variety of experimental techniques, such as molecular orientation in filaments through birefringence, filament and web crystallinity through differential scanning calorimetry and density measurement, crystalline structure by x-ray diffraction, morphology of the bonding area by scanning electron microscopy, and single filament mechanical properties by tensile testing. In addition, thermo-rheological properties, such as thermal mechanical analysis (TMA), and thermal deformation analysis (TDA) of the collected filaments, and nonwoven samples were evaluated under different temperature and stress.

The filaments were annealed at both constant and free length conditions. The effect of annealing time was also studied. Mechanical properties, filament diameter and birefringence of the fibers, before and after annealing, were investigated. In order to understand the effects of various process variables on the final web properties, the related nonwovens were characterized for strength (tensile, burst, and tear), tensile elongation,

isotropy, air permeability, stiffness, fiber diameter, and bond appearance through microscopy. The results were analyzed through a statistical design. The effect of temperature, throughput, and their interaction were evaluated through statistical means. To evaluate quality of nonwovens quantitatively and objectively, a mathematical model was established, based on the mechanical properties of the nonwovens, using factor analysis in multistatistics and comprehensive evaluation in fuzzy mathematics.

CHAPTER II

LITERATURE REVIEW

2.1 Spunbonding Process and Spunbonded Nonwovens

A spunbonded nonwoven fabric has been defined as a fabric formed by filaments that have been extruded, drawn, laid on a belt, and bonded thermally, chemically or mechanically. Spunbonded nonwovens can also be defined generally as continuous-filament fibrous structures which can be made in the form of fabrics, sheets and tapes, and are prepared from synthetic polymers in a process integrated with fiber manufacture [2].

Spunbonding is a unique process that links the innovative polymer, technological and textile research, which involves web formation (extrusion, attenuation and collection of filament bundle), and bonding of web to impart strength, cohesiveness and integrity to the structure. The attenuation of the web may be achieved either by the use of draw-off rolls and subsequently forcing the filament bundle through an aspirator jet with a spreading operation that involves charging the filament bundle with an electrostatic field to deposit the filaments in the form of a web on a conveyor belt, or by drawing filaments into a number of separated sheets with the help of air ducts and then laying the sheets sequentially, as in the Freudenberg process. Use of supersonic velocity air stream and the movement of air jet from side to side with some mechanical devices have been developed to prepare webs. Spunbonding system is the most productive of all the non-conventional methods of textile fabric formation. At a production rate of between 30 and 300 m/min, depending on weight

per unit area, it is many times faster than the conventional systems of fabric formation. Filament production speeds in excess of 2000 m/min have already been achieved and today in certain process variants speeds around 10,000 m/min are being operated [3].

2.1.1 Historical Perspective of The Spunbonding Process

The Spunbonding Process can be viewed as either an evolution of the existing staple fiber nonwoven production concept or the logical extension of the synthetic filament spinning processes commercialized during the 1940's and 1950's. The origins of the spunbonding process appear to date at least from 1940, when the processes of the spunbonding type were patented by Slather and Thomas of Corning Company to produce glass wool [4]. Similar processes for the fabrication of mineral wool from molten siliceous were patented by Calendar in 1945 [5]. Commercially manufactured spunbonded nonwovens of synthetic polymers are generally based on the technology patented by Freudenburg of West Germany and by Du Pont of the USA in the 1950's and 1960's. In 1965, Du Pont commercialized a product of polyester called 'Reemay®'. This was followed by polypropylene 'Typar®' and the flash spun polyethylene 'Tyvek®' [6]. At the same time, Freudenberg introduced a spunbonding process called 'Lutravil®'for the manufacture of mixed polyamides [7]. Five years later, the Lurgi Kohle & Mineral-oltechnik GmbH of Germany introduced their spunbonding process called 'Docan®'. In 1984, Reifenhauser GmbH of Germany introduced the spunbonding process, 'Reicofil®' for fabricating webs mainly from polypropylene [6].

There is a growing body of patent literature related to spunbonding [8,9], and

summaries can be found in Textile Progress [10] and in International Nonwoven Bulletin [11]. Most of the literature relates to the production processes and end uses of spunbonded nonwoven structures. Since the spunbonding process begins with the filament spinning, the most convenient fiber materials that have been commercially used are those of thermoplastic polymers such as polyamides, polyesters, polyethylene and polypropylene. Spunbonded nonwovens produced from viscose rayon with relatively low spinning speeds (125 m/min) have been researched and introduced in the market.

The applications of spunbonded nonwovens range from baby diapers to automotive and from surgical gowns to geotextiles [11]. Today spunbonded nonwovens are used throughout the automobile as a backing for tufted automobile floor carpets, trim parts, trunkliners, interior door panel, and seat covers. Spunbonded civil engineering webs are expanded into a multiple of related uses, e.g. erosion control, revetment protection, railroad beds stabilization, canal and reservoir lining protection, highway and airfield black top cracking prevention, roofing, etc. Spunbonded nonwovens as cover stock is also widely used in sanitary napkins. The medical applications include: disposable operating room gowns; shoe covers; and sterilizable packaging. The examples of packaging materials include: metal-core wrap, medical sterile packaging, floppy disk liner, high performance envelopes and stationery products. The global capacity of spunbonded production would have grown from less than 10% in to more than 40% of the 1990 capacity (Figure 2.1).

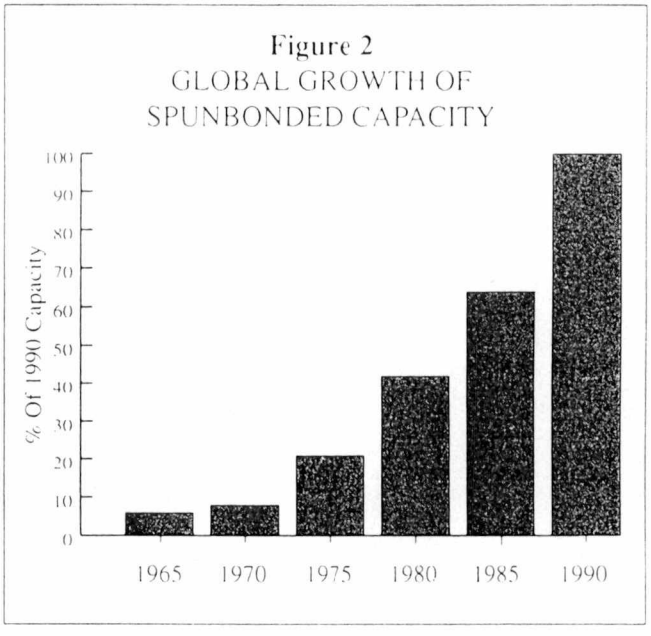

Figure 2.1 Global Growth of Spunbonded Capacity [3].

2.1.2 The Spunbonding Processes

A primary factor in the spunbonding process is control of four simultaneous integrated operations: filament extrusion, drawing, lay down, and bonding [11]. The first three operations are directly adapted from common fiber spinning and constitute the spun or web formation phase of the process, while the bonding process is the web consolidation or bond phase of the process, hence the generic term spunbond. The spunbonding process begins with a polymer resin and ends with a finished fabric. The spunbonded webs are made on an integrated and continuous production line. Generally, a spunbond line consists of the following elements: extruder for forming filaments; metering pump, die assembly, filament spinning, drawing and deposition system, collecting belt, bonding zone, and winding unit.

The polymers (pellets or granules) are fed into the extruder hopper. As the polymer moves along the barrel of the extruder, it melts by heating, friction of viscous flow and mechanical action. The pressurized molten polymer is then conveyed to the metering pump, which is a positive displacement constant volume device for uniform melt delivery to the die assembly. The molten polymer from the gear pump goes to the feed distribution system to provide uniform flow to the die block assembly. The die assembly is one of the most important elements of the spunbonding process. The die assembly consists of polymer feed distribution and spinneret. The feed distribution in a spunbonding die is more critical than in a film or sheeting die, which is usually designed in such a way that the polymer distribution is less dependent on the shear sensitivity of the polymer. The feed distribution balances both the flow and the residence time across the width of the die. From the feed distribution channel, the polymer melt goes directly to the spinneret. A spinneret is a single

block of metal having several thousand orifices, which is usually circular or rectangular in shape. The grouping of spinnerets is often called a block or bank. In commercial production lines, two or more blocks are used in tandem to increase the coverage of the fibers.

The filament spinning, drawing and deposition are the most critical steps in the spunbonding process. There are three spinning techniques used in the spunbonding process. They are melt spinning, dry spinning, and wet spinning. Among them, the melt spinning is widely used mainly due to its simplicity and economics. The drawing of the filaments follows spinning, which is achieved using a specially designed aerodynamic device. The filament deposition follows drawing and is achieved by an aerodynamic device, which is referred to as fanning or entangler unit. Hartman [12] proposed some of the basic principles involved in filament spinning, drawing, and deposition, which are described below:

Method 1 in figure 2.2A uses longitudinal spinnerets, with air slots on both sides of the spinneret for the expulsion of drawing air ①. The room air ② carried along and after laydown of the filaments, is removed by suction ③. This process is very well suited for tacky polymers, such as linear polyurethene. The web is truly 'spunbonded', that is the continuous filaments after web collection bond themselves due to their tackiness. Crystallization, which then sets in, eliminates adhesiveness of filaments after the bonding step.

Method 2 in figure 2.2B allows a higher draw ratio, with subsequently increased molecular orientation of filaments. Filaments are drawn with several air or gas streams ①, ②, and ③ using drawing conduits. The air is removed by suction ④ after web formation. This process has special advantages in preparing fine spunbonded webs with a textile-like appearance and handle of the web.

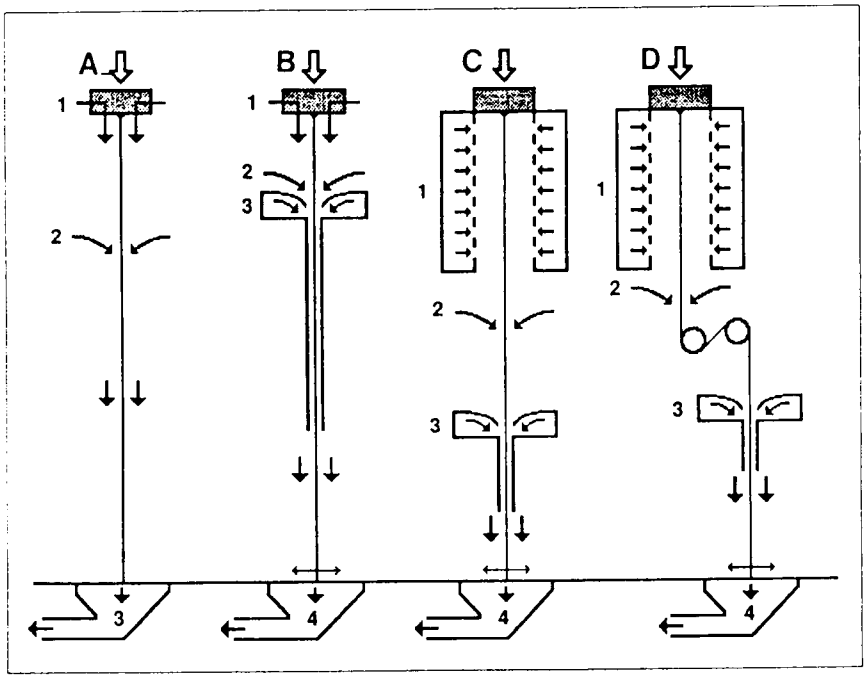

Figure 2.2 Schematic of Filament Spinning, Drawing, and Deposition [12].

Method 3 in figure 2.2C operates with regular cooling ducts ① and drawing jets ③. The drawing and cooling arrangements can be operated to give very high spinning speeds with the result that highly oriented filaments are produced. The room air ②, of controlled temperature and moisture content, can be entrained to control fiber properties. The air is removed by suction ④ after web formation.

Method 4 in figure 2.2D has a mechanical drawing step ② between spinneret and lay down zone. This method is similar to conventional spinning and is especially useful for polymers, which in regular air drawing do not give optimum filament molecular orientation. Again we find the use of air stream for cooling ① and for lay down ③, ④. The webs with high strength and low elongation can be made through this method. A lot of spunbonding processes can be classified into one of these four methods with some modification. For example, 'REICOFIL®' system, 'DOCAN®' system, solution 'FLASH-SPUN' system, 'LUTRAVIL®' system, burst fiber system, and wet spinning system.

Reicofil® system, which is shown in Figure 2.3 has been developed by Reifenhauser GmbH of Germany. The performance of the standard Reicofil spunbonding system can be characterized by the following data: Filament speed-1,200 m/min; air velocity-2400 m/min; maximum width-5.2 m, throughput-100 kg/h/m, filament size (PP)-1.6-3.5 den, production speed-125 m/min, low energy consumption (E<1kWh/kg) and excellent mechanical properties [13]. It is based on the melt spinning technique. The melt is forced by spin pumps through special spinnerets having a large number of holes. The primary blow ducts, located below the spinneret block, continuously cool the filaments with conditioned air. The secondary blow ducts, located below the primary blow ducts, continuously supply the

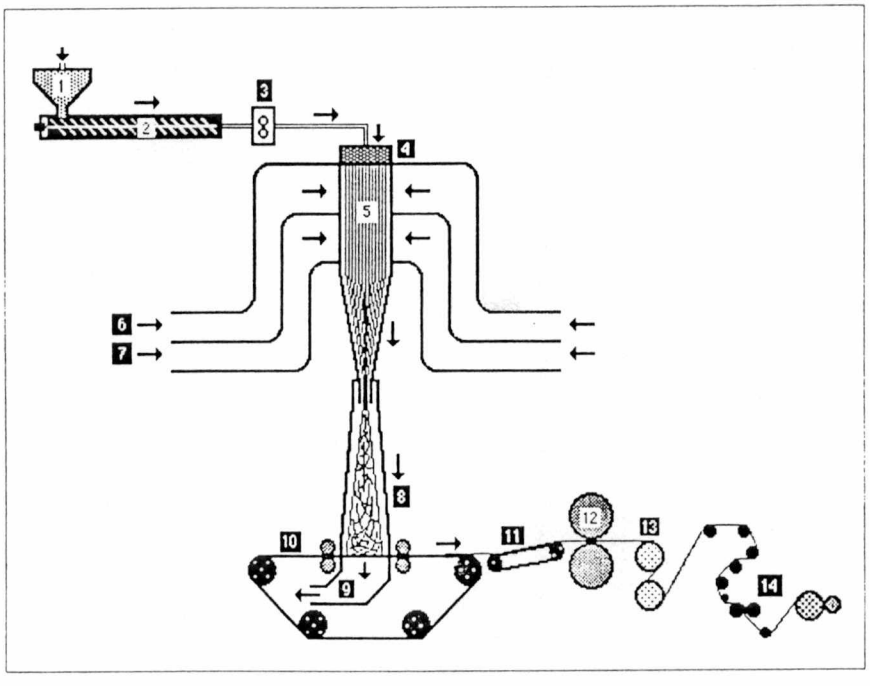

Figure 2.3 Schematic of Reicofil Spunbonding Unit [11].

auxiliary room temperature air. Over the line's entire working width, ventilator generated underpressure sucks filaments and mixed air down from the spinnerets and cooling chambers.

The continuous filaments are sucked through a venturi (high velocity low pressure zone) to a distributing chamber, which affects fanning and entangling of the filaments. Finally, the entangled filaments are deposited as a random web on a moving sieve belt. The randomness is imparted by the turbulence in the air stream, but there is a small bias in the machine direction due to some directionality imparted by the moving belt. The suction below the sieve belt enhances the random lay down of the filaments. Reicofil®2, based on the original Reicofil process and its modular design, has been developed which drastically changes the physical properties and the productivity [13].

In the Docan® system [11], the melt is forced by spin pumps through special spinnerets having a large number of holes. By suitable choice of extrusion and spinning conditions, desired filament denier is attained. The blow ducts located below individual spinnerets continuously cool the filaments with conditioned air. The force required for filament drawing and orientation is produced by a special aerodynamic system. Each continuous filament bundle is picked up by a draw-off jet operated on high pressure air and passed through a guide tube to a separator which effects separation and fanning of the filaments. Finally, the filament fan leaving the separators is deposited as a random web on a moving sieve belt. The suction below the sieve belt enhances the random lay down of the filaments.

The solution 'flash-spun' system is an alternative technique for the conversion of fiber

forming polymers into spunbonded webs using the dry spinning technique [11]. A product example of this process is Tyvek®. Flash spinning is the most complex and difficult method of manufacturing spunbonded nonwovens due to the need to spin heated pressurized solution under precise conditions. Lutravil system is based on the melt spinning technique and not available for commercial licensing. Burst fiber system has been developed in 1970's. In this process, fiber forming polymers are extruded through a radial die. However, the molten polymer, typically polypropylene, contains a foaming agent (e.g. azodicarbonamide), which evolves gas at the extrusion temperature. As the film is cooled immediately after extrusion by a blast of cold air, a foamed film is formed and is reheated to above its glass transition temperature and is stretched. The biaxial stretching or drawing process converts the foamed structure into a balanced fibrous tubular network which may be either collapsed or slit and wound up as textile roll goods.

Wet spinning system uses cellulose based raw materials and has been developed since 1972 in Japan and England. A polymer solution is extruded through a spinning funnel or a spinneret. The extruded filaments are diffused in the diffusion box, and are allowed to flow down together with solution through the slit on the bottom of diffusion box. The filaments are then laid on the conveyor belt for webbing [11].

2.1.3 Bonding and Mechanics of Fabric Formation

The process of making a spunbonded fabric includes web formation (mentioned above) and bonding of web to impart strength, cohesiveness and integrity to the structure. There are three basic bonding methods in the spunbonding processes: thermal (calendering),

chemical (adhesive), and mechanical (needle punching or hydroentangling).

Thermal bonding is the most widely used technique in spunbonding processes. This bonding is achieved by fusing of the filaments in the web at the cross-over sections. The fusion is obtained by direct action of heat and pressure via a calendar or an oven. The degree of fusion determines most qualities of the web, such as hand and softness. Normally, the thermal bonding can be achieved in combining a filament of the same material but of different softening point, or distributing different material in powder form through the web, or using bicomponent filaments in which the bonding agent forms a thin sheath around each web filament or is present as an integral sector of the filament cross-section [11].

Chemical bonding (adhesive bonding) is achieved using a polymer latex or a polymer solution deposited in and around the fibrous structure and then cured thermally to get bonding. In spray bonding, the bonding agent usually stays close to the surface of the material, resulting in a web with a little strength, high bulk, and a fair degree of openness. In case of saturated bonding, all the fibers are bonded to each other in a continuous matrix so that the rigidity, stiffness, and thinness of the web increase. In case of partial solvation bonding, the overall bonding is obtained using gaseous hydrogen chloride. The gaseous NC solvates the outer surface of the carrier fiber and bonds the fibers together at all fiber cross-over points by welding together the contacting solvated surface [11].

Mechanical bonding (needle punching) is achieved by entangling the fibers using bearded needles, which are set into a board and penetrate into the web and then recede, leaving the fibers entangled. Needle configuration, needle length, barb shape, and web advance rate can influence the degree of fibrous entanglement. The needle punched webs

are quite extensive, bulky, and comfortable. Needle punching is suitable for heavier spunbonded webs [11].

There have been numerous empirical studies dealing with the mechanical and physical properties of commercial products and the suitability and performance of spunbonded fabrics. Spunbonded fabrics exhibit extremely high tensile and tear strengths compared with conventional woven, or adhesive-bonded nonwoven fabrics. The mechanical properties of the spunbonded fabrics depend on filament properties, bonding parameters, and filament arrangement. Filament properties include linear density, tenacity, modulus, elongation, cross-section, crimp, and fiber morphology. Bonding parameters include binder type, binder concentration, binder distribution, and selfbonding. Filament arrangements include fabric weight uniformity, filament separation, and orientation. The understanding and prediction of the behavior of filaments during melt spinning and the pattern of laying down during fabric formation require the consideration of aerodynamics and the electrostatic and mechanical forces acting on spinline. The mechanics of structure formation in the melt-spun filament have been extensively reported in the literature, but the information on the threadline dynamics in the spunbonding process is scanty.

Analysis of the mechanics of spunbonded structures involves the study of the dynamics of the threadline and the effect of air drag on the spinline, fine structure development, and the formation, bonding, and the mechanics of fabric structure. Studies by Hearle *et. al.* tried to simulate the formation of web [14,15] and suggests that the mechanism of buckling (i.e. the form taken by threads being fed too rapidly onto a moving belt) is governed by the geometry of feeding and by the linear density and the bending and torsional

rigidities of the threads. In 1980, Gould and Smith [16] pointed out that since the speed at which filament or yarns flow can be extremely high, the air drag will have an effect on the development of fine structure and consequently on the mechanical properties of the filaments.

Recently, Spruiell, *et. al.* [16] investigated the spunbonding process using mathematical modeling. This model for the 'Reicofil®' spunbonding process, developed earlier at the University of Tennessee [17], was applied to investigate the effects of various process and polymer variables on the resulting filament structure and properties by a simulated spinline. The material parameters studied were polymer elongational viscosity and the kinetics of stress induced crystallization. The process parameters varied include the extrusion temperature, spinline length, temperature and flow rate of the cooling air and the shape of the draw down venturi. Effect of changing the mass throughput was also investigated. The model indicates that the elongational viscosity is a key factor in controlling the amount of drawdown, the temperature at which crystallization occurs and the level of molecular orientation developed in the spunbonded filaments. The polymer crystallization kinetics also has a major influence on the temperature of crystallization but relatively little effect on the filament drawdown. Among the process parameters, the cooling air temperature and the air flow rate appear to be the most significant variables. The model predicted that the final fiber diameter, final crystallinity and final birefringence of the filament decreased with the increase in cooling air temperature.

In 1993, Malkan, Wadsworth and Davey investigated the effect of processing parameters on the 'Reicofil®' spunbonding process [18]. The process-structure-property

relationships among the various processing variables were assessed in terms of the physical properties of the webs and the final fiber diameter (fiber diameter in webs). The variables studied were polymer throughput rate, bonding temperature, bonding pressure, polymer melt temperature, primary air temperature, attenuation air flow rate, and production speed. Polymer throughput rate and bonding temperature had the most significant effects on the final fiber diameter and stress-strain properties of the webs. The final fiber diameter was shown to be an important resultant variable in controlling many of the key properties of the spunbonded webs. The final fiber diameter was shown to decrease with an increase in cooling air temperature and polymer melt temperature, and with a decrease in polymer throughput rate.

2.2 Polypropylene Fiber Spinning

Production of fibers from polypropylene can be carried out by a variety of processes, from high-quality multifilament yarns produced in the long air-quench process to coarser fibers obtained by fibrillating slit film. To produce high-denier fibers, the water quench process for monofilament has been used. Recently, the short air quench system and spunbond process of nonwovens have been developed with considerable space saving.

2.2.1 Air-Quench Melt-Spinning

2.2.1.1 Long Air-Quench

Long air quench is used for spinning systems that utilize take-up speeds from 300-

4000 m/min and a filament free length 3-10 m. The long lengths are needed for sufficiently cooling the high speed threadline. Yarns with individual filament deniers from 2 to 25 and total deniers of from 75 to several thousand are produced by the long air-quench spinning. Staple fibers can also be produced using this method.

The melt-spinning of polypropylene begins at the hopper of an extruder, there the polypropylene, either a uniform blend or a volumetrically or a gravimetrically proportioned mixture of natural and colored materials (pellets, spheres, or powder), is fed to the throat of the extruder. Resins with melt flow rates of 3-35 are used in the process. Since polypropylene is nonhygroscopic, drying of the feed material is not required (surface moisture should be removed) and inert gas blanketing of the extruder hopper is optional. The raw material is then melted and conveyed through the electrically heated extruder. Extruders of at least 24/1 L/D are desirable for polypropylene, and some resin suppliers recommend that a portion of the screw be equipped with a mixing zone, or mixing downstream of the extruder, or twin-screw extrusion [19].

Some kind of filtration is normally supplied immediately downstream from the extruder. After the melt leaves the filter, it travels through the transfer lines or spin manifold to the metering pumps. The metering pumps are essentially positive- displacement precision-made gear pumps, especially designed for melt-spinning. After leaving the metering pumps, the melt travels through short transfer lines and into the spin pack. Good pack design assures that the melt inside the pack flows in a symmetrical manner with respect to the spinnerette. The pack filter, the breaker plate and the spinnerette are contained in the lower portion of the pack. These parts, along with metering pumps, are the heart of the melt-spinning process.

Die swell is always present in polypropylene spinning because the melts are viscoelastic. The viscoelasticity also gives rise to melt fracture if temperatures are too low or if orifice shear rates are too high. After exiting the spinnerette capillaries, the filaments begin their descent to the winder position. The filaments first enter into the quench cabinet (1 to 2 m in length), where they are solified. Further cooling takes place in the quench stack between the cabinet and the point of finish application. The quench zone is very important part of a melt-spinning process. With polypropylene, the emerging filaments are from 70 to 170 ^{0}C above the melting point (165 ^{0}C). Careful consideration should be given to aerodynamics within the quench cabinet. There is normally a cross-flow of air along the fiber bundle length. The cross-velocity is usually higher in the regions near the spinnerette. The threadline, travelling at high speed, develops an air boundary layer sufficiently. Turbulence or unstable flows anywhere along the threadline can cause filament unevenness.

In recent years, quenching of a large number of filaments produced from a circular spinnerette has been improved by blowing air rapidly outward from an air source placed on the spinnerette axis. Although some orientation is introduced into the melt during its passage through the spinnerette orifices, most of this orientation is lost at the orifice exit because of strain recovery. The orientation in the undrawn yarn is a result of the stretching of the filament between the position of maximum diameter (just below the spinnerette exit) and the position of final diameter. However, the development of crystalline orientation in polypropylene continues beyond the position of final diameter. The amount of orientation in undrawn yarn is determined by the resin properties and the spinning conditions. Any condition that gives higher stress in the stretching fiber gives higher degree of orientation.

Higher-molecular-weight resins, large quench rates, and large stretch rates give higher spin-line stresses. The take-up speed is one of the most influential parameters affecting orientation. Following are the finishing and drawing of yarns. There are variations of the spinning process that were not mentioned, e.g., biocomponent spinning. The operation is carried out usually by employing two extrusion systems that keep the resins separate until just before the streams exit the spinnerette. Sheath core or side-by-side yarns can be made by this process.

2.2.1.2 Short Air-Quench

A short air-quench process has been developed for the purpose of the design to save building space and reduce labor costs. The entire system can be located on one floor. In principle, the short air quench system is basically the same as the long quench process, but due to the shorter distance available for quenching, no more than a meter or so, the spinning rate possible is not no more than 150 m/min, although most operating speeds would be lower than that.

The systems are designed for producing staple fibers (3-100 denier), but some manufacturers suggest their use for making textured or bulk yarns. Anyway, the spinning systems are located in line with the traditional drawing, annealing, and bulking systems downstream. The products made from short air quench systems are obviously not as high in quality as those produced from long air quench systems.

2.2.1.3 Water-Quench

Monofilaments with higher denier (more than 100 denier) are usually produced in a water-quench system due to the inherent limitation of forced convective heat transfer with gases. Common screw extruders are used for melting and conveying the polypropylene resin, just as mentioned above. However, often there are no metering pumps used in the system. For polypropylene, one large spinnerette is employed with the number of spinnerette orifices corresponding to the number of filaments desired. The spinnerettes are heated by electricity, however, when filament uniformity is important, condensing organic vapors may be used for heating. Polypropylene monofilaments spin into such products as chair webbing, ropes etc., and wider limits of uniformity are normally acceptable in these products. Otherwise, metering pumps should be used for uniformity.

As soon as exiting the orifice, the filaments enter a water-quench bath. Guides are used in the bath for the filaments to travel a proper distance for quenching. The unique aspects to the water-quench of polypropylene are draw resonance and a difference in crystalline order under certain spinning conditions. In air-quench units, yarns with a crystallinity of about 55% may be obtained. The crystals are usually distributed throughout the yarns as lamellae and are normally in the monoclinic α-form. In the rapid cooling water-quench system, a less ordered smectic or paracrystalline structure may be produced with a morphology that is mainly fibrillar. Upon drawing under certain conditions, these smectic structures lead to high-strength fibers.

After the filaments leave the quench bath, they will be wiped or blown free of water in preparation for hot draw. The orientation of the spun filaments, and consequently the

draw ration necessary for producing a satisfactory product, depends on the stretch rate during spinning and quenching just as they do in the air-quench process. The larger the stretch rate, the higher the spin-line stress, the higher the orientation, and the lower the required draw ratio.

2.2.2 Film-forming Fibers

Films are fabricated in two conformations-sheet and blown film. Blown film is not widely used because its operation is more complicated and it produces a less fibrillable film (due to a more ordered crystalline structure and the lateral orientation). Sheet films are produced from long, narrow-slit dies, which are usually attached directly to a conventional single screw extruder. There is normally a filter between the extruder and the die. Metering pumps are almost never used. The die opening can be adjusted along the die length so that the film thickness may be maintained uniform across its width. The film thickness is measured by a gauge and resins with MFR 1-4 are usually used for these films.

Techniques for producing relatively coarse but very useful fibers or fiber-like tapes from film have been developed. The most prevalent general method is that which uses rotating rolls. This method is simple, easy to control, and gives more uniform products. The peripheral cutting devices can consist of pins, hacksaw blades, razor blades, or fine threads or serrations cut on the lands of a fluted roll. During processing, the running tape is fed over the rotating roll, which rotates so that its contacting surface travels in the tape direction at speeds of one to three times the tape speed. Oriented polypropylene is very adaptable to this fibrillating process, strong, and very fiber-like tapes with denier of 300 and up were

manufactured. Another (less-used) process for making fibers from film or tapes is that the film in the molten state is pressed between two rolls. One of the rolls is smooth, and the surface of the other contains closely spaced, shallow peripheral grooves. The film, then, is embossed all along its length, and in subsequent stretching and perhaps mechanical treatments, the film separates along the grooves. Relatively fine monofilament (6-10 denier) were fabricated in this method [20].

2.2.3 Fibers from Spunbonding Process

The spunbonding process is the method wherein the production of fibers and fabrics or webs is combined in one step. The conventional spunbonding process consists of laying down a web or mat of continuous filaments and then bonding the fibers within the fabric by mechanical, thermal, or chemical methods. Melt-blowing process also fits the general definition of a spun-bonding process, in which short and fine filaments are laid down.

The spunbonding process includes a spinnerette with means of conveying the continuous filaments out into the form of a web or several or more spinnerettes arranged in a row of length which may approximate the width of the web to be manufactured. The filaments are pulled from the spinnerette, perhaps by air jet, may be given an electric charge, and are then laid down on a moving screen. The filaments are usually only partially oriented, even though they are stretched at very high speeds. After they are formed, the fabrics may be thermally bonded by calendering or needle-punched or chemically bonded [21].

Melt-blowing process produces nonwoven fibrous webs from any thermoplastic resin

but has been used most extensively with polypropylene, which appears to be particularly suited for meltblowing. In melt-blowing, a long rectangular die or spinnerette containing a large number of capillaries in a single row all along its length is attached to a common screw extruder. Molten polymer is fed directly from the extruder through a filter and through the capillaries. Hot air at near-sonic velocities is forced through adjustable slots all along the length of both sides of the die. Fiber attenuation takes place as the hot melt issues from the capillaries in to the convergent high-velocity air streams. The cooling air from ducts located along both sides of the die is directed towards the filaments at a position further from the die and helps in quenching. The fibers are collected on a continuous, moving wire screen under which there may be located a suction chamber to help in the removal of large volumes of air. The web is fed from the collecting screen to a take-up roll or a hot calendering system. The width of the web is the same as the length of the die. The weight of the web is determined by the output of the extruder and the speed of the collecting screen. The average orientation of the fibers relative to the machine direction depends on the air flows and screen speed. The diameter of the fiber can be as small as 0.5 um, depending on process conditions. Finer and shorter fibers are produced from the lower polymer flow rate and the higher air flow rate. Continuous fibers are made at very low air rates. Higher temperatures, decreasing the distance between the die and collecting screen, and lower air rates result in a stiffer fabric. Usually, the melt-blowing fibers have fairly low orientation.

2.3 Properties of Polypropylene and Polypropylene Fibers

Polypropylene produced by the polymerization of propylene is of major importance

as a plastic and fiber forming material [22]. Polymerization to high molecular weight polymer is achieved by Ziegler-Natta polymerization. The polymer so produced is highly stereoregular being isotactic. This kind of polypropylene has been used [23] predominantly in commercial production.

Commercial polypropylene is 90-95% isotactic and has a number average molecule weight of 40,000-60,000 with a polydispersity of 6-12 [22]. It crystallizes with the molecular in a 3_1 helix. Several different types of spherulite may be formed on crystallization. The crystalline regions have a density of 0.94 g/cm^3 and the amorphous regions have a density of 0.85 g/cm^3, and typically, polypropylene has a density of about 0.90 g/cm^3 with a crystallinity of about 50%. Polypropylene melts may be quenched to give an amorphous polymer. The maximum melting temperature (T_m) is 165 ^{0}C with a narrow (about 5 ^{0}C) melting range, so polypropylene softens at a considerably higher temperature than polyethylene. Its major amorphous transition is about 0 ^{0}C, therefore, the polymer embrittles apparently on cooling. Commercial block copolymers with about 5-15% ethylene blocks, known as propylene copolymer, have relatively low brittleness.

Polypropylene is stiffer than polyethylene, having a tensile modulus of 1000-1300 MPa and a tensile strength of 25-35 MPa [22]. Its elongation at break is 50-300% and impact strength (Izod) 0.3-4.3 J (12.7mm)$^{-1}$. Polypropylene is highly solvent resistant and environmental stress cracking resistant. It had a very high electrical resistivity. However, the presence of a tertiary hydrogen on each repeat unit makes it very susceptible to oxidative degradation. Although usually opaque, thin film, especially if biaxially oriented, may show a sparkling degree of clarity. Uniaxially oriented fibers can be obtained by fiber spinning,

followed by drawing and heat-setting.

2.3.1 Solution Property; Molecular Weight, and Molecular Weight Distribution

Relations between physical properties of polymers and structural parameters such as molecular weight, molecular weight distribution, molecular size and shape (chain conformation) have been established by investigations of dilute solution properties. The main emphasis of this section will be focussed on molecular weight and molecular weight distribution which are both of utmost practical importance for the characterization of polymer samples.

Because of its crystalline character, PP, like other crystalline polyolefins, is soluble only at elevated temperatures. Polyolefin solutions in general, and PP solutions in particular are subject to oxidative degradation at elevated temperatures; for this reason the use of antioxidants or nitrogen atmospheres is required in the investigation of polyolefin solutions, and prolonged heating should be avoided. Isotactic PP displays good solubility above 80 ℃ in so-called 'good' solvents such as xylene, tetralin, chlorinated aromatic and aliphatic hydrocarbons, etc. In 'poor' solvents such as esters, ethers, higher alcohols, etc. PP becomes soluble only at considerably higher temperatures.

PP, like other vinyl polymers, consists of a mixture of homologous macromolecules of different molecular weight, and it is therefore termed polydisperse. The most commonly used molecular weight averages are: number average Mn, weight average Mw, z-average Mz, and viscosity average Mv. The ratio Mw/Mn is frequently used as a measure of the width of molecular weight distribution or polydispersity.

2.3.2 Melt Flow Rate

Melt Flow Rate (MFR, alternative name for melt flow index)is a measure of the melt viscosity of a polymer and hence also of its molecular weight. The weight of a polymer extruded through a standard cylindrical die at a standard temperature in a laboratory rheometer carrying a standard piston and load. The procedure for measuring polypropylene MFR is ASTM D1238 Condition L. The temperature of the test is 230 ^{0}C, and the forcing load is 2160g. The MFR is the amount of resin extruded through the 0.0825×0.315 inch die in 10 minutes. The MFR is inversely related to the apparent melt viscosity and the end pressure losses, both of which are strongly dependent on the polymer weight average molecular weight. The larger the melt flow, the lower the molecular weight. Polymers with melt flow rate from less than 1 to more than 35 are commercially produced. Most fibers are produced from resins having MFR between 3 to 35. For meltblowing process, up to 100 MFR of PP is used.

2.3.3 Crystalline Properties of Polypropylene

The physical properties of a polymer are determined by its microstructure. Particularly in the case of crystalline polymers, X-ray methods are the most important tools in elucidating property-structure relations. Polymer molecules with a particular molecular structure (for instance, isotactic PP) aggregate to form crystals, and these, in turn, aggregate to form spherulites. The manner of aggregation of molecules determines the crystal structure, the aggregation of crystals produces the morphological structure (spherulitic or single crystal). Polyolefins are only partially crystalline and the determination

of the degree of crystallinity (percentage of crystalline material) by X-ray or other methods is of great practical importance. Finally, the conditions and the rate at which crystallization takes place is of importance. General requirements for the crystallizability of polymer molecules are geometrical regularity of the molecular structure (high degree of tacticity), a sufficient packing efficiency of the polymer chains, and sufficiently favorable conditions for the kinetics of crystallization [25]. Even under the most favorable conditions, polymers will never achieve full crystallinity because of chain entanglements, structural imperfections, and insufficient rate of crystallization.

2.3.3.1 Crystal Structure of Polypropylene

The crystal structure of it. PP was clarified by Natta [24]. From X-ray fiber patterns a monoclinic unit cell containing 4 chains and 12 monomer units was derived which had a calculated density of 0.936 (compared to an experimental density of about 0.91) and the following parameters (in A): $a = 6.65$, $b = 20.96$, $c = 6.50$, $\beta = 99.3^0$. From the identity period in the c-axis $c = 6.50$ Å it was concluded that the chains have a threefold helical conformation: 3_1 helix. Three monomer units are distributed along one turn of the helix (Figure 2.4). The most probable model for packing PP helices in a Cc-space group was also discussed by Natta [24]. The conformation assumed by the chain molecules in the crystalline state should, in general, be a close approximation of the form corresponding to the lowest energy of the isolated chain. In crystalline PE the chains assume the planar zig-zag form of the all-trans conformation; crystalline it. PP assumes the form of 3_1 helices corresponding to a regular alternation of trans and gauche bonds: (Tg)n sequence. This

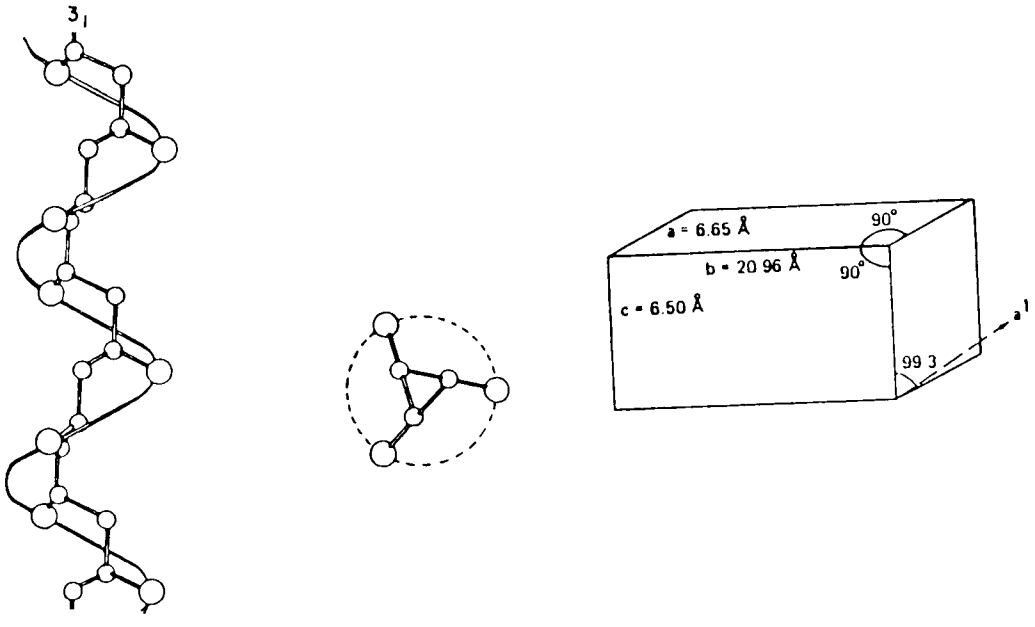

Figure 2.4 3_1 Helix for Isotactic Polypropylene [24].

conformational sequence corresponds to a minimum steric strain (expansion of the bond angle joining backbone carbon atoms from the tetrahedral angle of 109.5° to 114.5°). Besides the ordinary monoclinic form (α form) of it. PP other polymorphic forms are β and γ. β form is the hexagonal one (unit cell: a = 12.74, c = 6.35) which occurs in certain spherulite formations. The hexagonal form is also characterized by the threefold helical conformation of polymer chains. By rapid quenching of molten PP a so called γ or quenched form of it. PP can be obtained [24,26]. This form is believed to be closely related to the hexagonal form with, a lesser degree of lateral order and consisting mainly of very small hexagonal crystallites. X-ray diffraction diagrams of all three forms are shown in Fig. 2.5.

2.3.3.2 Degree of Crystallinity of Polypropylene

The degree of crystallinity, i.e. the fraction of crystalline material may be determined by X-ray diffraction, density measurements, and thermal analysis. Other methods such as infrared absorption and solvent extraction respond to tacticity rather than crystallinity. The entire subject, however, is rather controversial because the different methods furnish estimates of different though correlated properties of polymer samples. The dependence of properties on crystallinity rather than tacticity cannot always be clearly distinguished. The X-ray diffraction method [27] relates the intensity (area under the diffraction curve) of the main crystalline peaks *Oc*, (1200 for 100% crystalline PP), to that of the amorphous halo *O*a (925 for 100% amorphous PP); the degree of crystallinity *C* may be calculated as following:

$$C=Oc/(Oc+1.297Oa)$$

The density method is based on the assumption of a two phase model of the polymer

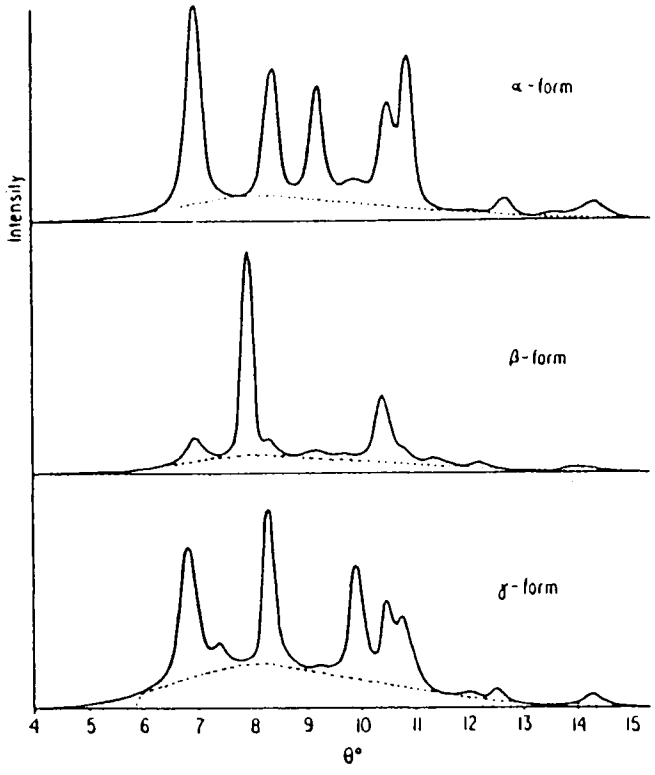

Figure 2.5 X-ray Diffraction Diagrams of Isotactic Polypropylene Crystalline Forms [26].

consisting of crystalline zones with a theoretical X-ray density (0.9363) and amorphous zones with the low density of wholly amorphous at. PP (0.8576); the density values were obtained at 20°C. The degree of crystallinity is derived by linear interpolation. The results obtained by these two methods show fair agreement and typical values for the degree of crystallinity of commercial PP samples are between 50 and 65%.

Thermal analysis data may also be used to determine the heat of fusion (or heat of crystallization respectively) per unit weight PP and to derive therefrom the percentage of crystalline material [28]. Commercial PP samples are highly isotactic and contain usually only a few percent of atactic material. The isotactic material is partially crystalline, the atactic one is practically wholly amorphous. The infrared spectrum of molten it. PP is practically identical with that of at. PP. Assignments of infrared bands have been summarized [29]. The intensity ratio of one of the isotactic bands, such as the one at 997 cm^{-1}, to one of the bands persisting in the amorphous system, that, for instance, at 975 cm^{-1}, is used as a measure of the degree of tacticity [30,31]. This ratio ranges from zero (100% atactic) to unity (100% isotactic). Since

the isotactic bands, such as the one at 997 cm^{-1} are due to the helical conformation of it. PP chains rather than to crystallinity. It is not surprising that, for instance, quenched PP shows very low X-ray crystallinity but is highly isotactic judged by its infrared spectrum [32]. Commercial PP samples usually have a tacticity of 90% and more. Numerical values for the degree of crystallinity will, of course, also depend on the conditions of crystallization, on thermal aftertreatment (annealing) [33,34], and on the molecular weight and molecular weight distribution of any particular sample.

2.3.3.3 Morphology of Polypropylene

Crystalline polymers may occur in two different morphological forms: crystallization from very dilute solutions leads to the formation of lamellar single crystals whereas crystallization from the melt leads to formation of spherulites. The orientation of polymer molecules in these structures has produced the concept of chain folding, particularly in the field of polyolefins.

By cooling extremely dilute solutions of crystallizable polyolefins the polymer solute material will precipitate in the form of single crystals. This phenomenon has been observed for PE, it. PP, and also for higher isotactic polyolefins. In all cases, the crystals are composed of lamellae with a thickness of the order of 100 Å and with lateral dimension of at least one micron. The simplest crystals are monolayers, more complicated ones may contain 10 to several hundreds lamellae, all originating from the same nucleus. Information on the orientation of polymer chains may be derived from micro X-ray methods; in practically all spherulites the molecules are arranged in a tangential fashion [34], i.e. the crystallographic a-axis of PP lies along the spherulite radius. Spherulites consist of radial fibrils composed of lamellae of the same order of thickness as those of single crystals. The polymer chains being oriented perpendicular to the spherulite radius and hence to the fibrils, are folded in a more or less regular fashion similar to the folding in solution-grown single crystals.

2.3.4 Rheological, Thermal and Mechanical Properties of Polypropylene

2.3.4.1 Rheological Behavior of Polypropylene

Polypropylene melts exhibit non-Newtonian viscosity, normal stresses in shear flow, excessive entrance and exit pressure drop, die swell, secondary entrance flows, melt fracture, and draw resonance. Differences in types of behavior were observed for the melts in the elongational flow experiment. The moderate and broad molecular weight distribution samples exhibited local necking just after they reached maximum stress, and ductile failure occurred. The narrow molecular weight distribution samples elongated uniformly and finally ruptured abruptly.

The speed of spinning is inversely related to the viscosity of the polymeric material [35]. The melt viscosity can be lowered by increased temperature, decreased molecular weight, increased shear rate, and widened molecular weight distribution. The velocity profile across the die is such that the maximum velocity is reached at the enter of the die; parabolic velocity distribution for Newtonian fluids and a more 'plug' like distribution for pseudoplastic polymer melts. In zone B [35] (near to the die) the flow pattern converges toward the die with stagnant regions around the die entrance; this effect may be reduced by tapering the die entrance. Shear rate, shear stress, and elastic shear strain in this zone increase to a maximum, and the viscosity decreases. Due to the high shear stress melt fracture may occur in this zone. In zone C the shear rate is constant and the shear stress decreases to a constant value. In zone D shear rate and shear stress decrease rapidly, elastic recovery occurs, the melt begins to be cooled, and viscosity increases. In zone E the modulus

(resistance to flow) increases due to cooling (solidification), development of orientation, and increase in viscosity (low shear rate). Maximum draw-down can be achieved for polymer melts with small elastic recovery and small viscosity increase (non-Newtonian behavior).

2.3.4.2 Thermal Properties of Polypropylene

The physical properties of isotactic PP are essentially determined by its molecular weight and degree of crystallinity. The temperature range within which PP is most commonly used is limited by the crystalline melting point Tm on the high side and by the glass transition temperature Tg on the low side. The crystalline melting point of high molecular weight it. PP has been shown to have a maximum value of 176 ^{0}C (under normal processing conditions the melting points are usually considerably lower). As with practically all crystalline polymers, melting does not all occur at this temperature; a melting range is observed which starts as low as about 120 ^{0}C. Literature values of the heat of fusion of hypothetical 100% crystalline PP show wide discrepancies ranging from 15.4 to 62 cal/g. The most reliable value seems to be 59 ± 8 cal/g as obtained by calorimetric measurements in connection with data on crystallinity derived from X-ray diffraction [36]. The experimental heats of fusion for both polyolefins are of course considerably lower than the above mentioned values because of their only partially crystalline character.

The glass transition is associated with the amorphous phase of a polymer and occurs at a temperature Tg at which segments of the main chain become mobile. The noncrystalline phase of PP will become glassy and brittle below Tg, soft and rubbery above Tg; the embrittlement of it. PP as a whole at low temperatures is a direct consequence of the

glass transition of the noncrystalline phase. It is obvious that the glass transition can be more easily observed in wholly amorphous at. PP whereas ordinary commercial it. PP contains only a small fraction of at. PP and of noncrystalline isotactic PP; yet the observed transition temperatures do not show any significant difference between atactic PP and ordinary isotactic PP. Various physical methods can be used to determine Tg, e.g. dilatometry, dynamic mechanical measurements (at low frequency), heat capacity, and nuclear magnetic resonance (narrowing of line width). The agreement of Tg-values from various experimental methods is not very good but ranges from about -30 to 20°C. The most reliable values are probably derived from dilatometry [37] Tg between -20 and 0 °C (depending on tacticity and thermal history); there are some indications that the low temperature transition may be due to amorphous atactic PP and a somewhat higher transition between 25 and 45 °C perhaps due to noncrystalline isotactic PP. PP does not show any transition in the very low temperature range such as PE (transition due to mobility of methylene sequences at 125°C).

2.3.4.3 Mechanical properties of Polypropylene

The mechanical properties of it. PP are largely due to its crystallinity; because of the comparatively high melting temperature, the crystalline phase retains mechanical strength up to rather high temperatures. On the low temperature side the usefulness of PP is limited by its embrittlement at the glass transition temperature. The two most important factors affecting the properties of PP are molecular weight and crystallinity. Rheological properties and hence processability depend primarily on the former, whereas mechanical and particularly elastic properties (e.g. stiffness) are mainly dependent on the latter. Yield point,

tensile strength, and elongation are commonly determined by the stress-strain curve. They represent the maximum elastic strength, the ultimate strength, and the extent to which the material can be drawn. At high rates of loading (strain rate) stress-strain curves deviate considerably from the pattern illustrated. Yield point, tensile strength, and elongation depend on a number of variables as shown in temperature, density, molecular weight, and rate of loading.

2.3.5 Effect of Spinning Parameters

The properties of spun polypropylene fibers are primarily determined by the stress existing in the spinline at the position of final fiber diameter [38]. The stress level is basically determined by take-up velocity, molecular weight, extrusion temperature, extrusion velocity, and air cross-flow rate and temperature. The stress of spinline is the determining factor in the orientation of the molecules prior to solidification and this orientation gives rise to rapid crystallization in the spinline. The stress is related to how rapidly the spinline is stretched and cooled, not how much drawdown exists in the spinning process. As molecular weight increases, the average apparent elongational viscosity increases, therefore, the orientation of the spun fibers increases. A decrease in spinning temperature results in an increase in average apparent elongational viscosity and, therefore, an increase in orientation. A decrease in spinning temperature gives a decrease in length over which spinline deforms, which also results in an increase in orientation. An increase in take-up velocity gives an increase in average elongation rate and a corresponding increase in orientation. An increase in capillary diameter will give a smaller value of extrusion velocity and a measurable

increase in orientation. An increase in air velocity results in a decrease in length over which spinline deforms and, therefore, an increase in average apparent elongational viscosity and orientation. In spinning, the orientation is due to stretch rate, not the amount of stretch as in the case of drawing.

In air-quenched filaments, only monoclinic crystal form was produced [39]. The crystallization was observed to occur on the spinline, and during crystallization the birefringence increased rapidly. Increasing the spinning temperature with other variables unchanged resulted in a low orientation.

Crystallization rate generally increase with an increase in take-up speed or stress. The degree of crystallinity as a function of spin-line stress increases as the stress increases. Although both the crystalline and amorphous orientations increase with stress, the orientation developed in the crystalline regions is always larger than that developed in the amorphous regions.

The spherulitic structure of polypropylene fibers at low spinning stresses undergoes a transition to a row-nucleated structure as stress is increased [40]. Polypropylene exhibits a distinctive bimodal orientation of the unit cells when crystallized from melts undergoing extension. There are crystals whose c-axis is oriented parallel with fiber axis and a small amount of crystals whose a'-axis is oriented parallel with fiber axis.

Birefringence, modulus, yield strength, and tensile strength increased as the spinline stress increased, as well as spinning speed. At lower spinning speed, density and birefringence were both dependent on spinning temperature. However, at high spinning speeds (about 3000 m/min.) the birefringence did not depend on temperature. Birefringence

was higher near the surface of the fibers [41]. This higher birefringence has been postulated to be due to the rapid cooling on the outside and the consequent increase in viscosity and load bearing in the outside layers.

2.3.6 Effect of Drawing

Drawing increases strength and modulus and decreases elongation, in which simple flow process results in profound change in the fiber structure. During the initial step of deformation, a crystalline fiber undergoes an affine transformation. Lamellae parallel to the applied stress may deform in a different manner from lamellae perpendicular to the stress. With sufficient deformation, the lamellae are broken up into folded chain blocks approximately 20 nm in width [42-45].

These blocks subsequently aggregate to form the basic unit (microfibril) of the drawn fiber. The microfibrils consist of alternating blocks of folded-chain crystals and amorphous regions that are mostly chain folds. The tie molecules in amorphous regions connect the blocks in the fiber axis direction and provide the major source of resistance to deformation and strength to the fiber, which are located mainly on the surface of the microfibrils and extend along many crystal blocks and are aggregated laterally to form the fibrils.

Drawing increased the crystalline orientation in all cases [42]. For highly oriented fiber during spinning, the increase in orientation was small. The higher the as-spun orientation, the lower was the draw ratio necessary to develop a given higher level of orientation. Samples that were hot-drawn and annealed displayed a well-formed monoclinic structure. Cold-drawing transformed the monoclinic form of the spun fibers into a more

oriented but disordered structure. Density of the hot-drawn and cold-drawn and annealed fibers were slightly higher than those of the spun fibers. Cold-drawing resulted in disruption of the entire structure including the unit cell as well as the morphological units. Annealing removed residual strains, increased perfection in the unit cell, increased crystallite sizes, and restructured the axial periodicity with a new long-period spacing.

2.3.7 Effect of Annealing

Annealing the fiber quickly relaxes the stress, heals the voids and structural defects, and leads to an increase in degree of crystallinity and to perfection and size of crystallites. If heated with free ends, the annealing causes the fiber to shrink. Annealing can lead to an improvement in mechanical properties and certainly stabilizes the structural and dimensional properties of the fiber for use at elevated temperature.

For viscoelastic materials, deformation is followed by either stress relaxation or strain recovery to some thermodynamically stable state. The relaxation or recovery process occurs because polymers are viscoelastic. In cooled polymers, relaxation or recovery occurs much more slowly, because the time constants are much larger.

The process can greatly speed up by the application of swelling agents or heat. For drawing polypropylene, the relaxation of tie molecules, shrinkage, and disorientation proceeded relatively fast, compared with the long period growth and the increase in density, which continued as a linear function of log time through 1000 minutes [46]. Cold-drawing of polypropylene caused voids and a decrease of crystallite size and greatly enhanced lattice strains and defects. Annealing the fibers at 140 ^{0}C restored a well-formed monoclinic

structure and healed the voids.

2.4 Polypropylene-based Polyethylene Copolymer

A polymerization in which more than one monomer (A, B, etc.) participates, results in a copolymer, which therefore contains more than one type of repeat unit. Copolymer is sometimes restricted to polymers involving only two different monomers. Chain copolymerization, with simultaneous polymerization of the monomers, produces an approximately random copolymer. Often copolymers produced by step-growth reactions are expected to result in block copolymers.

Random copolymerization of ethylene and propylene leads to amorphous elastomers. Comprehensive reviews on copolymers of this type have been published [47]. Graft copolymerization of various monomers on PP backbone chains [48] leads to products of very interesting properties which, however, have not attained any great practical importance so far. The preparation and manufacture of block copolymers , on the other hand, is of very great practical and commercial significance. From kinetic studies of propylene polymerization it was concluded that the average lifetime of growing PP chains is sufficiently long to permit the formation of block copolymers by alternate feeding (for several minutes) of ethylene and propylene into a catalyst system active towards both monomers, and by removal of the preceding monomer by evacuation or flushing with an inert gas. The alternate feeds may be either pure ethylene and propylene or ethylene-propylene mixtures and propylene; in the first case blocks of PE and PP sequences will be obtained and will be capable of forming PE and PP crystallites. In the second case, blocks

of random PE copolymer will alternate with PP block, as a result, and will be able to form PP crystallites. It has been pointed out that in view of the polymerization conditions it seems very likely that most so-called block copolymers are actually intimate blends of PE and PP homopolymers with comparatively small contents of true block copolymers.

The main advantage of so-called block copolymer (with ethylene contents preferably between 5 and 15 %) relative to PP homopolymers is the greatly improved impact strength, particularly at low temperature or, in other words, a shift of the brittle point (glass transition Tg) to lower temperature. Other mechanical properties (such as stiffness, hardness, etc.) are reduced compared to PP homopolymers.

A random copolymer with 10% ethylene displays impact strength comparable to a block copolymer with also 10% ethylene, but is much inferior with respect to tensile strength. The comparatively poor impact strength of a polyblend with 10% PE is believed to be largely due to the fact that the degree of dispersion which can be achieved by mechanical blending of these two incompatible polyolefins is not comparable to the one obtained by alternating polymerization of ethylene and propylene and the same catalyst system and the same catalyst sites in block copolymerization.

Another way to improve low temperature impact strength of PP is the addition of elastomeric material with a sufficiently low glass transition temperature (e.g. polyisobutylene, ethylene-propylene copolymer, etc.) by melt blending [49-51]. The two polymeric materials are usually not compatible with each other but under suitable processing conditions (high temperature; screw extruder) a sufficient degree of dispersion can be attained in the polyblend. The concentration of elastomeric material usually ranges between

5 and 20%. Temperature impact strength of such polyblends is accompanied by a reduction of other mechanical strength properties such as stiffness, hardness, etc.

CHAPTER III

EXPERIMENTAL DETAILS

3.1 Processing

Based on the established optimum process window for 35 MFR PP by earlier researchers [36], two kinds of polymers, one polypropylene homopolymer and another, a polypropylene-based copolymer, were processed using the Reicofil spunbonding line at the University of Tennessee, Knoxville. A series of filament samples (before bonding) and the corresponding nonwoven samples were collected. The two key process variables, mass throughput and primary air temperature were changed as shown in Figure 1. Other processing conditions are shown in Tables 3.1 and 3.2.

3.2 Characterization of the Filaments and Nonwoven Samples

3.2.1 Tensile Properties.

Tensile properties of the filaments and the nonwoven samples were measured using the United Tensile Tester with test conditions described in the ASTM D3822-91 for filaments and ASTM D1117-80 for nonwoven fabrics [52]. For filament samples, a gauge length of 2" (5.08 cm) and an extension rate of 2"/min (5.08 cm/min) were used. The filaments were carefully separated from unbonded webs avoiding any deformation of the sample during that process. The sample was then mounted in a window with a slight

Schematic of Processing Variables

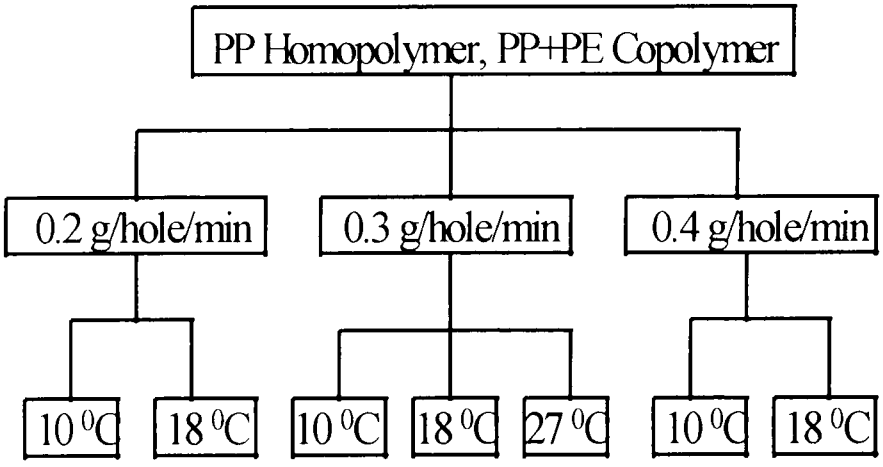

Figure 3.1. Schematic of Processing Variables

Table 3.1. Parameters of Processing Variables for PP Homopolymer

Sample Specification	1,2	3,4,5	6,7
Basic Weight (g/m^2)	40.0	40.0	40.0
Grade and Lot of PP Pellets	PP3445 59930	PP3445 59930	PP3445 59930
Melt Flow Rate of PP Pellets, g/min	35.18	35.18	35.18
Spin Pump Speed (rpm)	8.589	12.883	17.178
Gross Throughput/Hour (Kg/Hr)	44.6	66.9	89.2
Gross Throughput/Hole(g/hole/min)	0.2	0.3	0.4
Cooling Air Speed (rpm)	762.1	963.7	1267.2
Suction Blower Speed (rpm)	1652.9	2012.0	2252.4
Spin Belt Speed (mpm)	15.245	22.868	30.490
Calendar Nip Pressure (PLI)	385.0	385.0	385.0
Upper Roll Temperature ^0F (^0C)	297.0 (147.2)	297.0 (147.2)	297.0 (147.2)
Lower Roll Temperature ^0F (^0C)	292.0 (144.4)	292.0 (144.4)	292.0 (144.4)

Table 3.2 Parameters of Processing Variables for PP+PE Copolymer

Sample Specification	1,2	3,4,5	6,7
Base Weight Output (g/m^2)	40.0	40.0	40.0
Gross Throughput/Hour (Kg/Hr)	44.6	66.9	89.2
Gross Throughput/Hole (g/hole/min)	0.2	0.3	0.4
Spin Pump Speed (rpm)	8.589	12.883	17.178
Upper Roll Temperature ^0F (^0C)	260.0 (126.7)	260.0 (126.7)	260.0 (126.7)
Lower Roll Temperature ^0F (^0C)	255.0 (123.9)	255.0 (123.9)	255.0 (123.9)
Cooling Air Speed (rpm)	762.1	963.7	1267.2
Suction Blower Speed (rpm)	1652.9	2012.0	2252.4
Spin Belt Speed (mpm)	16.40	25.10	32.00
Calendar Nip Pressure (PLI)	385.0	385.0	385.0
Melt Flow Rate of Raw (g/min)	29.19	29.19	29.19
Grade and Lot of Raw Material	PD9355 59928	PD9355 59928	PD9355 59928

pretension for further testing. For nonwoven samples, gauge length of 4" (10.16 cm), width of 1" (2.54 cm), and extension rate of 4"/min (10.16 cm/min) were used in both machine direction and cross direction. The tenacity, breaking elongation and initial modulus were recorded and processed statistically by the connected computer.

3.2.2 Thermal Analysis

3.2.2.1 Differential Scanning Calorimetry.

Differential Scanning Calorimetry of all the filaments and nonwoven samples were carried out using the Mettler DSC 25. The samples were scanned at a heating rate of 10 ^{0}C/min in the nitrogen environment. Enthalpies of melting were determined so that the crystallinity of the samples could be calculated. A ΔH value of 146.5 J/g for 100% crystal polypropylene was used for estimating the crystallinity of the samples [53].

3.2.2.2 Thermomechanical Analysis.

Thermomechanical responses of the samples were recorded using the Mettler TMA 40 with a heating rate of 10 ^{0}C/min. The samples were scanned in the nitrogen environment with different levels of pretension. The gauge length for the samples was 10 mm, and for nonwoven samples approximately one mm wide webs were used. The samples were held by copper clips at both ends and a constant load was applied to the samples before starting the scan. The changes in length taking place with increase in temperature were recorded. Isothermal scanning of the samples was done to determine the length changes with time at

different temperatures and pretensions. These long-time measurements were used to evaluate time-dependent thermal properties of the samples.

3.2.3 Diameter and Birefringence.

Diameters of filaments in the unbonded web and the fabric samples were measured using an optical microscope. The filament samples were carefully taken from unbonded webs and laid on a glass slide for measuring. Thirty measurements were taken for each condition. Birefringence of the filament samples was determined using the retardation technique. Ten measurements were taken for each sample. The data were statistically analyzed for investigating the effect of processing variables.

3.2.4 X-ray Diffraction

X-ray diffraction photographs were obtained using a Phillips model x-ray diffractometer at 30 kV and 20 mA. The wavelength of the x-ray was 1.54183 Å and the exposure time, four hours. The samples were prepared by placing the filaments as a parallel array on a sample holder (a frame with a central circular opening). The distance between the film and the sample was 36.5 mm.

3.2.5 Scanning Electron Microscopy.

Scanning Electron Micrographs (SEM) of the fabric samples were obtained using an ETEC Autoscan Microscope operating at 20 kV. The samples were gold coated using a Hummer Sputter coater. Both the top and bottom side of the samples were scanned to

investigate the differences of bonding area between the two sides of the fabric samples. The cross-sections of the nonwoven in bond area were also photographed.

3.2.6 Thermal Deformation Analysis.

For thermal deformation analysis (TDA), a tubular oven mounted on rails (Figure 3.2) was used. One end of the leader filament was fixed, while the other end was passed over a smooth roll and pretensioned by applying required load. The tension or stress was adjusted by changing the mass hung at the free end. Changes in dimensions with time of the samples exposed to different temperatures were measured.

3.2.7 Density Measurement.

A gradient column was used to measure the density of the filament samples. The liquid used was a clear mixture of isopropanol ($CH_3CHOHCH_3$) and ethylene glycol (CH_2OHCH_2OH) with a density range of 0.875 to 0.9450 g/cm^3 for homopolymer samples and 0.835 to 0.915 g/cm^3 for copolymer samples, since the density of copolymer is lower than that of PP homopolymer. Five measurements were taken for each sample. Crystallinity of the samples was calculated using the following relationship [53]:

$$\text{Crystallinity (\%)} = [\rho_c(\rho-\rho_a)/\rho(\rho_c-\rho_a)]*100.$$

where: ρ = Measured Density;
ρ_c = 0.936 (g/cm^3), Density of 100% crystal PP;
ρ_a = 0.858 (g/cm^3), Density of 100% amorphous PP.

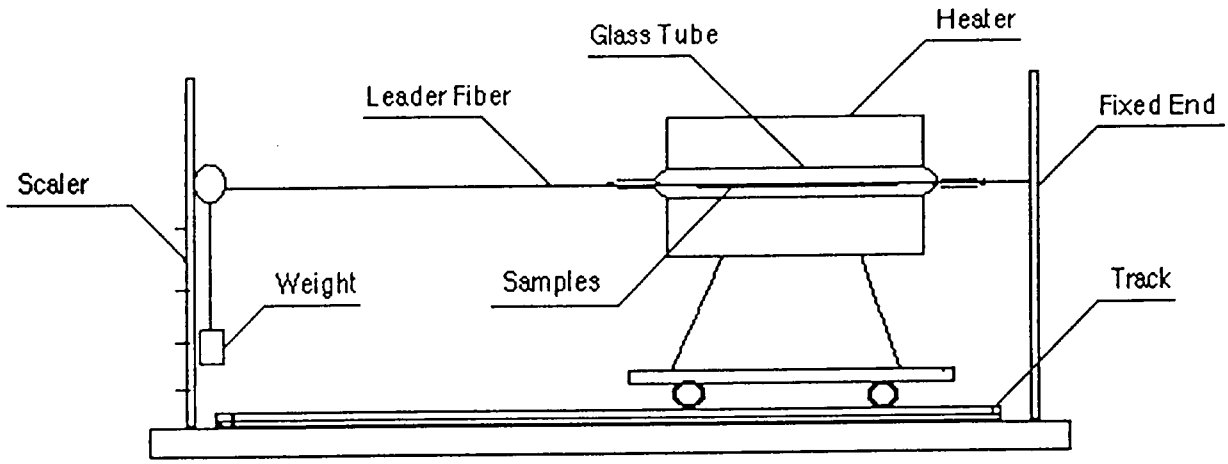

Figure 3.2. Experimental Set-up for TDA.

3.2.8 Melt Flow Rate.

The melt flow rates of the samples were measured according to the ASTM Test Method D1238, using the Tinius Olsen Melt Indexer. An average of five measurements is reported for each sample.

3.2.9 Bursting Strength, Stiffness and Air Permeability.

The bursting strength, stiffness and air permeability of nonwoven samples were determined using the INDA standard test methods. Five measurements were taken for each sample. Air permeability was measured according to the INDA standard test IST 70.1-70 (R82) [54] using the six mm diameter orifice at 70 ^{0}F and 65% R.H. For bursting strength measurement, the INDA standard test IST 30.0-70 (R82) was used. The INDA standard test IST 100.0-70 (R82) was used for the tear test. Tear strength was measured in both machine and cross-machine directions. Also, the stiffness of the nonwoven samples was measured in both the directions.

3.2.10 Annealing Studies.

Annealing of filament samples was carried out using a DK-63 constant temperature oven at varying temperatures and time. The filaments carefully taken from the unbonded webs were placed as a parallel array on the sample holder. The samples were inserted into the preheated oven and after exposure to predetermined time, taken out of the oven for further characterization.

Free length annealing was carried out by fixing one end of the filament while leaving

the other end free. For fixed length annealing, both ends of the filaments were fixed on a glass slide with slight pretension. X-ray diffraction photos, DSC scans, diameter, birefringence and tensile properties of the filaments were carried out before and after annealing. Whereas diameter and birefringence were measured for the same set of filaments, before and after annealing, tensile property data of annealed filament samples are compared with the same lot of fibers.

3.2.11 Statistical Analysis.

Statistical analysis of the results with respect to the processing variables was carried out using the statistical analysis of the SAS program [55, 56]. Birefringence, tensile strength and breaking elongation were used to evaluate the effect of primary air temperature, throughput, and their interaction. The tensile strength and breaking elongation were analyzed to determine the effect on properties and birefringence for structure. The test hypotheses were as follows:

1. H_0: No effect of Primary Air Temperature;

   H_R: The effect of Primary Air Temperature is significant;

2. H_0: No effect of Throughput;

   H_R: The effect of Throughput is significant;

3. H_0: No interaction of Temperature and Throughput;

   H_R: The interaction of Temperature and Throughput is significant.

CHAPTER IV

RESULTS AND DISCUSSION WITH PP HOMOPOLYMER SAMPLES

4.1 Effect of Processing Variables on Fiber Diameter and Birefringence

PP filaments were produced at different throughput and primary air temperatures and collected before thermal bonding. The fiber diameter increased as the throughput and primary air temperature increased as shown in Table 4.1. The increase in fiber diameter with increase in throughput has been observed before [57]. However, the diameter increase with the increasing temperature is contrary to what has been predicted [17]. The difference in observed trend of fiber diameter with cooling air temperature from the previous research and the ones predicted from the model [17] can be explained by the changes in the compensating effects of threadline stress and temperature during attenuation on the effective draw-down for the range of conditions studied. The model assumes that increase in quench air temperature results in reduction of fiber diameter due to lower viscosity in the fiber formation zone allowing higher drawability. Another point to be taken into consideration is that the model was probably built based on experimental data wherein the measurement of the fiber diameter was done in bonded webs and not with the formed filaments. This research has clearly shown that the fiber diameters before and after bonding are not the same. The change in fiber diameter during calendaring is dependent on the morphology of the filaments. This change is responsible for the reversal in trend for fiber diameter with quench air temperature.

Another possibility for the observed difference is the relaxation of the filaments. It was observed by Spruiell, et al, [58] that there were significant differences of the structure and properties of the filaments between the on-line and the off-line data. Their model predicted the on-line fiber diameter. It is reported [58] that the diameter increased about 10 to 25 percent after off line. For 35 MFR polypropylene, the diameter increased about 15% for off-line. It is also shown that the different conditions influence the amount of relaxation. Also the birefringence of the filaments changed along the spin-line. This is due to the relaxation of the filaments. The diameter of the filaments for this research was measured in the method of off-line. So the relaxation of the filaments already took place.

The birefringence of the fibers decreased as the throughput and primary air temperature increased. The higher the birefringence, the higher the orientation of the filaments. Therefore, as the cooling temperature increased, the orientation of the fiber decreased. This trend is related to changes in diameter of the fiber, as at the same throughput, lower primary air temperature results in smaller diameter of the fiber. This means the fiber is drawn more when cooler air is used. The low primary air temperature also helps in increasing the orientation of the fibers. This phenomenon is confirmed by other characterizations too. The linear density of the filaments, calculated based on the fiber diameter, are shown in Table 4.1.

4.2 Tensile Properties of Filament and Nonwoven Samples

Tensile properties of the formed filaments are shown in Table 4.2. The strength-at-break decreased with increase in the cooling air temperature. The elongation-at-break

Table 4.1 Sample Specification and Physical Properties of Filaments from PP Homopolymer

Sample	Throughput g/hole/min	Cooling Air Temperature ^{0}F (^{0}C)	Diameter (um)	Birefringence	Linear Density (Denier)
S_1	0.2	50 (10 ^{0}C)	21.76	0.0244	3.04
S_2	0.2	65 (18.33 ^{0}C)	23.63	0.0213	3.59
S_3	0.3	50 (10 ^{0}C)	24.82	0.0224	3.96
S_4	0.3	65 (18.33 ^{0}C)	26.18	0.0209	4.41
S_5	0.3	80 (26.67 ^{0}C)	27.14	0.0191	4.81
S_6	0.4	50 (10 ^{0}C)	27.2	0.0203	4.76
S_7	0.4	65 (18.33 ^{0}C)	28.9	0.0195	5.37

Table 4.2 Tensile Properties of PP Spunbond Filaments

PP Spunbond Filament	Break (mN/tex)	Elongation at Break (%)	Initial Modulus (mN/tex)
S_1	424.3	180.6	72.01
S_2	217.5	280.7	70.42
S_3	153.1	269.4	69.87
S_4	100.8	279.6	66.92
S_5	87.5	294.3	64.50
S_6	202.3	285.0	69.63
S_7	101.2	289.9	62.69

increased as the cooling air temperature and throughput increased. That was consistent with the observation that the orientation of the molecules in filaments was higher for low primary air temperature, i.e. the filaments with higher birefringence had lower breaking elongation and higher tenacity.

Tensile properties of nonwoven samples are shown in Table 4.3. Since the thermal bonding conditions were same for all the samples, the differences between the tensile properties of the samples reflect the differences of spinning processes. The tensile strength decreased as the primary air temperature and throughput increased. For the same reason, the elongation-at-break increased as the two process parameters increased. The strength-at-break of samples in the machine direction is apparently larger than that in the cross-direction. The elongation-at-break for MD is smaller than that for CD for the same samples indicating that the orientation of filaments in the webs is not random and is higher along the machine direction.

4.3 Thermal Properties

Figure 4.1 shows the DSC scans of filament samples produced at the same throughput and different cooling air temperatures. The melting peaks appear to be same, obvious in their heat of melting although melting temperatures show no differences. The crystallinity of the filaments decreased as cooling air temperature increased (Table 4.4). The crystallinity decreased with increasing throughput as well. The results indicating that low primary air temperature is helpful for the crystallization of PP filaments are consistent with that from density data as well as shown in Table 4.4. The crystallinity of the nonwoven

Table 4.3 Tensile Properties of Related Spunbond Nonwovens

PP Spunbond Nonwovens	Strength MD (mN/tex)	Strength CD (mN/tex)	Elongation at Break MD (%)	Elongation at Break CD (%)
NS_1	45.4	20.6	168.4	171
NS_2	44.8	23.4	175.0	212.6
NS_3	41.3	13.2	168.3	148.0
NS_4	37.5	20.9	179.3	217.6
NS_5	33.7	21.2	182.7	241.5
NS_6	37.0	16.1	171.4	163.9
NS_7	34.6	21.8	178.7	201.9

Table 4.4 Density and Crystallinity of PP Spunbond Filaments

PP Spunbond Filaments	Density (g/cm^3)	Crystallinity (%)	Crystallinity (%) from DSC
S_1	0.8968	52.04	57.54
S_2	0.8933	47.55	55.36
S_3	0.8947	49.35	55.77
S_4	0.8899	43.14	53.17
S_5	0.8888	42.01	52.60
S_6	0.8957	50.63	54.40
S_7	0.8938	48.19	53.24

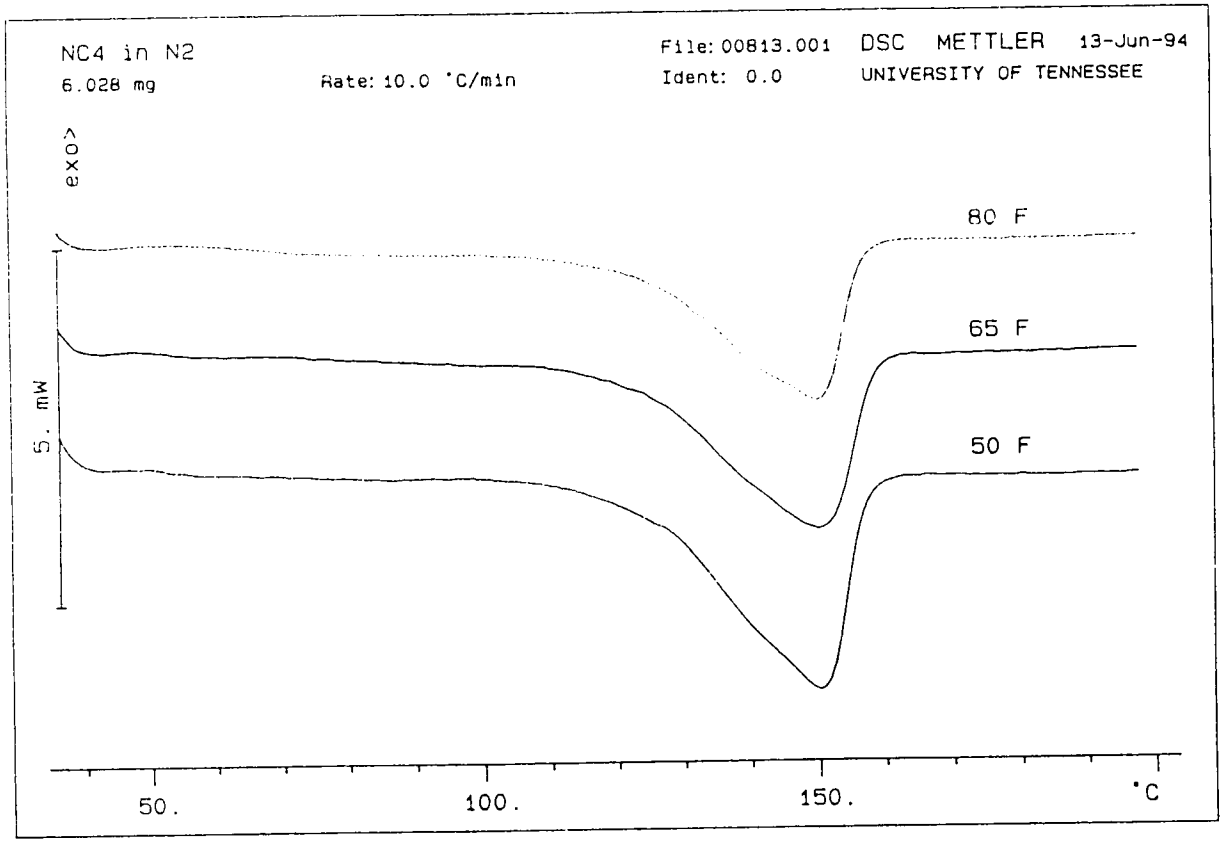

Figure 4.1. DSC Scans for Filament samples Produced at Different Primary Air Temperatures.

samples also showed the same trend as those of the corresponding filaments.

Thermo-mechanical behavior of the filaments and nonwoven samples are shown in Figures 4.2-4.7. Figure 4.2 shows the thermomechanical responses of filaments produced at different cooling air temperatures. The filaments produced at lower primary air temperatures were more stable than those spun at higher quench air temperatures. For the same primary air temperature, the filaments became more stable at higher temperatures with decreasing throughput as shown in Figure 4.3. That indicates that the morphology of the filaments spun at lower throughput was better developed than those produced with higher throughput. Figures 4.4 and 4.5 show the TMA scans of nonwoven samples produced from different primary air temperature and throughput, respectively. The responses are consistent with those of the filament samples. The results indicate that TMA is a useful tool in determining the filament and fabric responses to mechanical forces at elevated temperatures.

Figure 4.6 shows thermo-mechanical responses of unbonded webs with different compression loads. An effort was made to understand how deformation of the filaments took place during the thermal calendering under compression. For a constant compression load, the thickness of the web decreased as the temperature increased between 30 to 60 ^{0}C, the thickness changed notably as the temperature increased. From 60 to 140 ^{0}C the change in the thickness was minimal. After 140 ^{0}C, the thickness of the web changed rapidly until it melted around 165 ^{0}C. The thickness of the web decreased as the applied compression load during the scan increased. However, because of the limitation of the instrument, the load used was much lower that actual pressures used in calerdering.

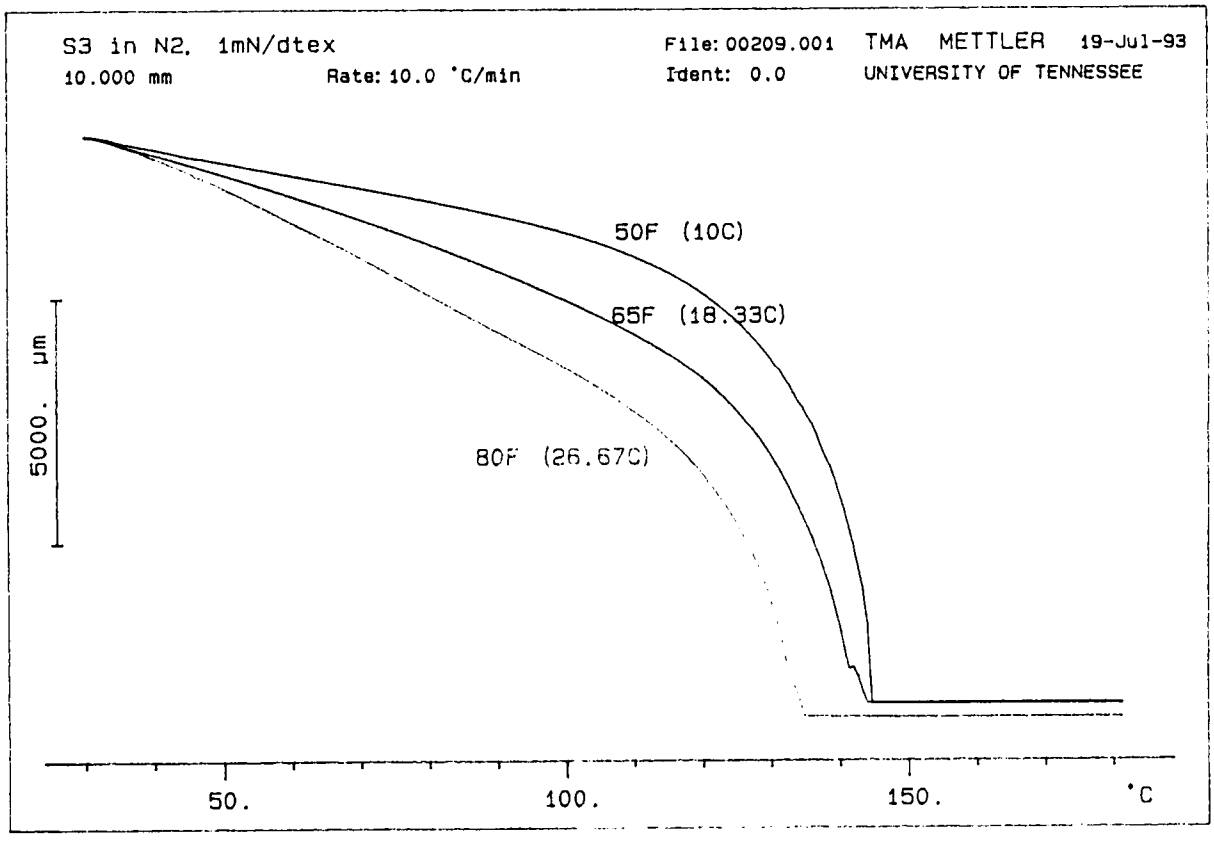

Figure 4.2 TMA Scans for Filament Samples Produced at Different Primary Air Temperatures.

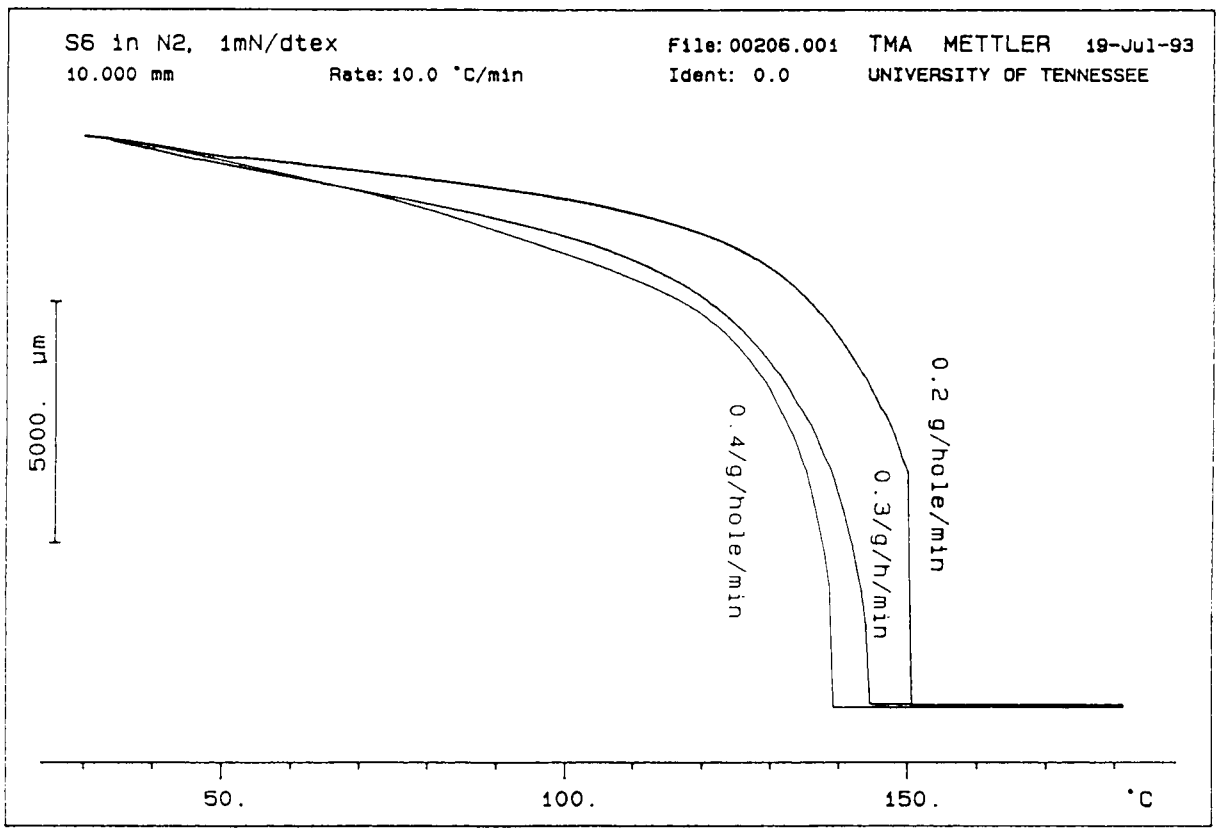

Figure 4.3. TMA Scans for Filament Samples Produced from Different Throughput.

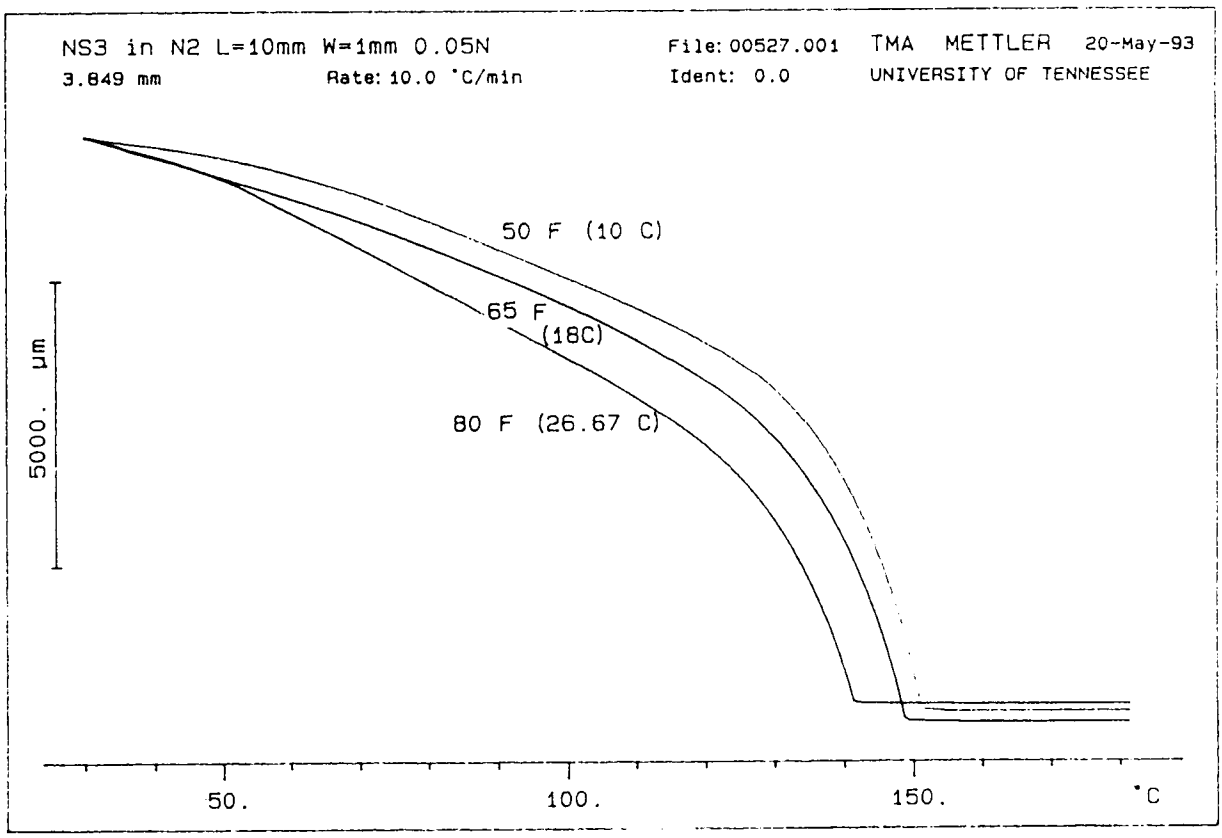

Figure 4.4 TMA Scans for Nonwoven Samples Produced at Different Primary Air Temperature.

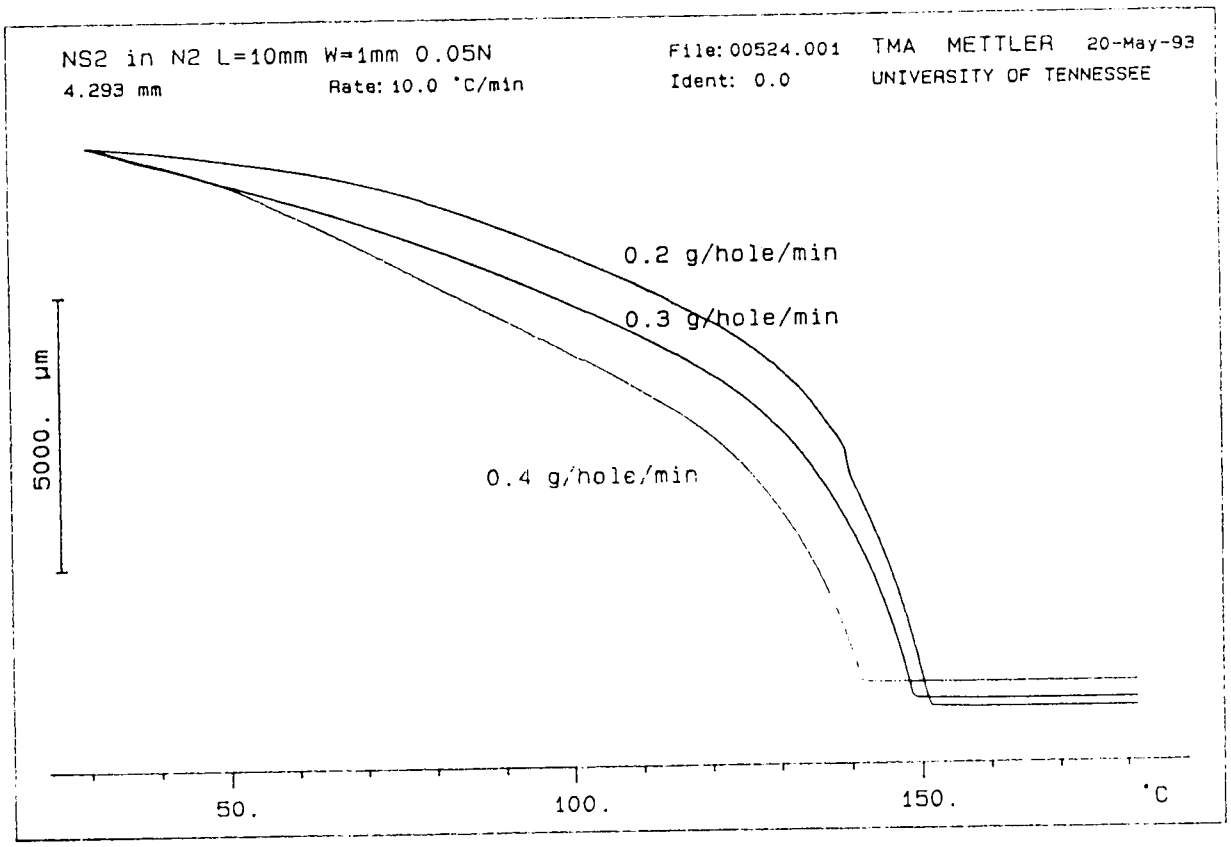

Figure 4.5. TMA Scans for Nonwoven Samples Produced from Different Throughput.

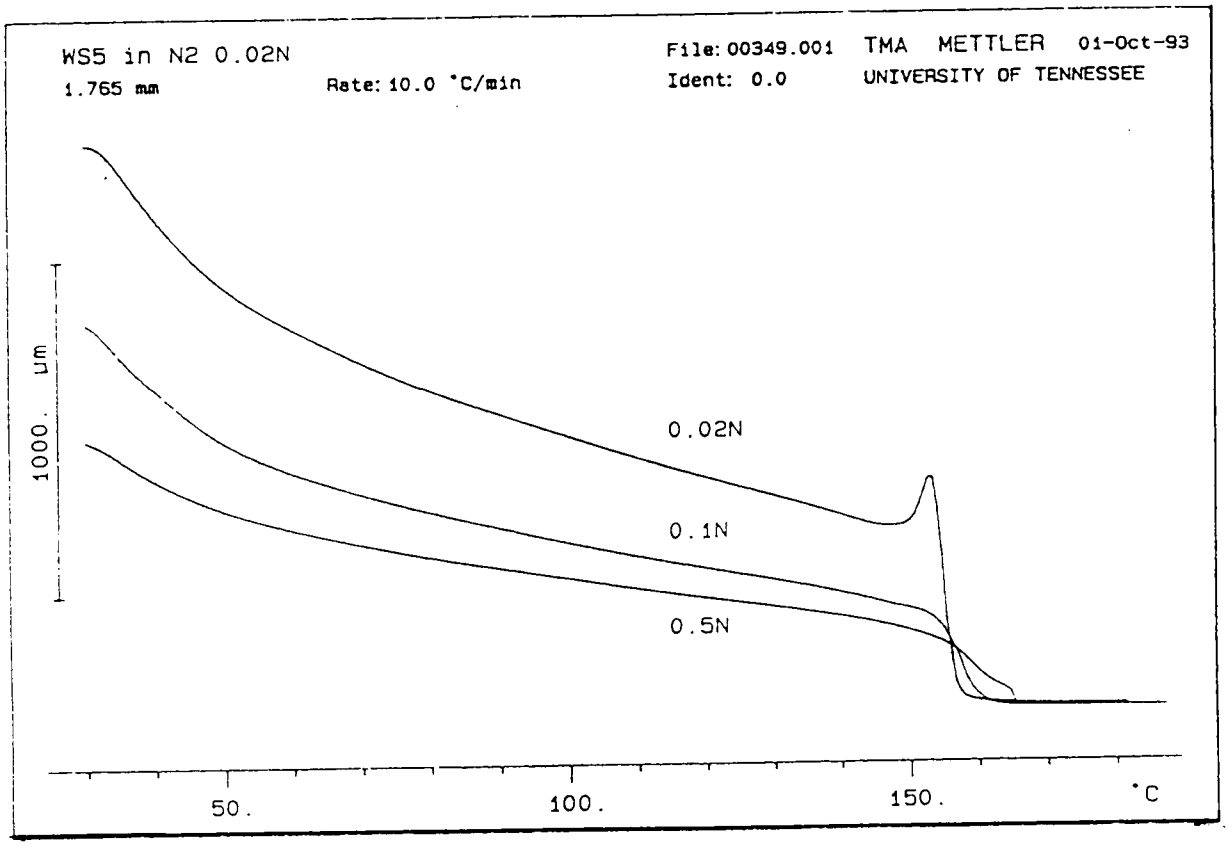

Figure 4.6 TMA Scans for Unbonded Webs with Different Compression Loads.

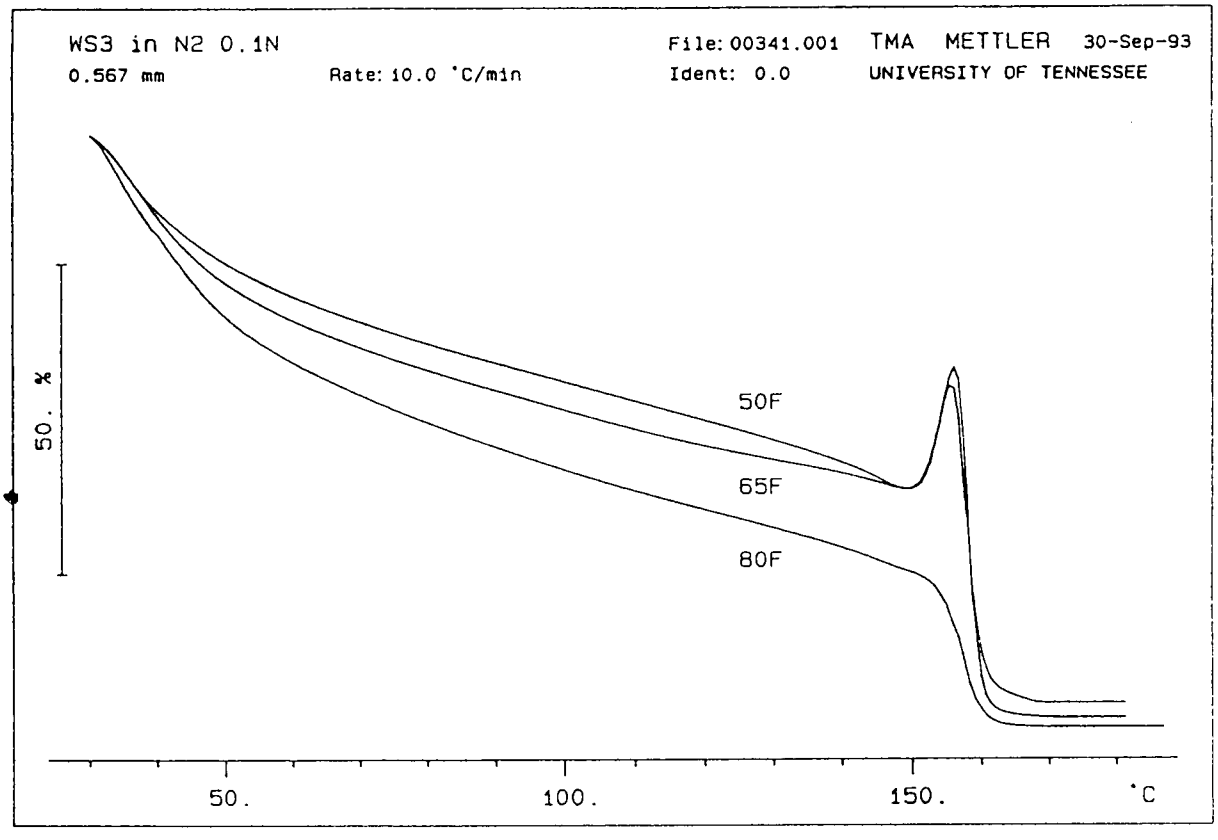

Figure 4.7 TMA Scans for Unbonded Webs Produced at Different Primary Air Temperatures.

Figure 4.7 shows the TMA scans at the same compression load of the unbonded webs produced at different primary air temperatures. For the same temperature, the change in thickness of the web from low primary air temperature was smaller than those with high primary air temperatures. That means the filaments spun from low cooling air temperature were not easily deformed compared to those from high primary air temperature. That is further confirmed from SEM photographs of bonded fabrics, that will be discussed later. In the case of low primary air temperature, the bonded area is smaller than that of high cooling air temperature. That is due to the fact that the filaments from low primary air temperature had high crystallinity and orientation.

Thermal elongation of samples at 140 ^{0}C for two minutes measured at two different tensions is shown in Table 4.5. At both 0.1 g/den and 0.0033 g/den pretension, the thermal elongation increased as the primary air temperature and the throughput increased. The relatively large thermal elongation showed that the filaments produced at lower primary air temperatures have a lot of potential for drawing. Lower the crystallinity and orientation of the samples, thermal elongation was higher. The higher thermal elongation values are expected of these samples due to the low draw down in the fiber formation step.

4.4 Time-dependent Thermal Properties for Filament Samples

Figure 4.8 shows the isothermal TMA scans of filament samples at different temperatures for 60 minutes with a constant tension of 1 mN/dtex. As shown, the creep increased with time and temperature. The maximum extension took place in the first 10 minutes. After that, time-dependent elongation increased as the time increased slowly and

Table 4.5 Thermal Elongation at 140 ^{0}C for 2 min. with Given Tension

PP Spunbond Filaments	Elongation at 0.1 (g/den)	Elongation at 0.033 (g/den)
S_1	17%	7.7%
S_2	23%	15%
S_3	31%	17%
S_4	35.6%	18%
S_5	42.1%	26.5%
S_6	33.2%	9.7%
S_7	54.2%	12.7%

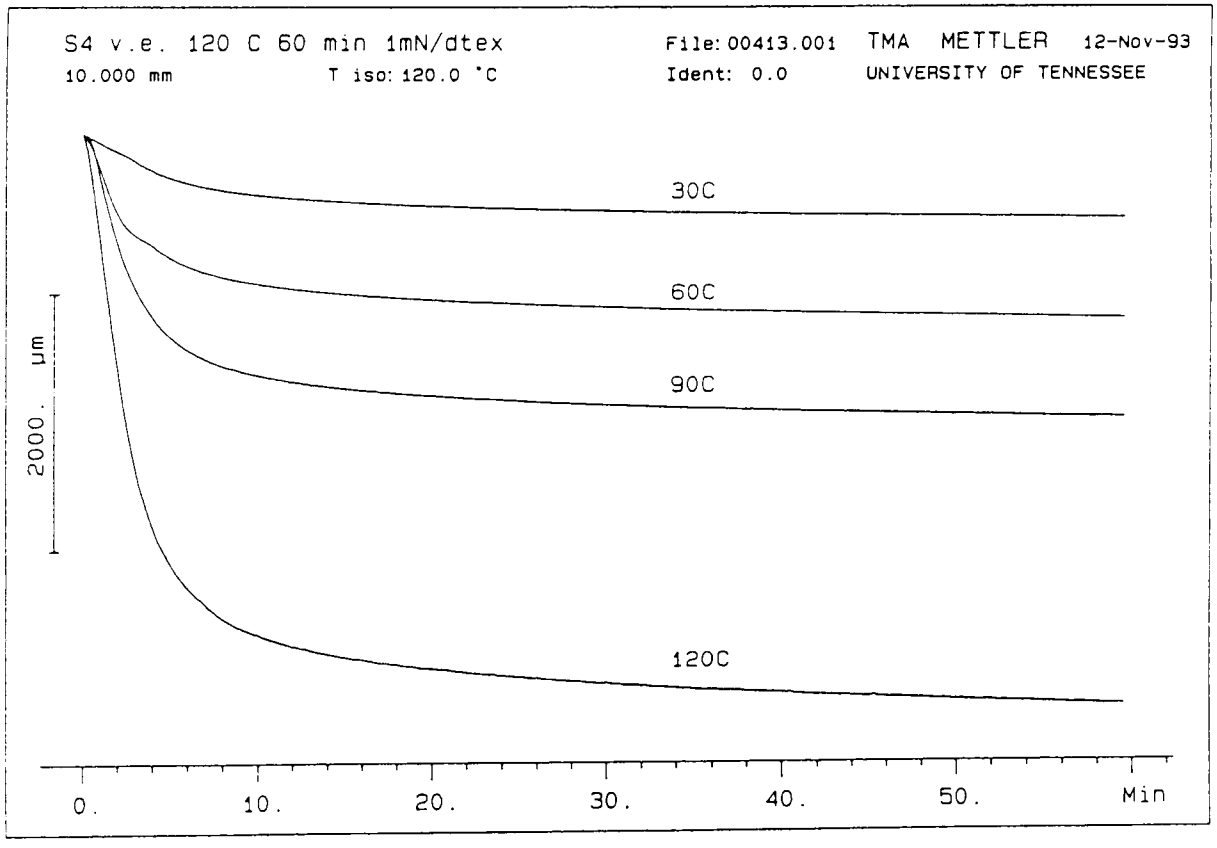

Figure 4.8 TMA Scans of Different Constant Temperatures for Filament Samples.

evenly. Apparently, the creep increased proportionately as the temperature of scan increased from 30 to 90 ^{0}C. However, there is a larger difference in the observed response between 90 and 120 ^{0}C. This suggests that there is a significant effect on mechanical properties at temperatures between 90 to 120 ^{0}C for the PP filaments. Figure 4.9 shows the flow behavior of filament samples at a constant temperature of 30 ^{0}C for 60 minutes, but with tensions of 1, 2, 4, and 5 mN/dtex. At 1 mN/dtex tension, the time dependent elongation changed smoothly and slowly with time. The response was similar for 2 mN/dtex tension. However, when the tensions were 4 and 5 mN/dtex, the time-dependent elongation increased much faster. In about 10 minutes, the time-dependent elongation reached 100% of its original length.

Figure 4.10 shows the TMA scans of filament samples produced at same throughput and different primary air temperature at a constant heating temperature of 30 ^{0}C, and a constant tension of 1 mN/dtex for 60 minutes. Creep of the filament of 50 ^{0}F (10 ^{0}C) quench air is slightly lower. TMA scans of filament samples with same primary air temperature but different throughput, at a constant heating temperature of 30 ^{0}C, and a constant tension of 1 mN/dtex for 60 minutes as shown in Figure 4.11. The creep of the filaments increased as the throughput increased. The observed difference in flow behavior of filaments is due to the difference in structure of these filaments. The smallest creep was observed for the filaments of high birefringence.

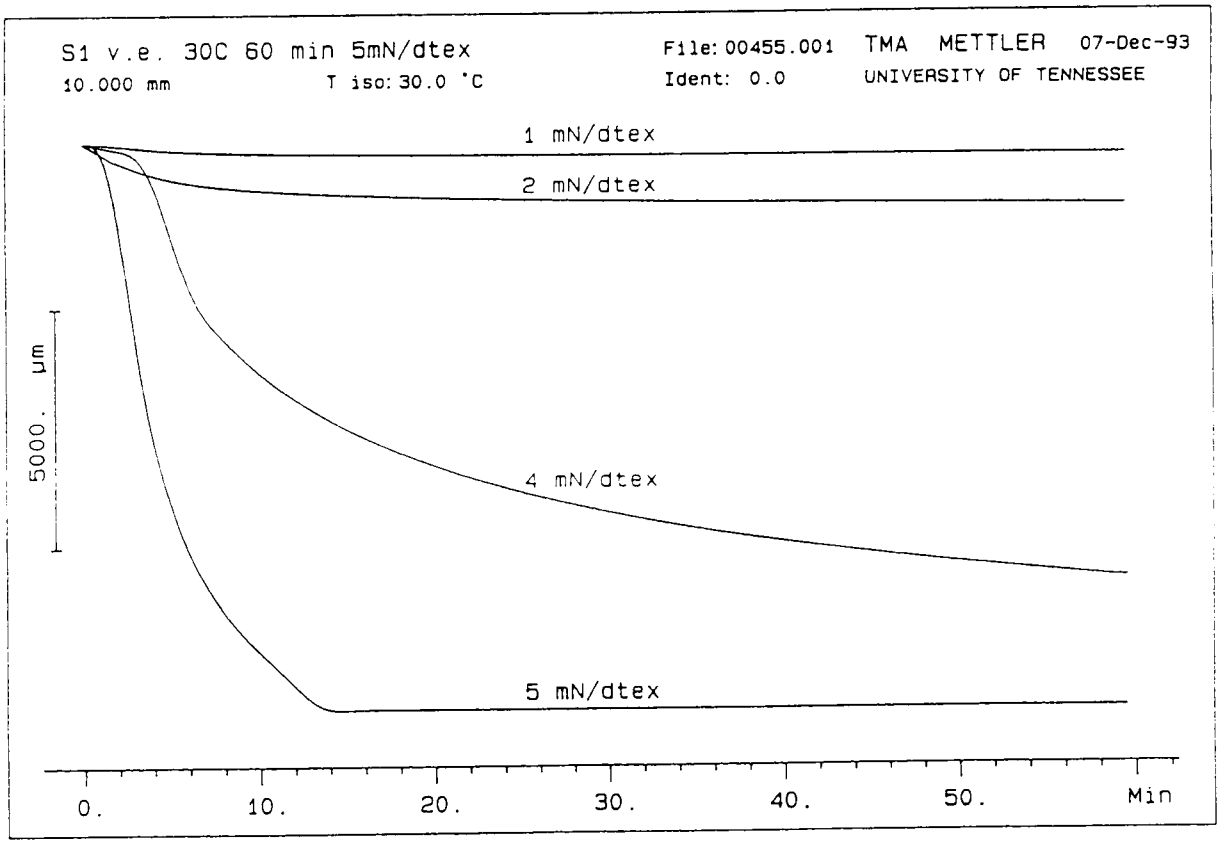

Figure 4.9 TMA Scans of Different Constant Tension for Filament Samples.

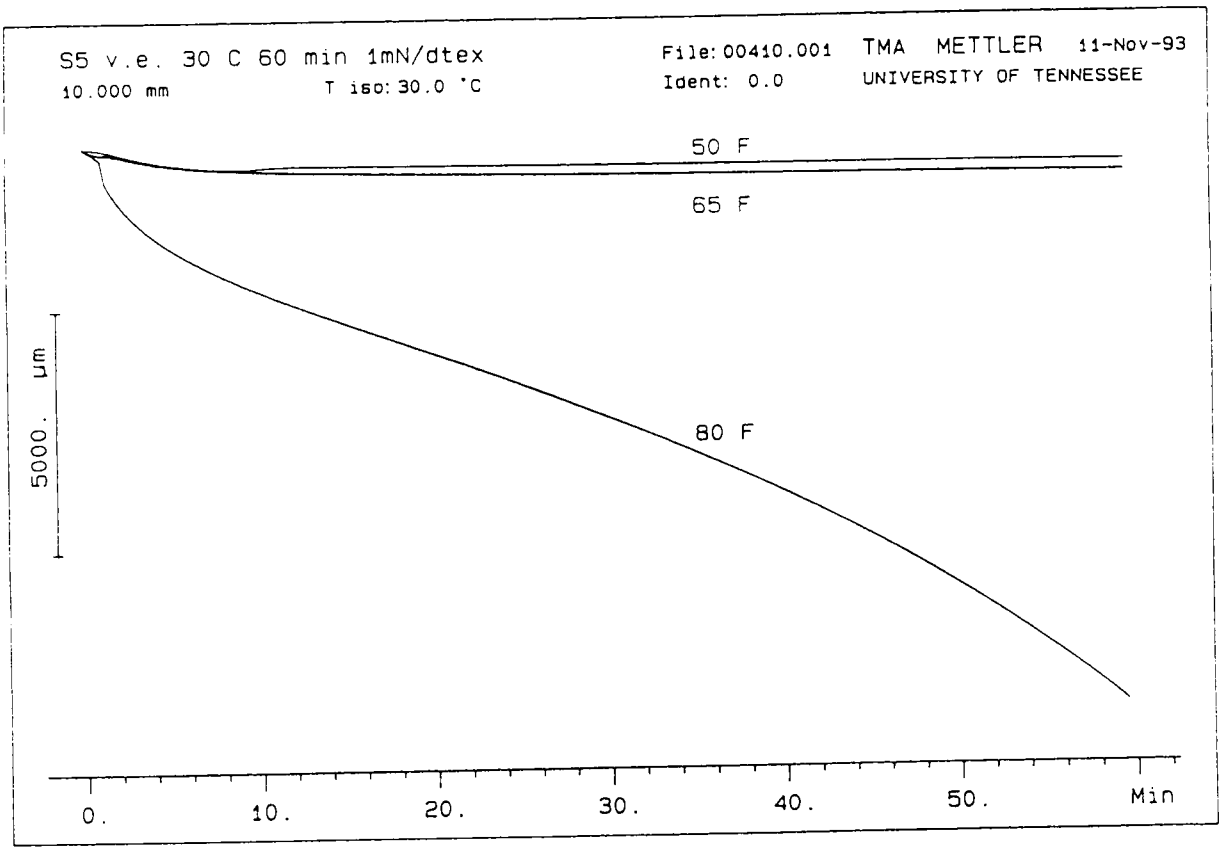

Figure 4.10 TMA Scans for Filament Samples Produced at Different Primary Air Temperature.

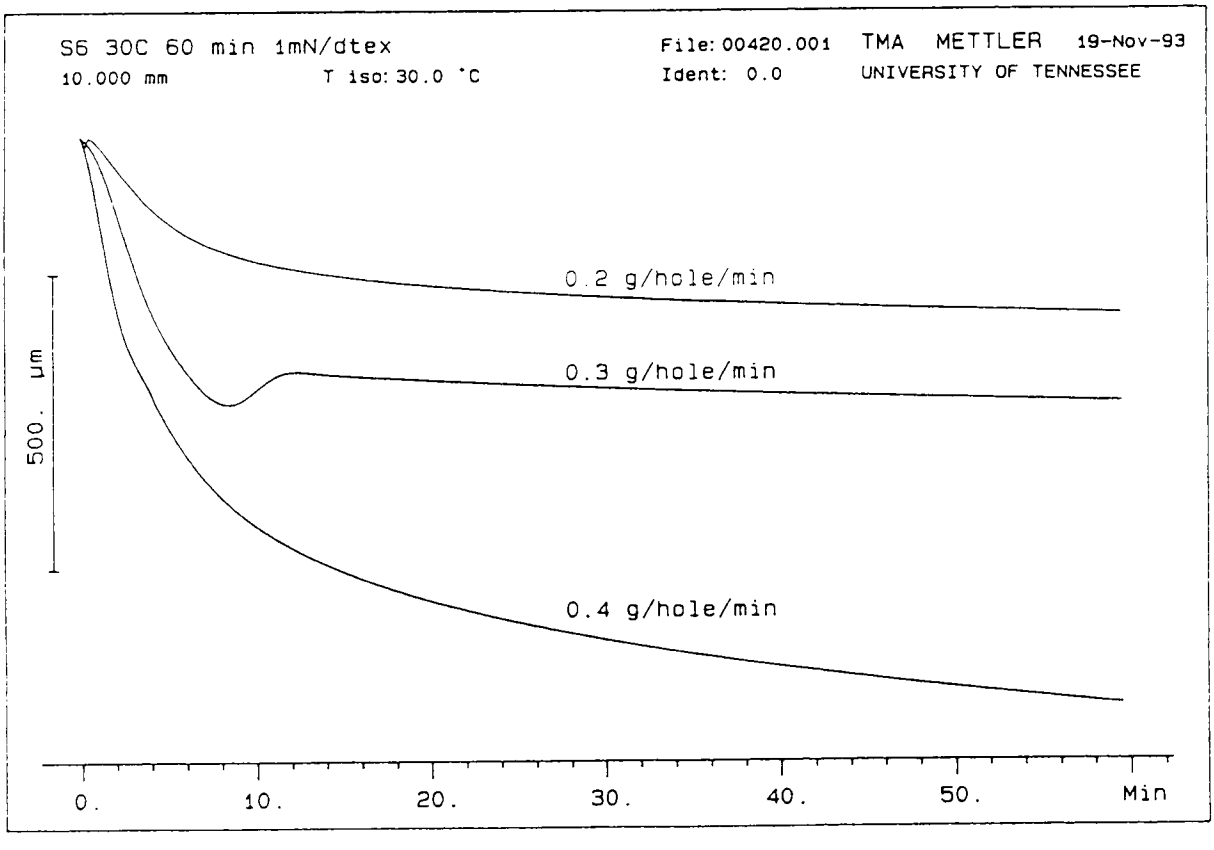

Figure 4.11 TMA Scans for Filament Samples Produced at Different Throughput.

4.5 Properties of Nonwoven Samples

The results of air permeability, MFR, burst strength, and tear strength of the bonded webs are shown in Table 4.6. The air permeability increased as the primary air temperature and throughput increased. Increase in diameter of the filaments with increase in the two parameters leading to lower fabric density after calendering was responsible for observed higher air permeability. The burst strength was consistent with the tensile strength and decreased as the primary air temperature and throughput increased.

The tear strength did not show any consistent trend and the values were almost same for most of the cases, except the high throughput condition, which had slightly higher values. The reason for that is that the tear strength is influenced by the strength of the filament, the fabric density and bonding. The higher tear strength values in CD are due to the greater amount of resistance offered by filaments preferably oriented in the MD.

The MFR of the PP pellets was 35.18. The MFR of nonwoven samples increased as primary air temperature increased. That indicates that more thermal degradation took place for higher primary air temperatures. The thermal degradation continues to take place even after the polymer melt is extruded from die since the melt is exposed to air (oxygen). The higher primary air temperature helps this continued thermal degradation. Table 4.7 shows the stiffness of nonwoven samples in both MD and CD. The stiffness increased as the primary air temperature decreased. The stiffness in MD was higher than in the CD.

Table 4.6 Air Permeability, MFR, Bursting and Tear Strength of Spunbond Nonwovens*

PP Spunbond Nonwovens	Melt Flow Rate (g/min)**	Air Permeability ($mm^3/mm^2/sec$)	Burst Strength (g/mm^2)	Tear Strength MD (Kg)	Tear Strength CD (Kg)
NS_1	36.750	462.18	12.21	11.86	15.08
NS_2	44.899	464.16	12.14	11.32	14.09
NS_3	40.853	520.70	10.53	11.03	13.84
NS_4	44.372	525.12	10.11	11.75	13.82
NS_5	48.47	553.65	9.34	11.71	13.42
NS_6	42.538	527.76	9.49	13.32	14.40
NS_7	48.930	553.11	9.45	13.30	13.82

* INDA STANDARD TEST.

** The MFR for PP pellets is 35.178 (g/min).

Table 4.7 Stiffness of PP Spunbond Nonwovens*

PP Spunbond Nonwovens	Bending Length (cm)		Flexural Rigidity (mg*cm)	
	MD	CD	MD	CD
NS_1	4.49	2.535	18.38	10.38
NS_2	4.04	2.465	16.49	10.06
NS_3	4.215	2.525	17.14	10.27
NS_4	4.085	2.38	16.928	9.86
NS_5	3.805	2.29	15.17	9.16
NS_6	3.86	2.33	15.47	9.34
NS_7	3.715	2.215	15.22	9.07

* ASTM D1388-64

4.6 Crystal Structure Analysis by X-ray Diffraction

X-ray diffraction photos of filament samples of different processing conditions are shown in Figure 4.12. The crystallinity and crystalline orientation increased as the primary air temperature decreased. This can be seen from the intense rings and shorter arcs in the diffraction patterns compared with the faint rings and larger arc for the samples for higher cooling air temperature. Figure 4.12(a) is the diffraction pattern of 50 ^{0}F (10 ^{0}C) and shows the pattern resulting from high orientation of crystals and high crystallinity. Figure 4.12(b) is the diffraction pattern of 65 ^{0}F (18.33 ^{0}C) quench air and shows the rings of medium intensity resulting from intermediate orientation of crystals and crystallinity. Figure 4.12(c) is the diffraction pattern of 80 ^{0}F (26.67 ^{0}C) and shows the rings of low intensity resulting from low orientation of crystals and low crystallinity.

4.7 Effect of Annealing on Properties and Structure of Filament Samples

The changes in diameter and birefringence of the filament samples after free length annealing at 140 ^{0}C for 2 minutes are shown in Table 4.8. After annealing, the diameter of all the filament samples slightly decreased from 0.68% to 2.1%. The filaments from spunbond line are not completely drawn due to insufficient draw-force. Some molecules in amorphous region may attach to already existing oriented crystals during annealing, resulting in small draw. During unconstrained annealing, the high birefringence filaments produced with lower primary air temperature showed a decrease in birefringence. On the other hand, the filaments from higher quench air temperature with low birefringence showed a tendency for increase in birefringence.

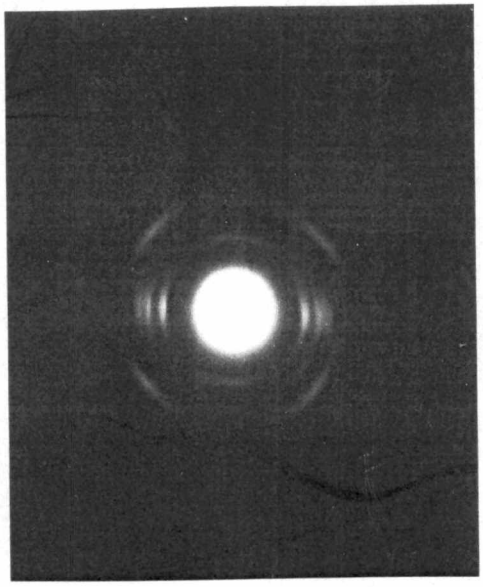

(a)

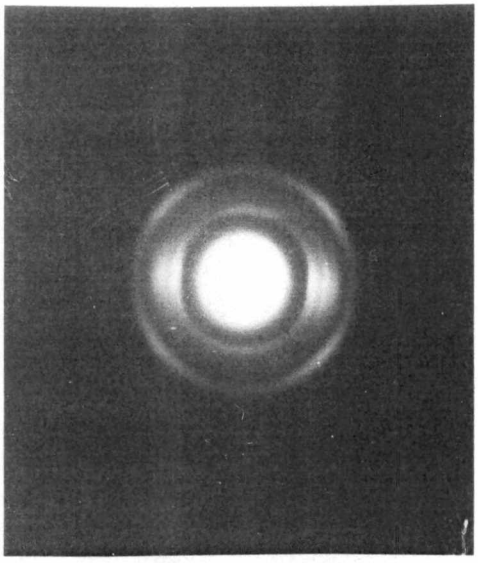

(b)

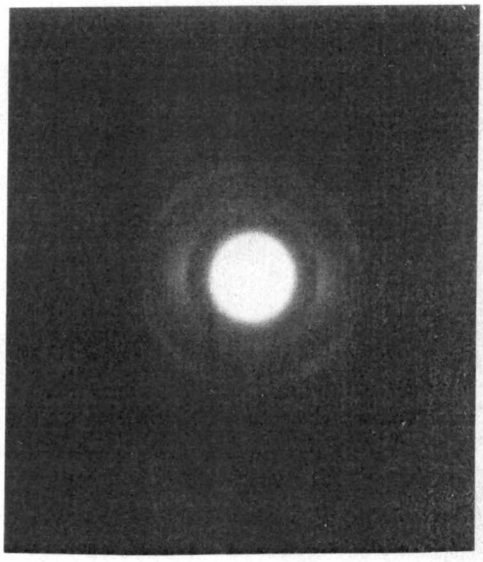

(c)

Figure 4.12. X-ray Diffraction Pattern for Filament Samples produced from Different Cooling Air Temperatures (a) 50 ^{0}F (10 ^{0}C), (b) 65 ^{0}F (18.33 ^{0}C), (c) 80 ^{0}F (26.67 ^{0}C).

Table 4.8 Diameter and Birefringence Change of PP Spunbond Filaments after Free Length Annealing at 140 °C for 2 min.

PP Spunbond Filament	Change* of Diameter (%)	Change** of Birefringence (%)
S_1	-2.26	-19.06
S_2	-1.44	+3.67
S_3	-1.78	-14.11
S_4	-1.20	+14.84
S_5	-2.10	+12.90
S_6	-1.42	-20.29
S_7	-0.68	+22.59

* "-" is decrease; ** "+" is increase.

Table 4.9 shows the changes in tensile properties of filament samples after free length annealing at 140 ^{0}C for 2 minutes. Tensile strength of filaments with high birefringence decreased, while strength of other samples increased. Breaking elongation of the filament samples except S1 (the filament with highest birefringence) decreased after annealing. The initial modulus increased for most filament samples. The reason for change in tensile properties is that the structure of the filaments changed significantly after annealing (As discussed above).

In the case of fixed length annealing (Table 4.10), the diameter of all the filament samples decreased from 3.8% to 7.46%, and the birefringence increased from 4.12% to 58.2%. The increase in birefringence was higher for samples with low orientation. During annealing, as the molecules in the amorphous, less-oriented region tend to recrystallize, the molecules reorient along the fiber axis, which can be proved from the x-ray diffraction patterns of the annealed filaments (Figure 4.13). From Figure 4.13, it can be seen that both the crystal orientation and crystallinity increased after the fixed length annealing.

Table 4.11 shows the changes in tensile properties of filaments after fixed length annealing at 140 ^{0}C for 2 minutes. The tensile strength decreased for most cases, while breaking elongation decreased for all the filament samples except the filament with the highest birefringence. Change in initial modulus was small for most of the samples.

Tables 4.12 and 4.13 show the results of diameter and birefringence changes of filament samples after free length annealing at 140 ^{0}C for 5 seconds and 30 seconds. The results from exposure to 5 second are almost same as those from annealing for 30 seconds, (same as the 2 minute situation shown in Table 4.9).

Table 4.9 Change of Tensile Properties of PP Spunbond Filaments after Free Length Annealing at 140 ^{0}C for 2 min.

PP Spunbond Filament	Change* of Strength (%)	Change* of Break Elongation (%)	Change* of Initial Modulus
S_1	-14.34	+54.18	+13.11
S_2	-58.63	-6.58	+3.87
S_3	-34.49	-8.20	-13.55
S_4	+25.23	-11.36	+18.60
S_5	+17.20	-5.10	+12.80
S_6	-48.52	-12.85	+1.78
S_7	+23.15	-27.81	-20.99

Table 4.10 Diameter and Birefringence Change of PP Spunbond Filaments after Fixed Length Annealing at 140 °C for 2 min.

PP Spunbond Filament	Change* of Diameter (%)	Change** of Birefringence (%)
S_1	-7.46	+18.83
S_2	-6.89	+39.80
S_3	-6.42	+23.72
S_4	-6.63	+56.24
S_5	-5.40	+58.20
S_6	-3.80	+4.12
S_7	-4.18	+24.43

* "-" is decrease; ** "+" is increase.

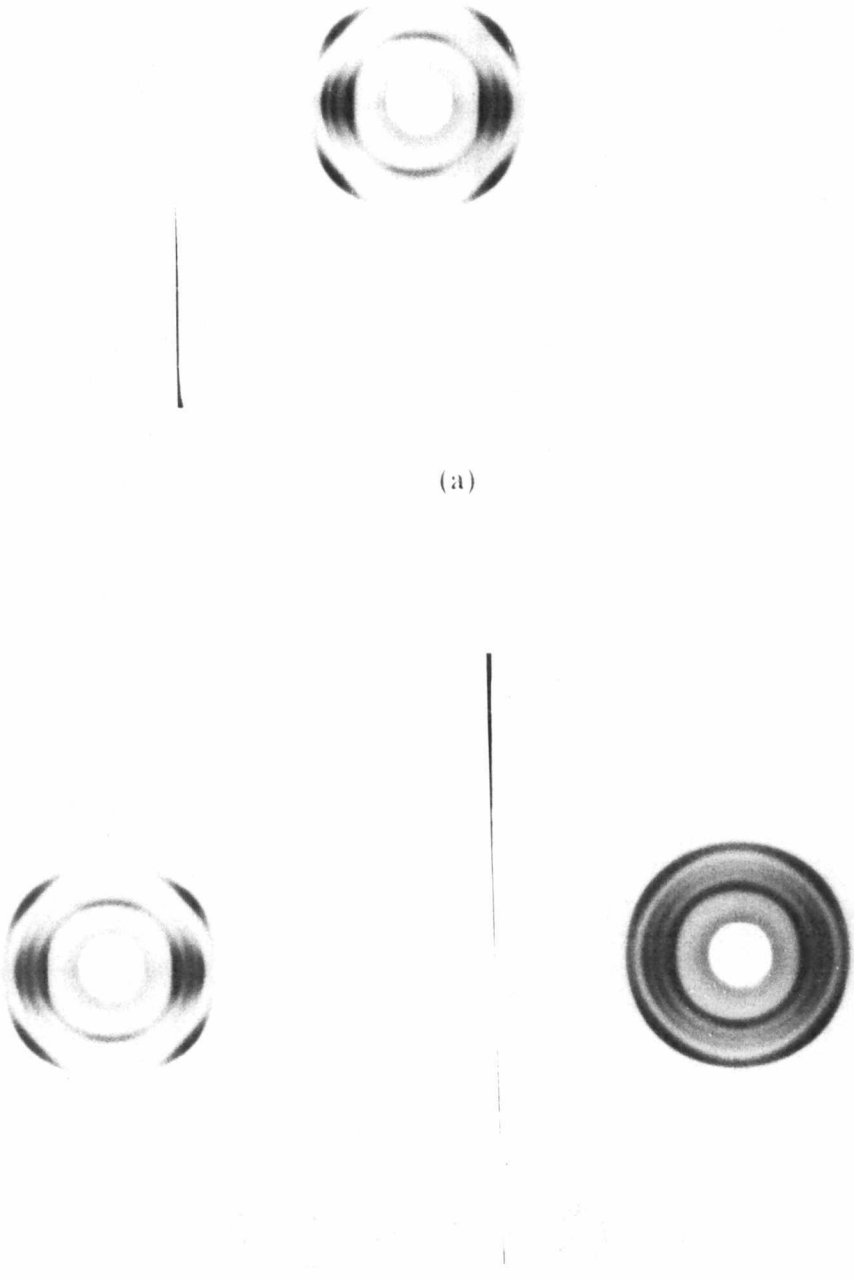

(a)

(b)

(c)

Figure 4.13. Effect of Annealing on X-ray Diffraction Pattern for Filament Samples produced from Different Cooling Air Temperatures (a) 50 ^{0}F (10 ^{0}C), (b) 65 ^{0}F (18.33 ^{0}C), (c) 80 ^{0}F (26.67 ^{0}C).

Table 4.11 Change of Tensile Properties of PP Spunbond Filaments after Fixed Length Annealing at 140 °C for 2 min.

PP Spunbond Filament	Change* of Strength (%)	Change* of Break Elongation (%)	Change* of Initial Modulus
S_1	-58.91	+28.11	-8.07
S_2	-3.42	-30.51	-17.48
S_3	-17.48	-12.86	+26.20
S_4	+13.88	-21.59	+2.45
S_5	-14.10	-22.40	-2.80
S_6	-47.67	-23.30	+24.01
S_7	+1.32	-29.80	+11.21

* "-" is decrease;
** "+" is increase.

Table 4.12 Diameter and Birefringence Change of PP Spunbond Filaments after Free Length Annealing at 140 °C for 5 sec.

PP Spunbond Filament	Change* of Diameter (%)	Change** of Birefringence (%)
S_1	-6.95	+9.18
S_2	-6.39	+16.70
S_3	-6.80	+10.56
S_4	-8.80	+13.73
S_5	-5.51	+18.25
S_6	-5.77	+11.60
S_7	-5.96	+7.39

* "-" is decrease; ** "+" is increase.

Table 4.13 Diameter and Birefringence Change of PP Spunbond Filaments after Free Length Annealing at 140 °C for 30 sec.

PP Spunbond Filament	Change* of Diameter (%)	Change** of Birefringence (%)
S_1	-5.95	+10.64
S_2	-1.38	+9.53
S_3	-4.38	+5.44
S_4	-7.50	+13.88
S_5	-5.61	+21.50
S_6	-6.67	+12.92
S_7	-5.25	+8.69

* "-" is decrease; ** "+" is increase.

4.8 Morphology of Nonwoven Samples By Scanning Electron Microscopy

Figure 4.14 shows the SEM photographs of nonwoven samples at 0.3 g/hole/min of throughput for different primary air temperatures. Figure 4.14(a) is the fabric from filaments quenched by air at 50 ^{0}F (10 ^{0}C) which shows small and well defined bonding area. Because the filaments had high orientation and crystallinity, they are not easily deformed. Figure 4.14(b) and (c) are for quench air temperatures of 65 and 80 ^{0}F (18.33 and 26.67 ^{0}C), respectively. In both the cases, the filaments were relatively easily deformable and the bonding area increased compared to samples from low primary air temperatures. The bond patterns showed a similar trend for samples with 0.2 and 0.4 g/hole/min throughputs.

4.9 Statistical Analysis of the Processing Variables

4.9.1 Statistical Analysis from Structure.

Birefringence was selected for statistical analysis. The reason for using Type IV in GLM was the presence of empty cells in the data set. From the analysis (Appendix A), it is concluded that the effect of primary air temperature and throughput are significant, based on the type IV P-value of 0.0001 for both temperature and throughput (Appendix A page 5). The interaction between temperature and throughput is also significant (P-value=0.0007).

From the plots of temperature and throughput vs birefringence, it is evident that as the temperature increased, the birefringence decreased, and that the orientation of the molecules of crystalline and noncrystalline region was low. Also, as the throughput increased, the birefringence decreased. To determine whether the decrease is significant or

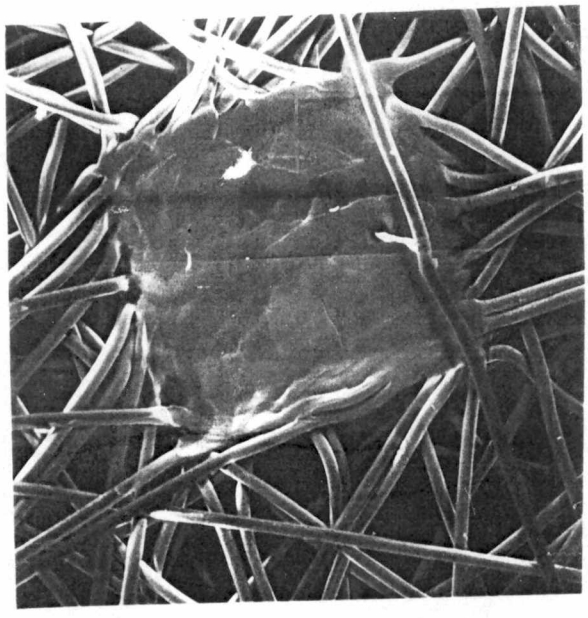

(a)

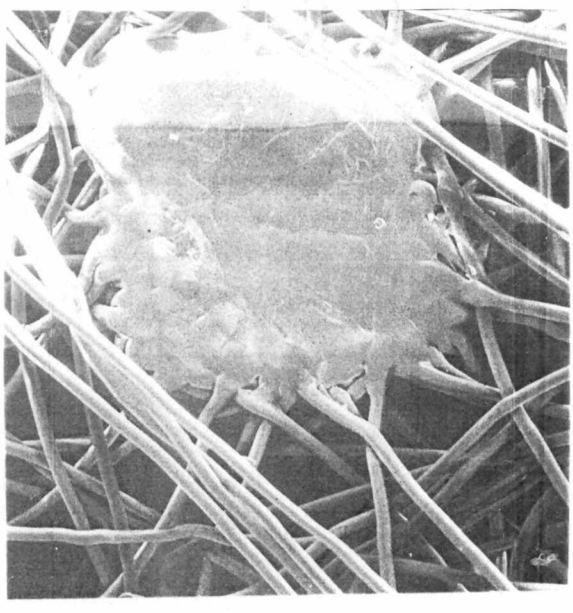

(b)

(c)

Figure 4.14 SEM Photographs for Nonwoven Samples produced from Different Cooling Air Temperatures (a) 50 ^{0}F (10 ^{0}C), (b) 65 ^{0}F (18.33 ^{0}C), (c) 80 ^{0}F (26.67 ^{0}C).

not, four contrasts were performed to estimate the significance. The difference in birefringence was contrasted when temperatures of 50 ^{0}F (10 ^{0}C) or 65 ^{0}F (18.33 ^{0}C) were used. From the p-value of 0.0001 (Appendix A page 16) it can be concluded that the difference between 50 ^{0}F (10 ^{0}C) and 65 ^{0}F (18.33 ^{0}C) is significant. The second contrast was to determine the significance of the difference in birefringence when a throughput of 0.2 or 0.3 g/hole/min was used. The p-value of 0.0001 (Appendix A page 16) shows that the difference is significant.

In order to make orthogonal contrasts, the third contrast was to estimate the significance of the difference between throughputs 0.2, 0.3, and 0.4 g/hole/min. The results show the difference is significant (P-value 0.0001, Appendix A page 16). The last contrast was to determine the significance of the difference in birefringence when temperatures of 50 ^{0}F (10 ^{0}C), 65 ^{0}F (18.33 ^{0}C) and 80 ^{0}F (26.67 ^{0}C) were used with throughput 0.3/g/hole/min. The low p-value of 0.0001 (Appendix A page 16) shows that the difference is significant. The slope between 65 ^{0}F (18.33 ^{0}C) and 80 ^{0}F (26.67 ^{0}C) is higher than that between 50 ^{0}F (10 ^{0}C) and 65 ^{0}F (18.33 ^{0}C), showing the same results as the previous contrast.

The highest mean value of birefringence of 0.0244 (Appendix A page 7) was for filaments cooled at 50 ^{0}F (10 ^{0}C) combined with a throughput of 0.2 g/hole/min. The lowest birefringence of 0.0191(Appendix A page 7) was for fibers cooled at 80 ^{0}F (26.67 ^{0}C) when a throughput of 0.3 g/hole/min was used. We demonstrated that low primary air temperature and low throughput will result in highly oriented fibers. Of the variables tested, the best combination for nonwoven fabric production is a cooling air temperature of 50 ^{0}F (26.67

^{0}C) and a throughput of 0.2 g/hole/min.

4.9.2 Statistical Analysis from Tensile Properties.

Tensile Strength and Breaking Elongation were selected for statistical analysis. The effect of cooling air temperature and throughput are significant, based on the type IV P-value of 0.0001 for strength and 0.0008 for breaking elongation (Appendices B and C page 5), for temperature, and a P-value for throughput of 0.0001 for both the cases. The interaction between temperature and throughput is also significant with a P-value=0.0001 from strength and 0.0027 from breaking elongation.

From the plots of temperature and throughput vs strength and breaking elongation, it was found that as the primary air temperature increased, the strength decreased, while the breaking elongation increased. Also, as the throughput increased, strength decreased and breaking elongation increased. To determine whether the changes are significant or not, four contrasts were performed to estimate the significance. The difference in strength and breaking elongation was contrasted when temperatures of 50 ^{0}F (10 ^{0}C) or 65 ^{0}F (18.33 ^{0}C) were used. From the p-value of 0.0001 from strength and 0.0024 from breaking elongation (Appendices B and C page 11) it can be concluded that the difference between 50 ^{0}F (10 ^{0}C) and 65 ^{0}F (18.33 ^{0}C) is significant. The second contrast was to determine the significance of the difference in tensile properties when a throughput of 0.2 g/hole/min or 0.3 g/hole/min was used. The p-value of 0.0001 from strength and 0.0044 from breaking elongation (Appendices B and C page 11) show that the difference is significant. In order to make orthogonal contrasts, the third contrast was to estimate the significance of the difference

between 0.2 g/hole/min, 0.3 g/hole/min, and 0.4 g/hole/min. The results show the difference is also significant (P-value 0.0001 from strength and 0.0086 from breaking elongation, Appendices B and C page 11) which means that this difference between each of the three throughputs is real. The last contrast was to determine the significance of the difference in tensile properties when temperatures of 50 °F (10 °C), 65 °F (18.33 °C) and 80 °F (26.67 °C) were used with 0.3 g/hole/min throughput. The low p-value of 0.0001 from elongation (Appendices B and C page 11) also shows that the difference for breaking elongation is significant. However, the large p-value of 0.5396 from strength shows the difference for strength is not significant. This is due to the interaction effect between primary air temperature and throughput.

The highest mean value of strength was 424.316 and the lowest breaking elongation was 180.6 (Appendices B and C page 7) for filaments cooled at 50 ^{0}F (10 ^{0}C) and at a throughput of 0.2 g/hole/min. The lowest strength was 87.5 mN/tex and highest elongation was 294.3 (Appendices B and C page 7) for fibers cooled at 80 ^{0}F (26.67 ^{0}C) when a throughput of 0.3 g/hole/min was used. The results indicated that low primary air temperature and low throughput will produce fibers with better mechanical properties, which in turn produced a nonwoven with better mechanical properties. Of the variables tested, the best combination for nonwoven fabric production was a cooling temperature of 50 ^{0}F (10 ^{0}C) and a throughput of 0.2 g/hole/min.

4.10 The effect of Filament Structure and Properties on Nonwovens

Since the nonwovens consist of filaments, the morphology and the properties of the filaments should influence the properties of the nonwovens as the filaments undergo the calendering process. Figure 4.15 shows the crystallinity of filament and nonwoven samples. For the samples of same throughput, the crystallinity of both filament and nonwoven samples increased as the primary air temperature decreased. For the samples produced with the same cooling air temperature, the crystallinity of filament and nonwoven samples increased as the throughput decreased. Therefore, the structure of filaments and the corresponding nonwovens show the same trend with processing conditions.

Figure 4.16 shows the relationship between the nonwoven properties and filament diameter. As the diameter decreased, tensile strength of nonwoven samples increased and breaking elongation decreased. This is due to the fact that fine diameter filaments have well developed morphology and properties, compared to larger diameter filaments. The effect of filament structure can be seen from Figure 4.17, which shows the relationship between the properties of nonwoven samples and filament birefringence. The tensile strength of nonwoven samples increased as the birefringence of filaments increased, while the breaking elongation decreased, except S_2, which had lower birefringence than that of S_3, but had a higher strength. That is due to the interaction of the primary air temperature and throughput as mentioned earlier.

The relationship of tensile strength of filament and nonwoven samples is shown in Figure 4.18 . The nonwoven samples with better tensile strength are those that consist of the filaments with better tenacity. However, the difference in tensile strength between the

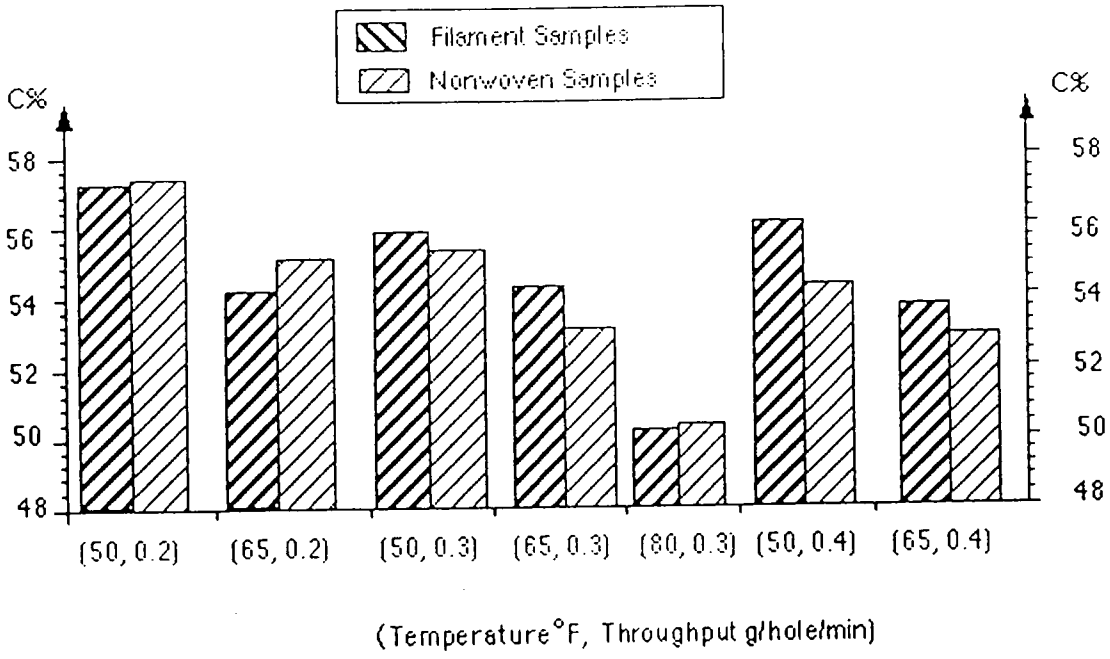

Figure 4.15 Relationship of Crystallinity Between Filament and Nonwoven Samples.

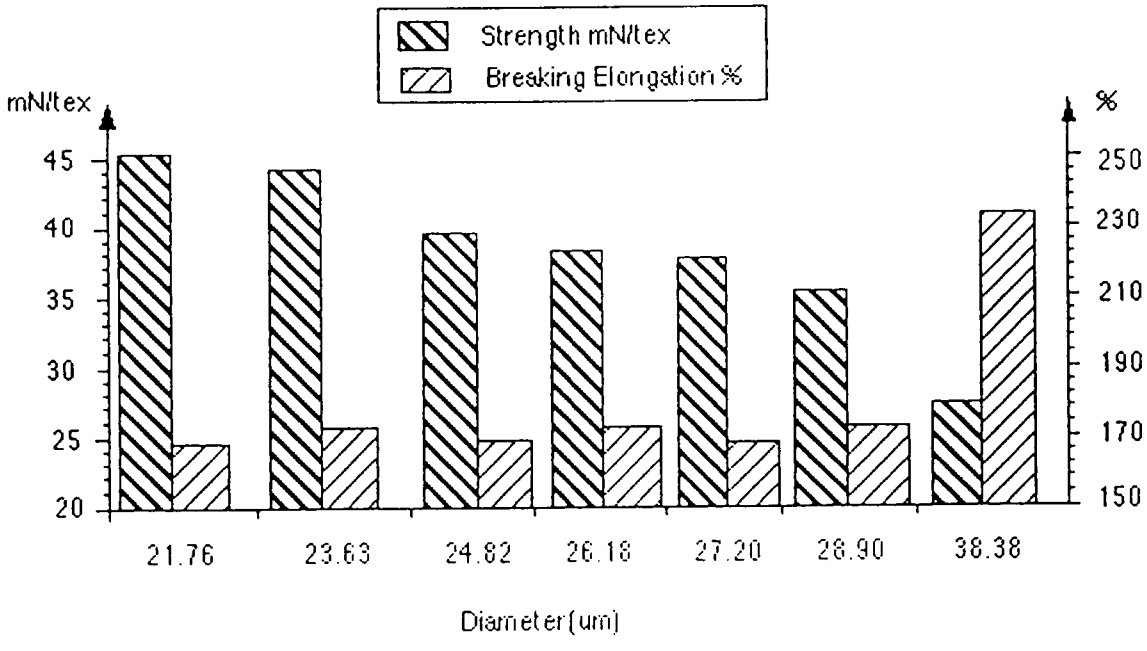

Figure 4.16 Relationship Between Nonwoven Properties and Filament Diameter.

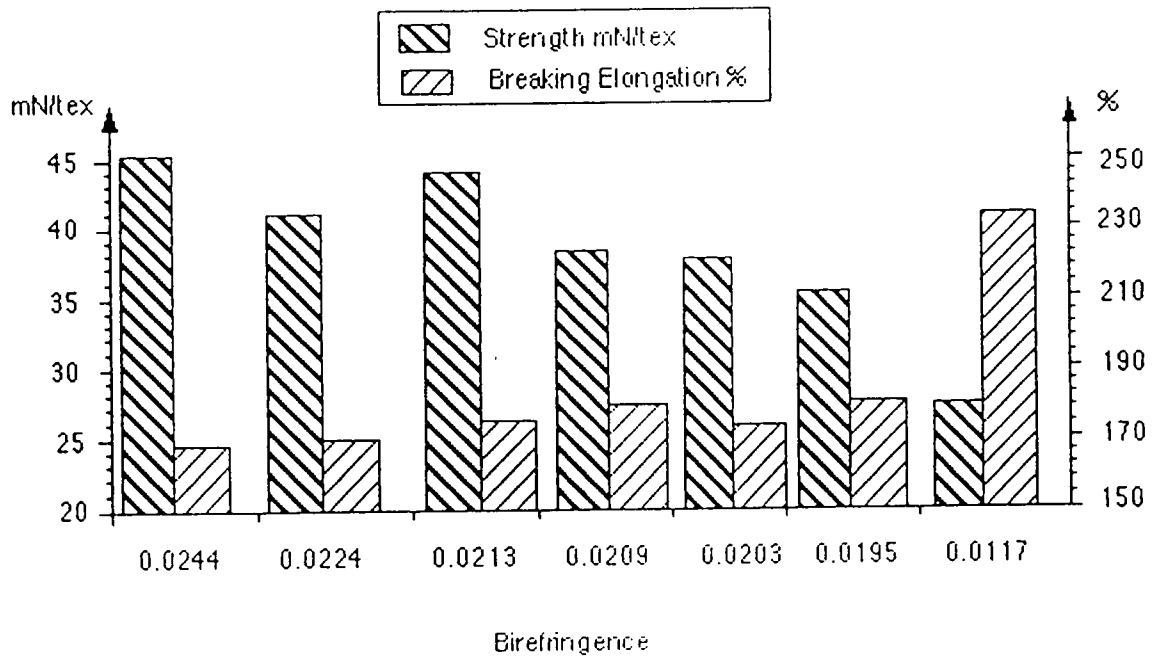

Figure 4.17 Relationship Between Nonwoven Properties and Filament Birefringence.

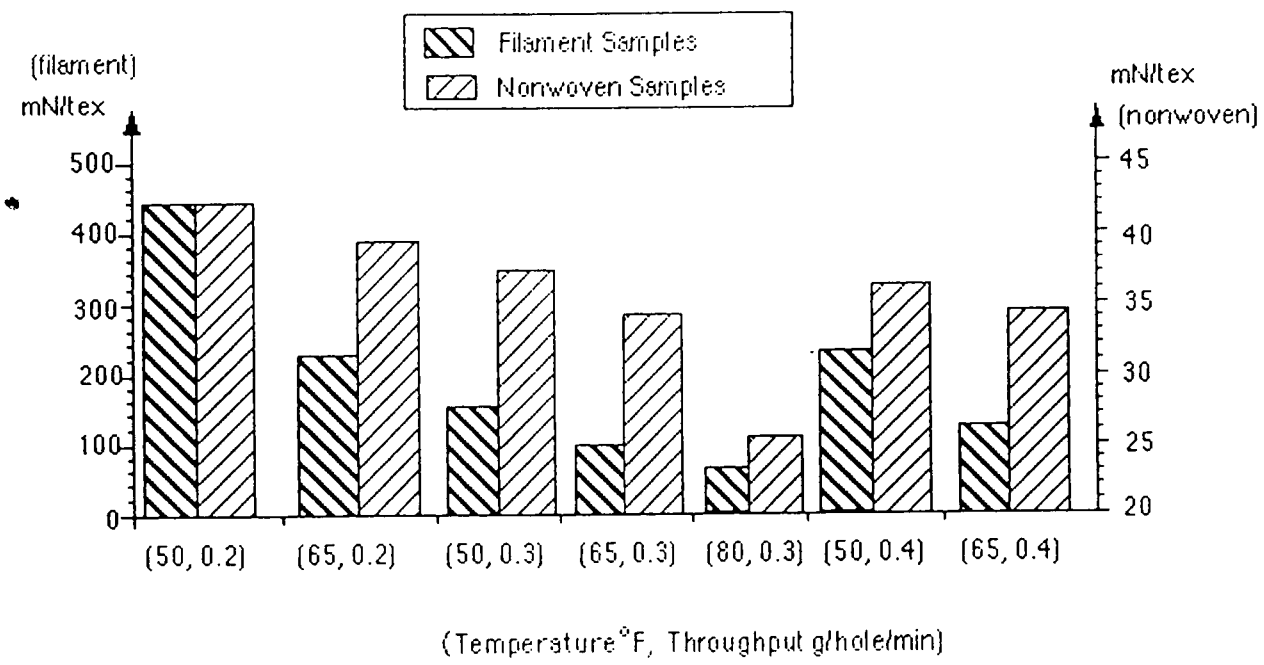

Figure 4.18. Relationship of Tensile Strength Between Filament and Nonwoven Samples.

nonwoven samples is smaller than that of filament samples. That is due to the compensating effect of thermal calendering. As discussed earlier, annealing showed greater improvement for filaments with poor structure and properties. Also bonding characteristics were different for these webs, and the properties of bonded fabrics depend on the bonds as well as properties of filaments in the fabrics in the unbonded regions.

The relationship of breaking elongation between the filament and nonwoven samples is shown in Figure 4.19. The higher the filament breaking elongation, the higher the elongation of the nonwoven samples. The trends were similar to those observed with tensile strength and TMA analysis for both filament and nonwoven samples. As shown in Figure 4.15 to Figure 4.19, at elevated temperatures, the filaments from higher quench air temperatures deformed easily, so did the nonwovens from higher quench air temperature. Also SEM photographs show a good relationship with TMA results as easily deformable filaments show high level of deformation in the nonwovens. The bonding area of nonwovens from higher quench air temperature clearly shows this effect.

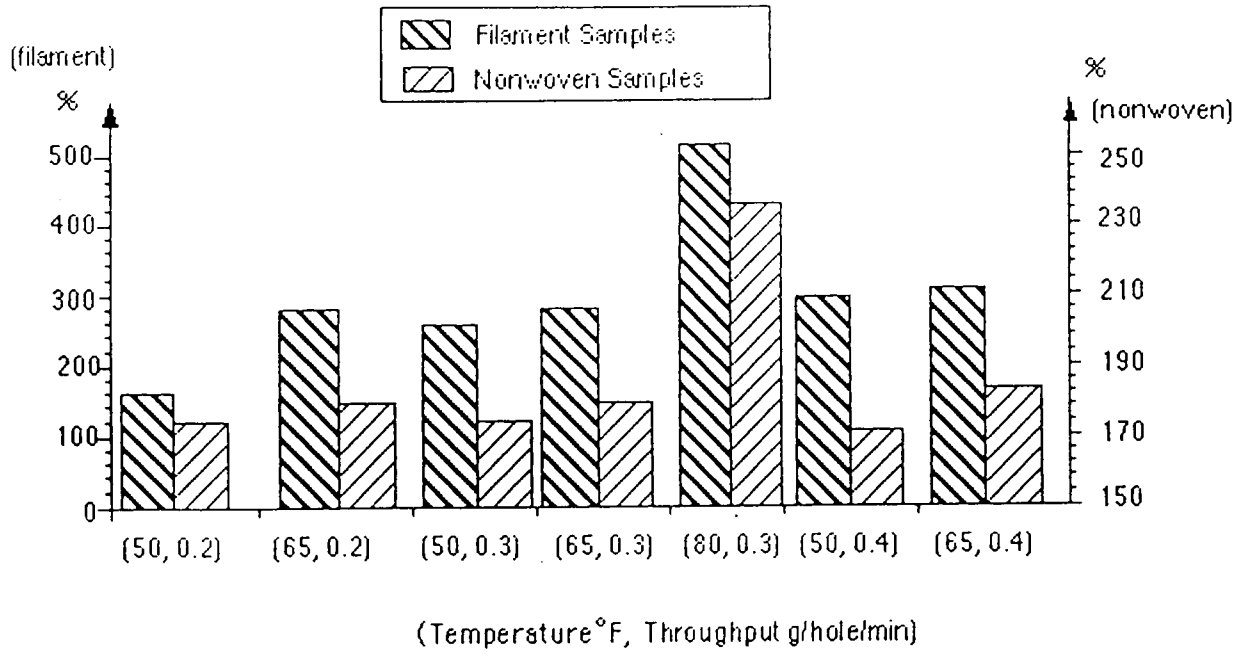

Figure 4.19 Relationship of Breaking Elongation Between Filament and Nonwoven Samples.

CHAPTER V

RESULTS AND DISCUSSIONS WITH PP+PE COPOLYMER SAMPLES

5.1 Effect of Processing Variables on Fiber Diameter and Birefringence

Polypropylene copolymer filaments were produced at different throughput and primary air temperatures and collected before thermal bonding and thoroughly characterized. The fiber diameter increased as the throughput and primary air temperature increased as shown in Table 5.1, which showed the same trends as seen with the homopolymer PP . This may be due to the same reason that the low temperature is helpful in generating higher spinline stress, which leads to reduction in fiber diameter. Other important fact or discussed earlier is stress relaxation. The birefringence of the fibers decreased as the throughput and primary air temperature increased as in the case of homopolymer. Therefore, as the cooling air temperature increased the orientation of the fiber decreased. This trend is related to changes in diameter of the fiber, as at the same throughput, lower primary air temperature results in smaller diameter of the fiber. This means the fiber is drawn more by cooler air than that by the higher temperature air. The low primary air temperature also helps in increasing the orientation of the fibers. This observation is confirmed by other characterizations as well. The linear density of the filament was calculated and is shown in Table 5.1. The difference in observed trend of fiber diameter with cooling air temperature from the previous research and the ones predicted from the model has been explained in the previous chapter. This research has clearly shown that the fiber diameters before and after

Table 5.1 Sample Specification and Physical Properties of Filaments from PP+PE Copolymer

Sample	Throughput (g/hole/min)	Cooling Air Temperature ^{0}F (^{0}C)	Diameter (um)	Birefringence	Linear Density (Denier)
C_1	0.2	50 (10 ^{0}C)	23.78	0.02077	3.59
C_2	0.2	65 (18.33 ^{0}C)	24.52	0.01810	3.82
C_3	0.3	50 (10 ^{0}C)	25.07	0.01852	3.96
C_4	0.3	65 (18.33 ^{0}C)	26.10	0.01657	4.00
C_5	0.3	80 (26.67 ^{0}C)	27.53	0.01363	4.82
C_6	0.4	50 (10 ^{0}C)	27.77	0.02031	4.90
C_7	0.4	65 (18.33 ^{0}C)	28.15	0.01611	5.04

bonding are not the same. The change in fiber diameter during calendaring is dependent on the morphology of the filaments. This change is responsible for the observed reverse trend for fiber diameter with quench air temperature by other researchers [36].

5.2 Tensile Properties of Filament and Nonwoven Samples

Tensile properties of the formed filaments are shown in Table 5.2, which show the same trends as seen with the homopolymer. The strength-at-break decreased with increase in the cooling air temperature. The elongation-at-break increased as the cooling air temperature and throughput increased. That further proved that the orientation of the molecules in filaments was higher for low primary air temperature than that for high primary air temperature.

Tensile properties of nonwoven samples are shown in Table 5.3. Since the thermal bonding conditions were same for all the samples, the differences between the tensile properties of the samples reflect the differences in spinning conditions. The tensile strength decreased as the primary air temperature and throughput increased. For the same reason, the elongation-at-break increased as the two process parameters increased. The strength-at-break of samples in the machine direction is apparently higher than that in the cross-direction. The elongation-at-break for MD is smaller than that for CD for the same samples. This suggests that the orientation of filaments in the webs is not random and is preferential along the machine direction.

The tensile strength and initial modulus of copolymer filaments are lower than those of the homopolymer filaments. The elongation of copolymer filaments was higher than that

Table 5.2 Tensile Properties of PP+PE Spunbond Filaments

PP+PE Spunbond Filament	Break (mN/tex)	Elongation at Break (%)	Initial Modulus (mN/dtex)
C_1	200.12	422.78	51.859
C_2	182.73	540.36	40.580
C_3	151.0	385.53	32.565
C_4	100.99	495.15	18.539
C_5	83.65	595.23	15.050
C_6	90.86	446.16	31.926
C_7	55.37	534.15	26.187

Table 5.3 Tensile Properties of Related Spunbonded Nonwovens

PP+PE Spunbond Nonwovens	Strength MD (mN/tex)	Strength CD (mN/tex)	Elongation at Break MD (%)	Elongation at Break CD (%)
NC_1	32.1	21.7	102.0	136.9
NC_2	31.0	19.6	109.9	152.3
NC_3	27.2	19.9	106.1	150.8
NC_4	26.3	15.3	130.0	161.9
NC_5	25.7	14.0	146.5	166.4
NC_6	25.9	17.7	105.7	150.5
NC_7	22.2	16.5	119.3	173.6

of homopolymer filaments as shown in Figure 5.1. This is due to the fact that the PE molecules in polypropylene reduce the crystallinity and molecular orientation of the filaments.

5.3 Thermal Properties

Figure 5.2 shows the DSC scans of filament samples produced at the same throughput and different cooling air temperatures. The melting peaks show some differences, especially in their heat of melting although melting temperatures show no difference. DSC studies did not show any difference in melting point for the filaments or nonwoven samples, but the melting enthalpy increased as primary air temperature decreased. That means the low primary air temperature results in better fine structure of copolymer filaments. The values of the crystallinity (Table 5.4) of both filament and nonwovens decreased as cooling air temperature increased. The crystallinity decreased with increasing throughput. The results indicate that low primary air temperature is helpful for crystallization of copolymer filaments. These results are consistent with that from density as shown in Table 5.5. Figure 5.3 shows the difference of DSC scan between PP homopolymer and the copolymer. As shown, the melting temperature and enthalpy of melting for the copolymer are lower than those of the homopolymer. That is the reason that the bonding temperature and processing temperature of the copolymer can be lower than that of the homopolymer. The lower enthalpy for the copolymer is an indication of lower crystallinity. Thermo-mechanical behavior of the filaments and nonwoven samples are shown in Figures 5.4-5.7. Figure 5.4 shows the thermomechanical responses of the filaments

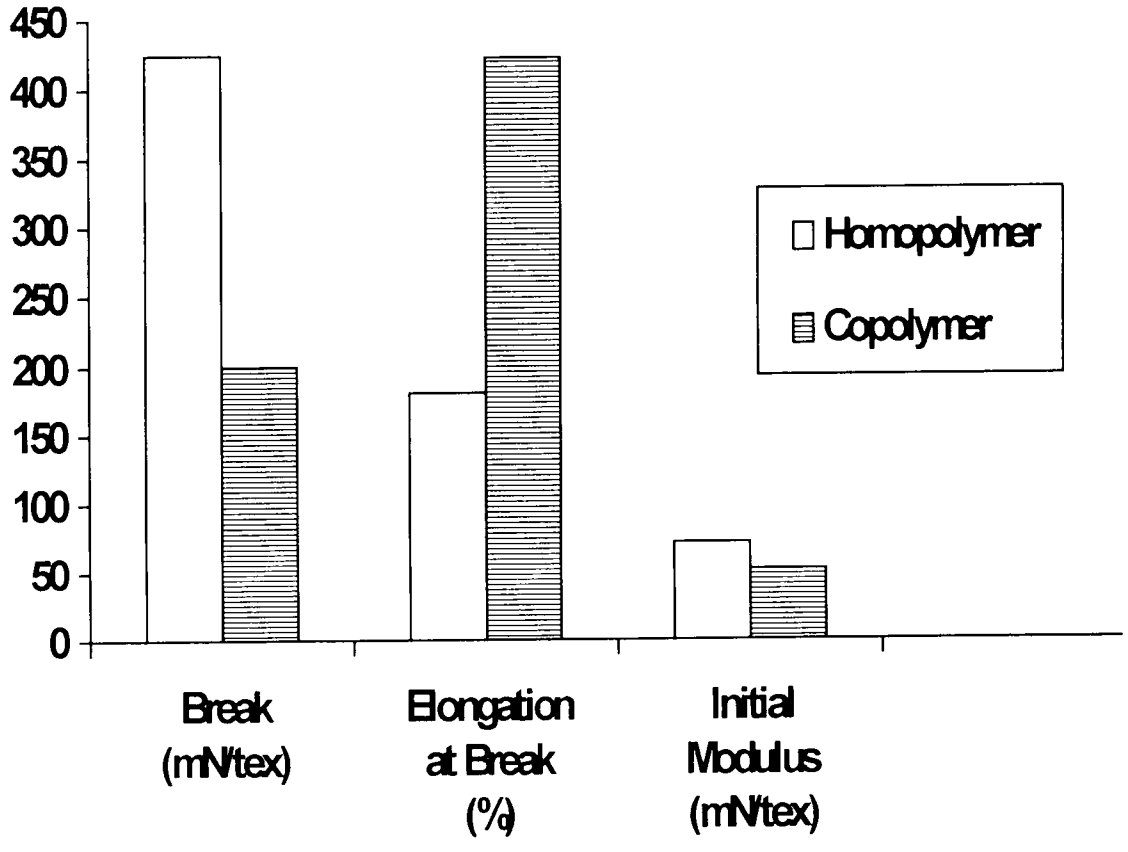

Figure 5.1. Comparison of Tensile Properties for As-spun Filaments

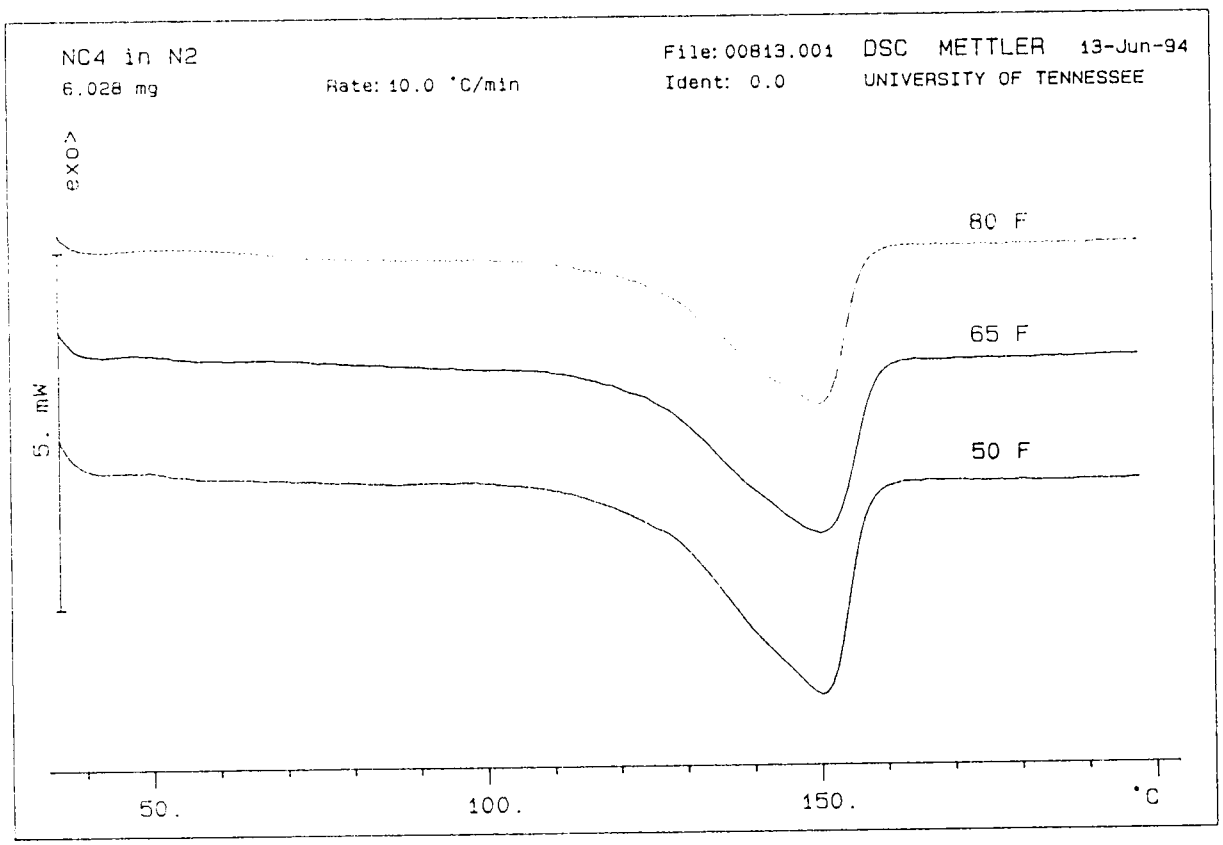

Figure 5.2 DSC Scans for Filament samples Produced at Different Primary Air Temperatures.

Table 5.4. Crystallinity from DSC for PP+PE Spunbonded Filaments and Nonwovens

Sample	Crystallinity (%)	Crystallinity (%)
C_1	44.44	42.52
C_2	43.89	39.52
C_3	44.23	40.22
C_4	43.62	39.80
C_5	43.07	39.66
C_6	43.34	40.27
C_7	41.71	39.52

Table 5.5 Density and Crystallinity of PP+PE Spunbond Filaments

PP+PE Spunbond Filaments	Density (g/cm^3)*	Crystallinity (%)**
C_1	0.8887	41.45%
C_2	0.8879	40.41%
C_3	0.8886	41.32%
C_4	0.8876	40.18%
C_5	0.8872	39.49%
C_6	0.8885	41.19%
C_7	0.8875	39.89%

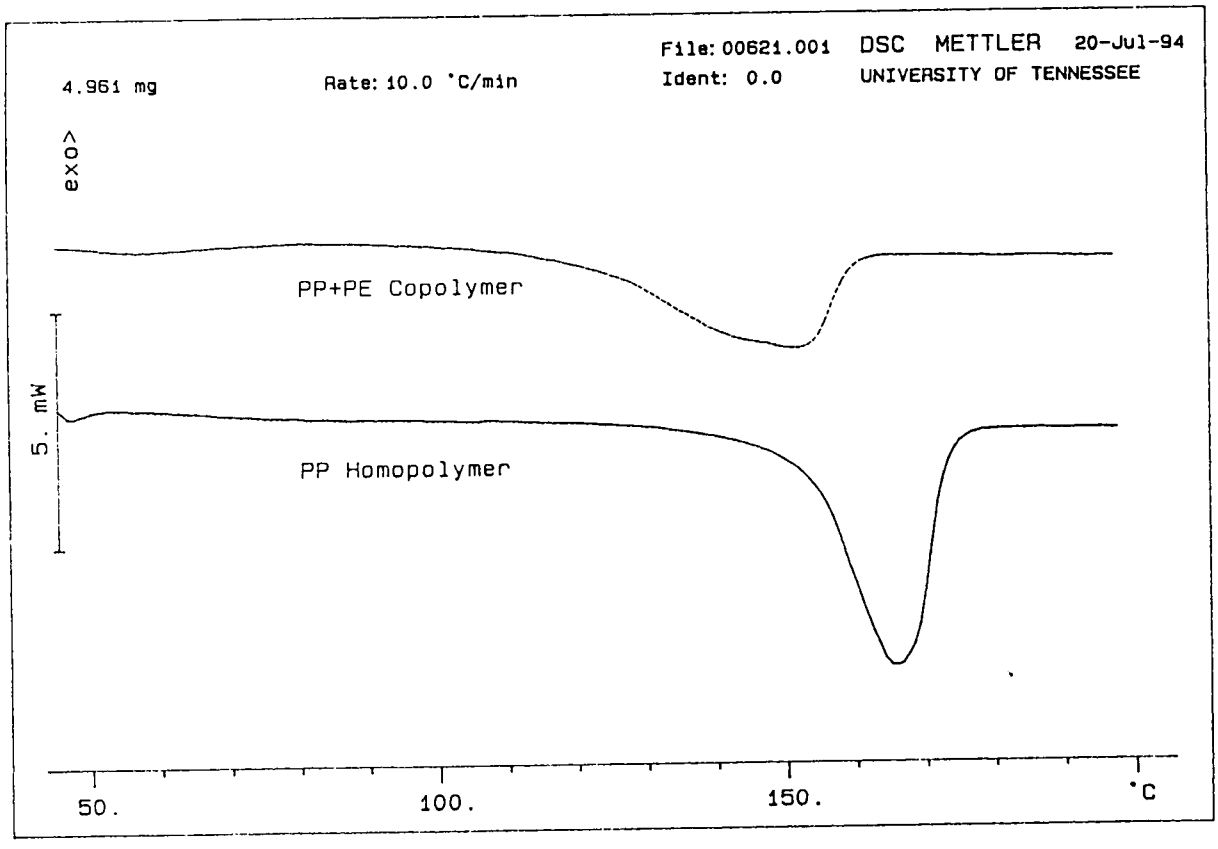

Figure 5.3 DSC Scan for PP Homopolymer and PP+PE Copolymer.

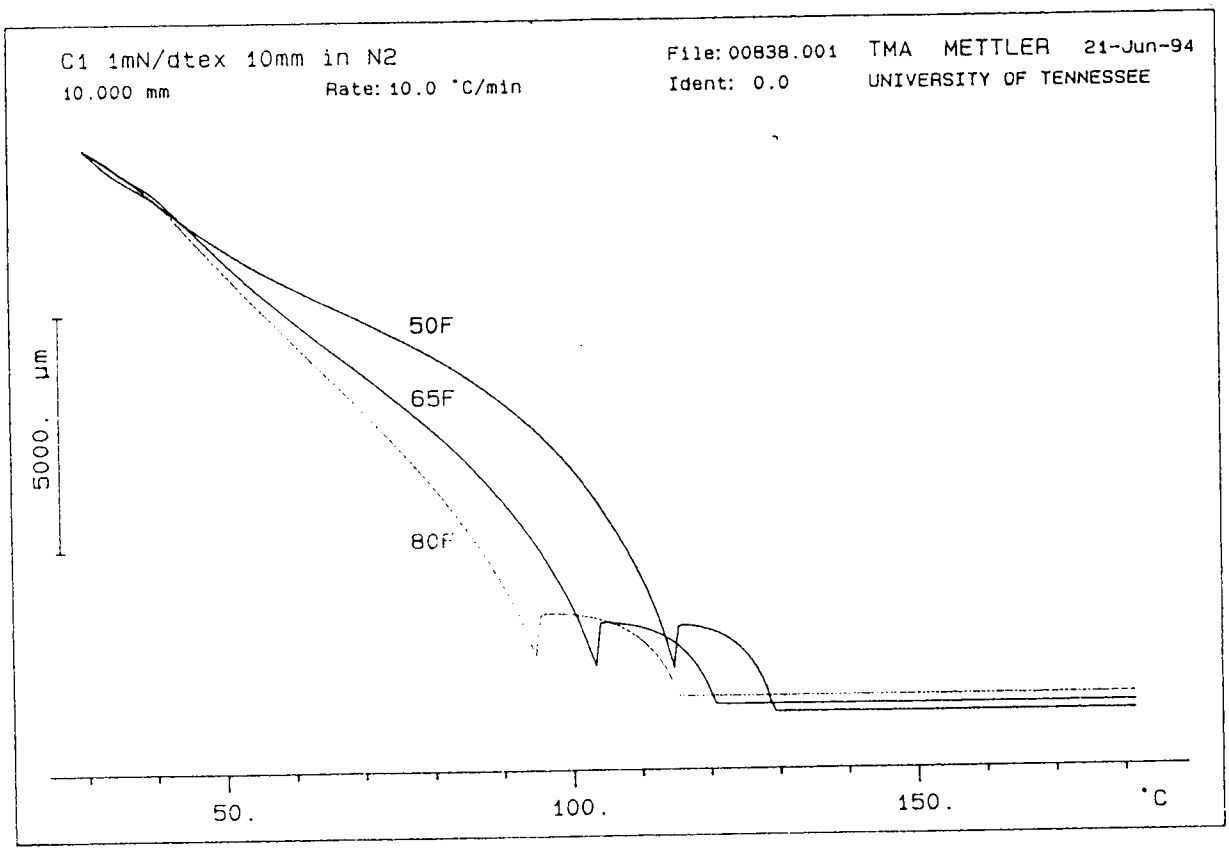

Figure 5.4 TMA Scans for Filament Samples Produced at Different Primary Air Temperatures.

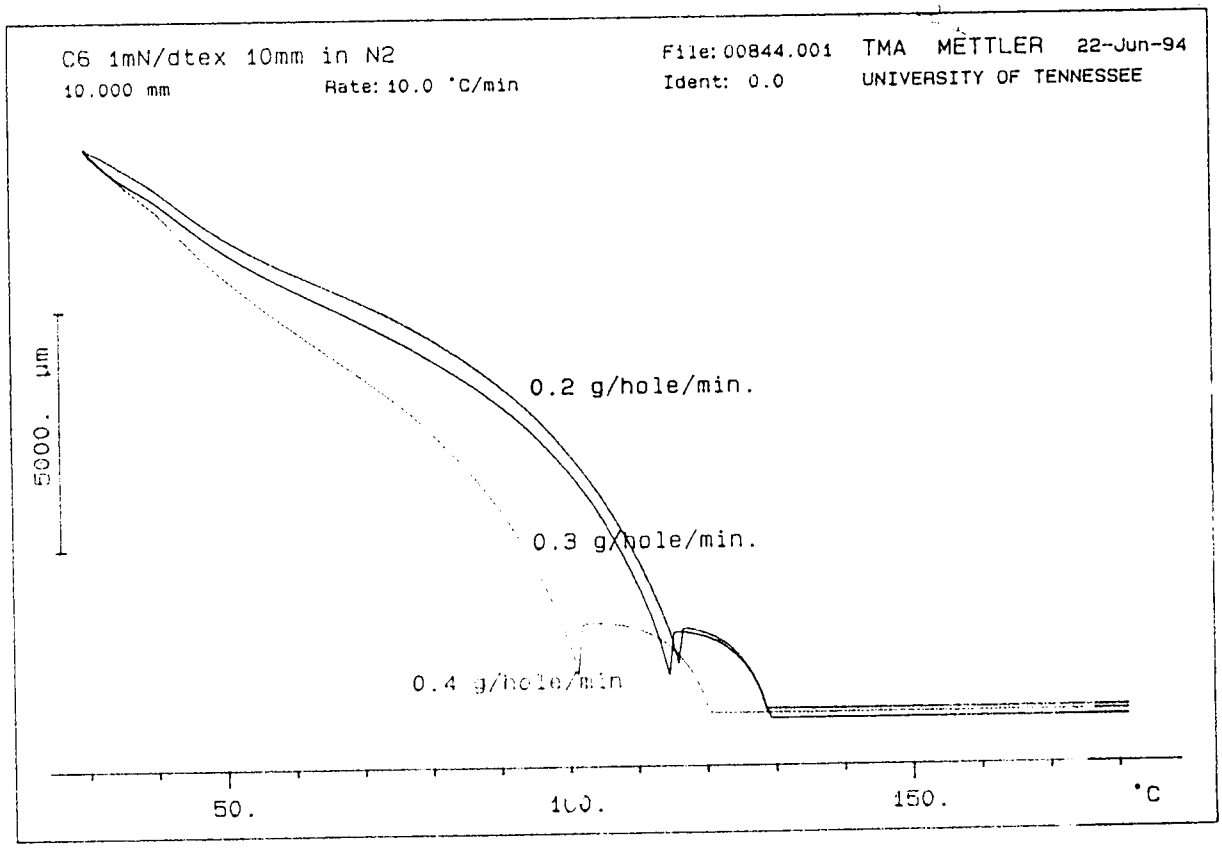

Figure 5.5 TMA Scans for Filament Samples Produced from Different Throughput.

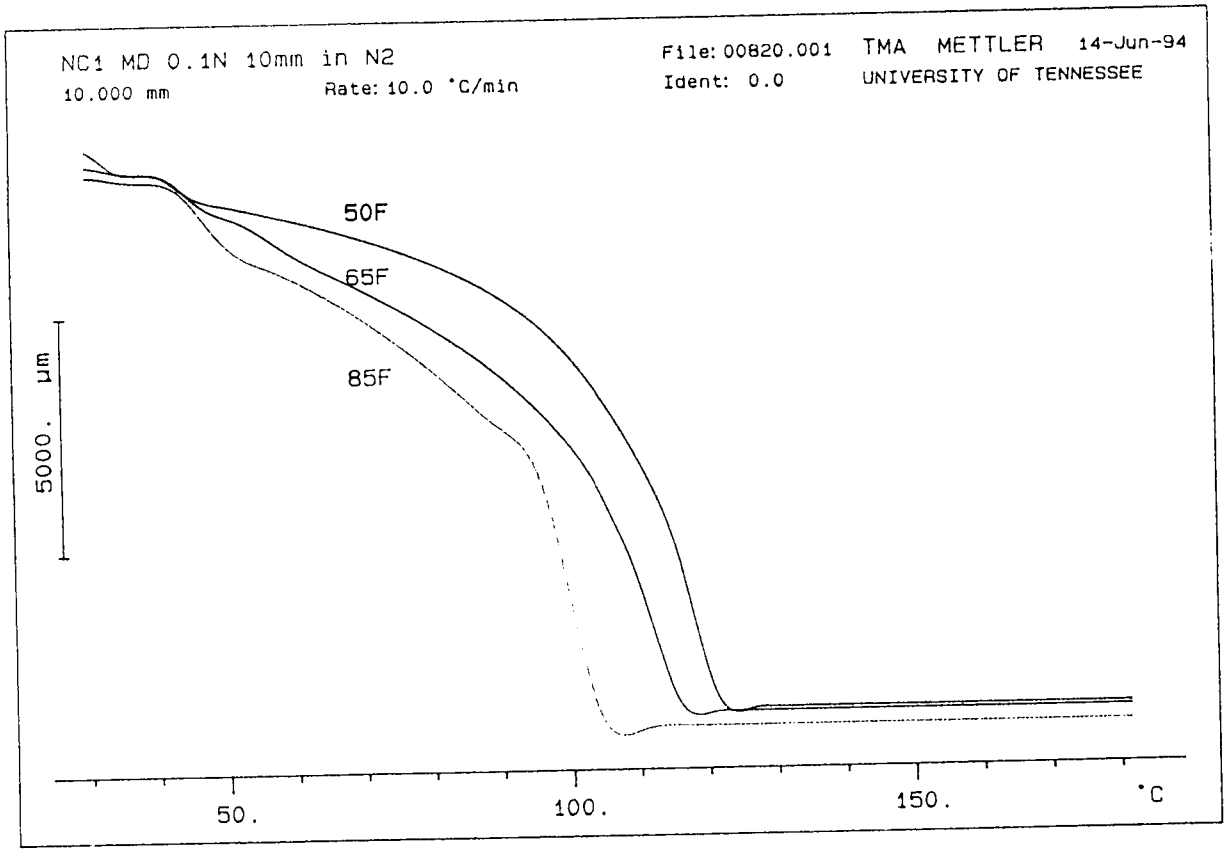

Figure 5.6. TMA Scans for Nonwoven Samples Produced at Different Primary Air Temperature.

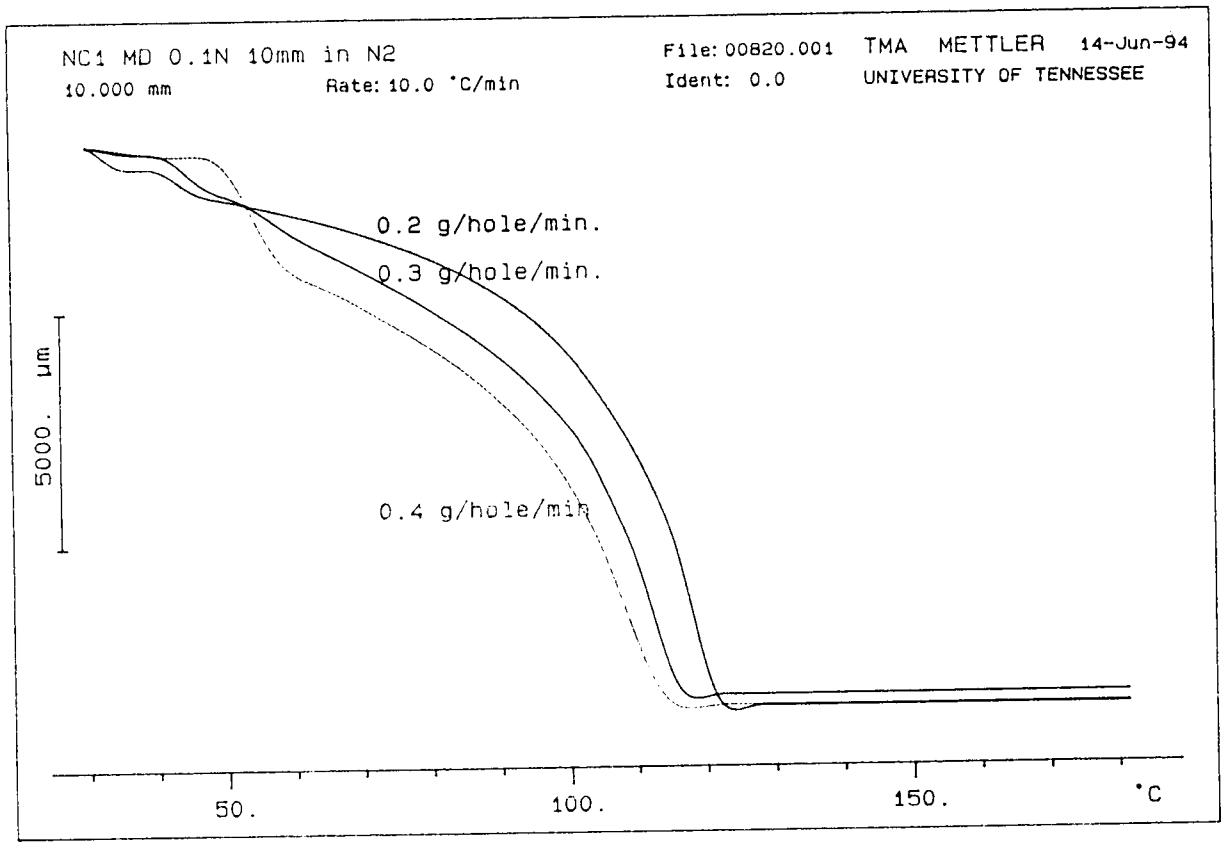

Figure 5.7 TMA Scans for Nonwoven Samples Produced from Different Throughput.

produced at different cooling air temperatures. The filaments produced at lower primary air temperatures were more stable than those spun at higher temperatures. For same primary air temperature, the thermomechanical stability of filaments improved with decreasing throughput as shown in Figure 5.5. That indicates that the morphology of the filaments spun at lower throughput was better developed than those produced with higher throughput. Figures 5.6 and 5.7 show the TMA scans of nonwoven samples produced from different primary air temperature and throughput, respectively. The responses are consistent with those of filament samples. TMA studies indicate there is a large difference in the observed response for the filaments, especially in the temperature range of 90 to 120 ^{0}C.

Figure 5.8 shows the dynamic TMA scan for copolymer filament samples. As shown, there is a transition temperature around 100 ^{0}C. That mean the mechanical properties of these samples can change dramatically after this temperature. Cooling air temperature shifts the transition temperature by about 20 ^{0}C. Lower cooling air temperature helps in crystallization and molecular orientation, and, therefore, results in high transition temperature of the filaments. Figure 5.9 shows the difference of TMA scan of filament samples between the PP homopolymer and PP+PE copolymer. PP homopolymer filament shows better thermo-mechanical properties than those of PP+PE copolymer filaments. That is due to the fact that the PP homopolymer filaments are of higher crystallinity and molecular orientation than those of PP+PE copolymer filaments. This also results in the thermomechanical properties of PP homopolymer nonwovens being better than those of PP+PE copolymer nonwovens, as shown in figure 5.10. More importantly, response of the filaments during the calendering process will be different in the two cases, which in turn

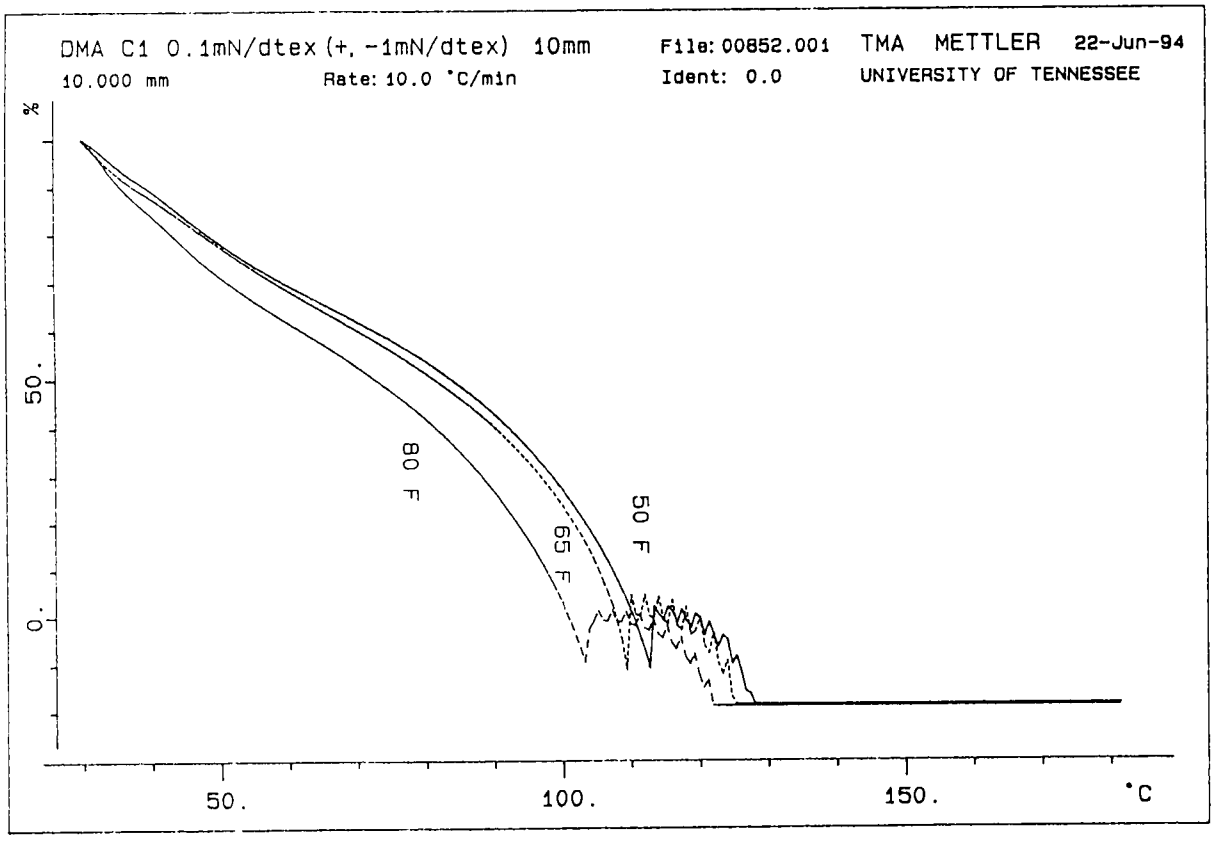

Figure 5.8 Dynamic TMA Scan for Copolymer Filament Samples at Different Cooling Air Temperature

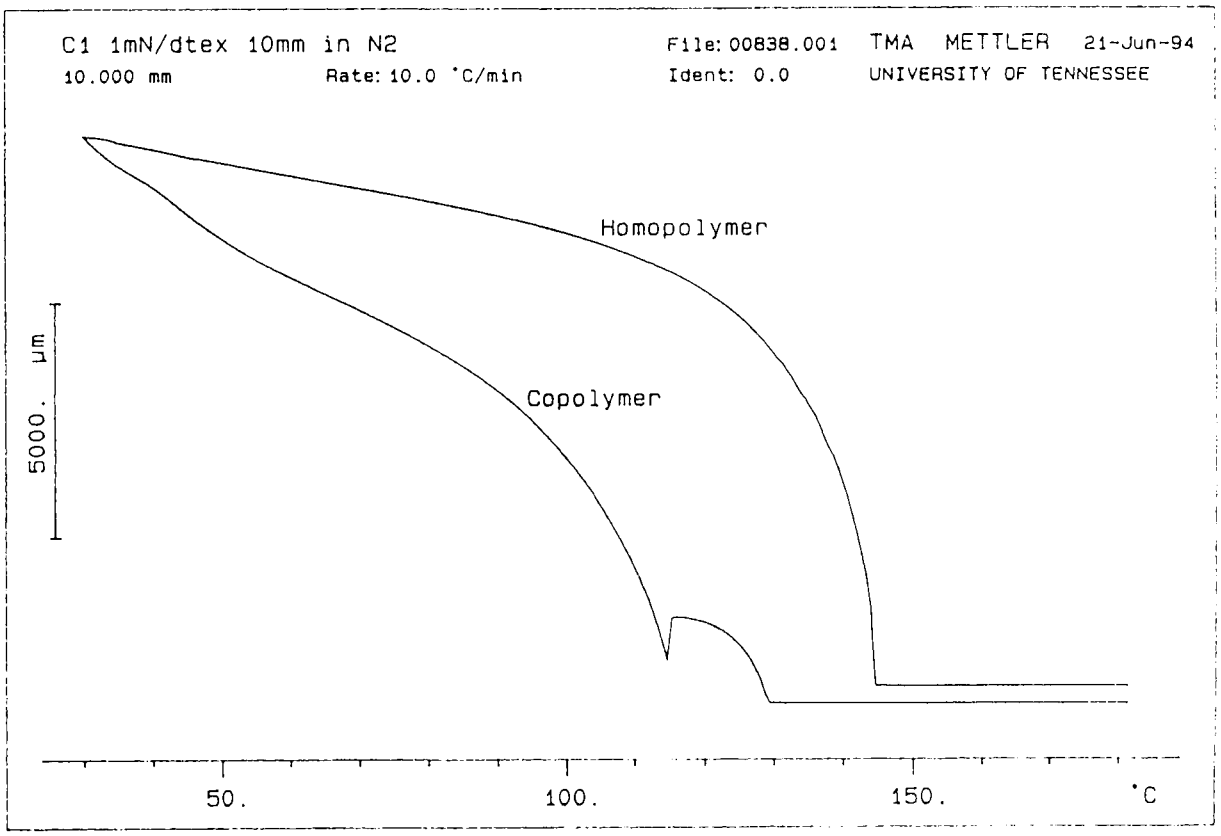

Figure 5.9 TMA Scans for Comparison of Copolymer and Homopolymer of Filaments

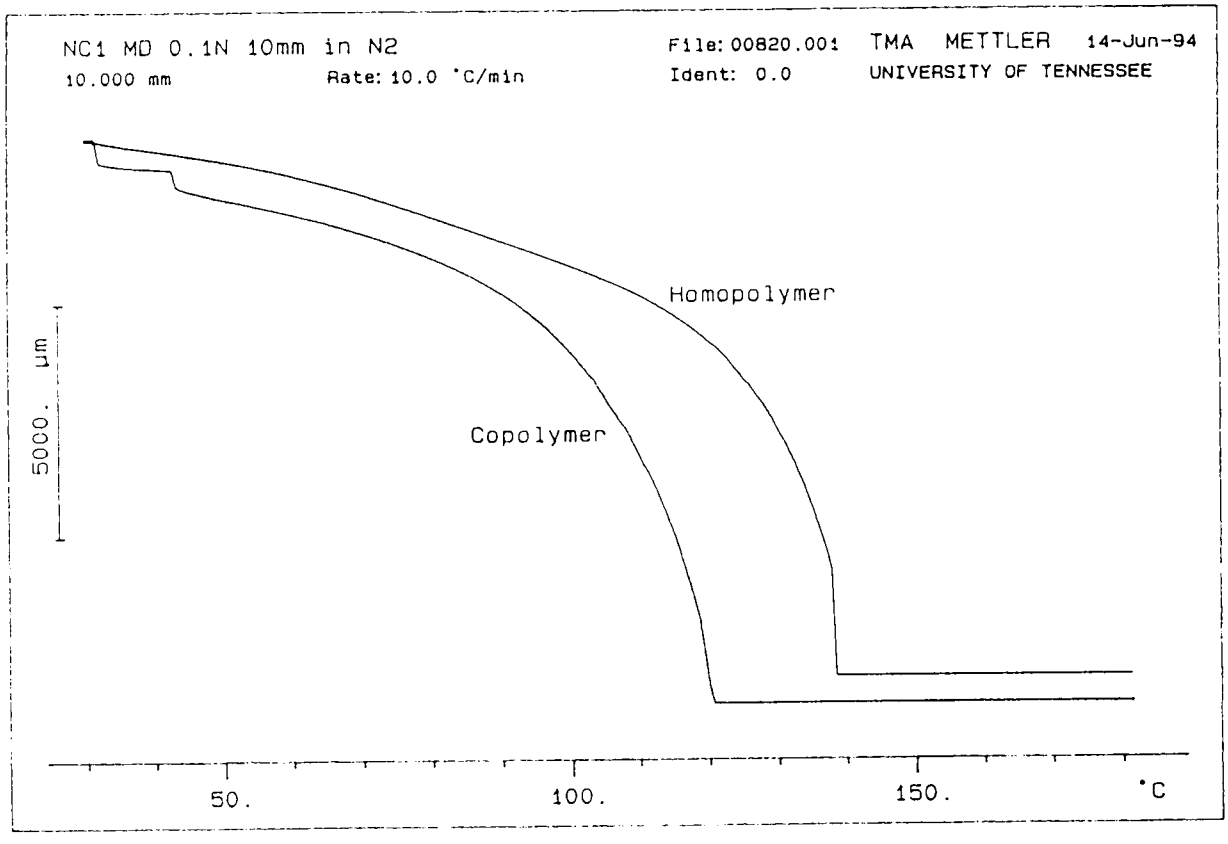

Figure 5.10 TMA Scans for Comparison of Copolymer and Homopolymer of Nonwovens

determine the properties of the bonded nonwovens.

Thermal elongation of samples at 125 °C for two minutes measured at two different tensions is shown in Table 5.6. At both 0.1 g/den and 0.033 g/den pretension, the thermal elongation increased as the primary air temperature and throughput increased. The relatively large thermal elongation showed that the filaments have a lot of potential for drawing by decreasing the primary air temperature or increasing the drawdown air speed. Lower the crystallinity and orientation of the samples, thermal elongation was higher. The trend observed is same as seen with the homopolymer filaments.

5.4 Properties of the Nonwoven Samples

The results of air permeability, MFR, burst strength, and tear strength of the copolymer nonwovens are shown in Table 5.7. The air permeability increased as the primary air temperature and throughput increased. Increase in diameter of the filaments with increase in the two parameters leading to lower fabric density after calendaring was responsible for observed higher air permeability. The burst strength was consistent with tensile strength and decreased as the primary air temperature and throughput increased. The tear strength was consistent with the burst strength only for primary air temperature. The tear strength increased with increasing throughput and with decreasing cooling air temperature. The strength of the fabrics decreased as the throughput increased. The decrease in tear strength in those conditions is due to the higher level of bonding. Due to the ease of deformation as can be seen by TMA, filaments melt easily during calendering, resulting increase in bonding area. The higher tear strength values in CD are due to the greater amount of resistance

Table 5.6 Thermal Elongation at 125 ^{0}C for 2 min. with Given Tension for Copolymer Filaments

PP Spunbond Filaments	Elongation at 0.1 (g/den)	Elongation at 0.033 (g/den)
C_1	31%	11%
C_2	38%	19%
C_3	40.4%	22%
C_4	45.2%	24%
C_5	48.8%	29.5%
C_6	39%	13%
C_7	47.1%	17.1%

Table 5.7 Air Permeability, MFR, Bursting and Tear Strength of Spunbonded Nonwovens*

PP Spunbond Nonwovens	Melt Flow Rate (g/min)**	Air Permeability ($mm^3/mm^2/sec$)	Burst Strength (g/mm^2)	Tear Strength MD (Kg)	Tear Strength CD (Kg)
NC_1	39.25	515.18	20.05	10.10	9.06
NC_2	45.54	528.85	18.18	9.35	8.82
NC_3	38.01	589.28	17.41	11.41	9.54
NC_4	41.56	604.52	15.59	10.37	8.48
NC_5	43.30	619.76	14.76	9.15	8.39
NC_6	44.33	538.48	15.49	11.77	9.36
NC_7	46.68	589.68	14.76	9.70	9.16

* INDA STANDARD TEST.

offered by filaments arranged preferably in the MD.

The MFR of the copolymer pellets was 29.45. The MFR of nonwoven samples increased as primary air temperature and throughput increased, indicating a slightly higher level of thermal degradation taking place at higher primary air temperature. The thermal degradation takes place even after the polymer melt is extruded from die since the melt is exposed to air (oxygen) as it solidifies. The higher primary air temperature helps the thermal degradation because the polymer is at elevated temperature for longer period of time. Table 5.8 shows the stiffness of nonwoven samples in both MD and CD. As in the case of tear strength, stiffness is affected by bonding and bond area and observed trends are consistent. The stiffness increased as the primary air temperature decreased. The stiffness in the MD was higher than in the CD, which is consistent with the observed anisotropy of the webs.

5.5 Morphology by X-ray Diffraction

Figure 5.11 shows the x-ray diffraction photos of filament samples produced under different processing conditions. The crystallinity and crystalline orientation increased as the primary air temperature decreased. This can be seen from the dark rings and short arcs of the diffraction patterns compared with the faint rings and larger arcs from the samples of higher cooling air temperature. Figure 5.11(a) is the diffraction pattern of 50 ^{0}F (10 ^{0}C) quench air temperature, and shows the rings of high intensity resulting from high orientation of crystals and high crystallinity. Figure 5.11(b), is the diffraction pattern of 65 ^{0}F (18.33 ^{0}C), shows the rings of medium intensity resulting from intermediate crystallinity and crystal orientation. Figure 5.11(c) is the diffraction pattern of 80 ^{0}F (26.67 ^{0}C) and shows the low

Table 5.8 Stiffness of PP+PE Spunbond Nonwovens*

PP Spunbond Nonwovens	Bending Length (cm)		Flexural Rigidity (mg*cm)	
	MD	CD	MD	CD
NC_1	6.40	4.27	24.72	17.48
NC_2	5.70	3.82	23.33	15.64
NC_3	5.56	3.88	22.76	15.88
NC_4	5.46	3.52	22.35	14.41
NC_5	5.30	3.36	21.69	13.75
NC_6	5.98	3.71	24.48	15.19
NC_7	5.64	3.56	23.09	14.57

* ASTM D1388-64

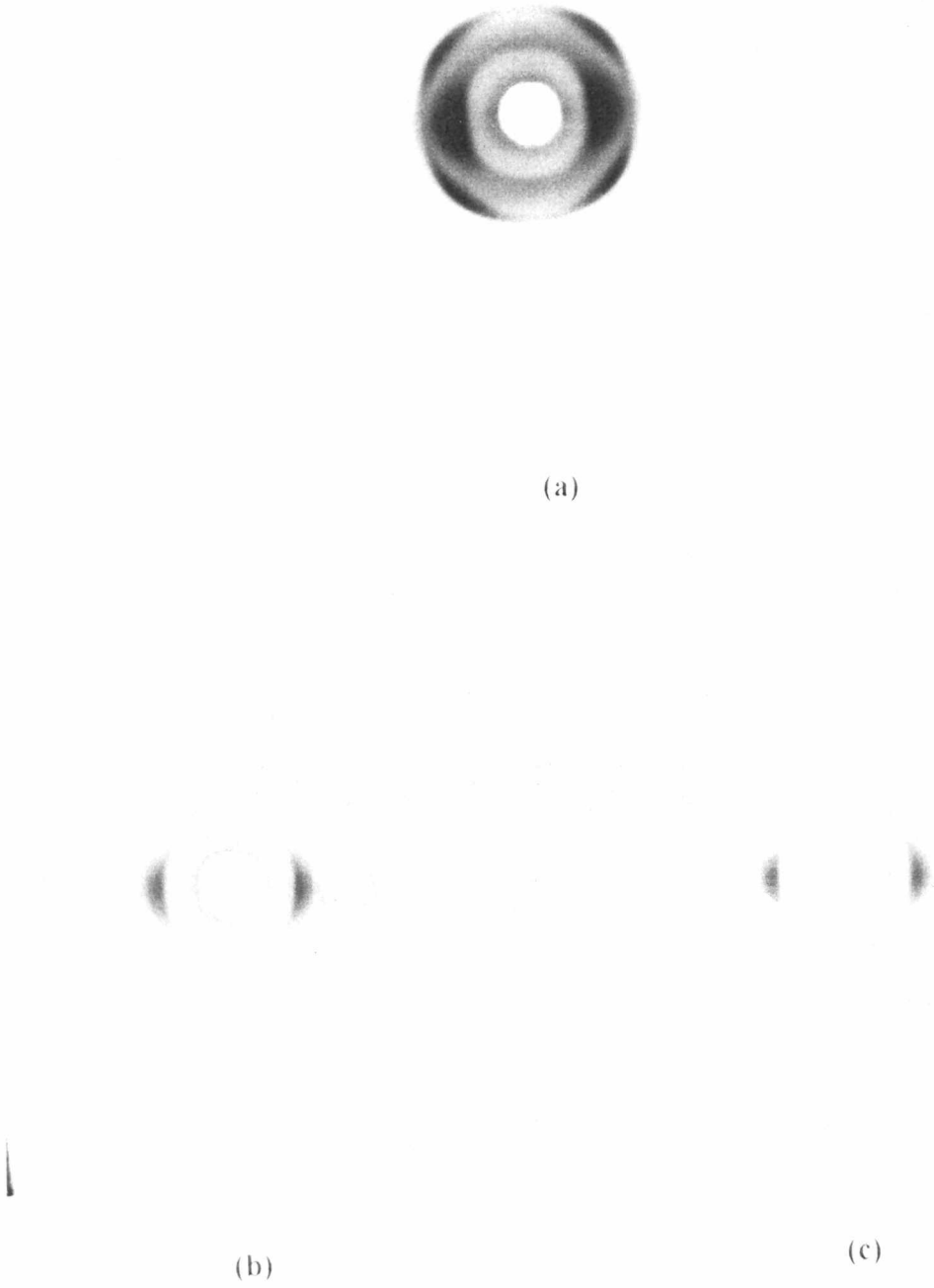

(a)

(b)

(c)

Figure 5.11 X-ray Diffraction Photographs for Filament Samples Produced from Different Cooling Air Temperature (a) 50 ^{0}F (10 ^{0}C), (b) 65 ^{0}F (18.33 ^{0}C), (c) 80 ^{0}F (26.67 ^{0}C).

intensity rings resulting from low crystal orientation and crystallinity.

5.6 Effect of Annealing on Structure and Properties of Filament Samples

The changes in diameter and birefringence of the filament samples after free length annealing at 115 ^{0}C for 30 seconds are shown in Table 5.9. After annealing, the diameter of all the filament samples decreased slightly from 1.21% to 3.44%. The reason is that the filaments from spunbond line are not completely drawn due to insufficient draw-force. Some molecules in the amorphous region may attach to already existing crystals during annealing, resulting in small draw. However, during unconstrained annealing, the birefringence change of the filament samples was different. The high birefringence filaments produced with lower primary air temperature showed a smaller increase in birefringence. The filaments from higher quench air temperature with low birefringence showed a tendency for higher increase in birefringence. By increasing the annealing temperature from 115 ^{0}C to 125 ^{0}C, the changes of diameter and birefringence increased as shown in table 5.10.

Table 5.11 shows the changes in tensile properties of filament samples after free length annealing at 115 ^{0}C for 30 seconds. Tensile strength of the filaments with lower birefringence increased more than that of filaments with higher birefringence. Breaking elongation of the filament samples decreased after annealing. The initial modulus increased just as the strength. The reason is that the structure of the filaments changed significantly after annealing (see above and following analysis for structure changes after annealing). By increasing the annealing temperature from 115 ^{0}C to 125 ^{0}C, the changes of tensile

Table 5.9 Diameter and Birefringence Change of PP+PE Spunbond Filaments after Free Length Annealing at 115 °C for 30 Sec.

PP+PE Spunbond Filament	Change* of Diameter (%)	Change** of Birefringence (%)
C_1	-1.70	+7.6
C_2	-2.04	+9.21
C_3	-1.21	+6.94
C_4	-1.97	+7.78
C_5	-2.60	+18.91
C_6	-2.14	+1.39
C_7	-3.44	+11.19

* "-" is decrease;
** "+" is increase.

Table 5.10 Diameter and Birefringence Change of PP+PE Spunbond Filaments after Free-Length Annealing at 125 °C for 30 Sec.

PP+PE Spunbond Filament	Change* of Diameter (%)	Change** of Birefringence (%)
C_1	-2.35	+6.39
C_2	-3.75	+11.67
C_3	-1.96	+8.93
C_4	-2.57	+12.16
C_5	-3.82	+20.61
C_6	-0.54	+9.41
C_7	-3.48	+16.39

* "-" is decrease;
** "+" is increase.

Table 5.11 Diameter and Birefringence Change of PP+PE Spunbond Filaments after Fixed-Length Annealing at 115 °C for 30 sec.

PP+PE Spunbond Filament	Change* of Diameter (%)	Change** of Birefringence (%)
C_1	-1.34	+9.74
C_2	-1.62	+12.65
C_3	-1.01	+3.12
C_4	-1.64	+4.41
C_5	-4.55	+11.00
C_6	-1.12	+3.62
C_7	-1.85	+7.22

Table 5.12 Diameter and Birefringence Change of PP+PE Spunbond Filaments after Fixed-Length Annealing at 125 °C for 30 sec.

PP+PE Spunbond Filament	Change* of Diameter (%)	Change** of Birefringence (%)
C_1	-0.79	+6.59
C_2	-1.04	+4.92
C_3	-0.86	+2.76
C_4	-1.10	+4.98
C_5	-2.57	+12.05
C_6	-0.91	+3.00
C_7	-1.92	+7.38

properties increased as shown in table 5.12. The reason is the increase in orientation as can be seen from the increase in birefringence (table 5.10).

In the case of fixed length annealing (Table 5.13) at 115 ^{0}C for 30 seconds, the diameter of all the filament samples decreased slightly from 1.01% to 4.55%, and the birefringence increased from 3.12% to 12.65%. The increase in birefringence was higher for higher quench air temperature samples. During annealing, as the molecules in the amorphous, less-oriented region tend to recrystallize, the molecules reorient along the fiber axis. By increasing the annealing temperature from 115 ^{0}C to 125 ^{0}C, the changes in diameter and birefringence were different as shown in table 5.14.

Table 5.15 shows the changes in tensile properties of filaments after fixed length annealing at 115 ^{0}C for 30 seconds. The tensile strength and initial modulus increased, with higher increase for lower birefringence samples. However, breaking elongation decreased for all the filament samples. The changes in tensile properties are more than those observed in free length annealing as seen from birefringence data. The reason for that is the higher orientation resulting from fixed length annealing. Changes in tensile properties on increasing the annealing temperature from 115 ^{0}C to 125 ^{0}C are shown in table 5.16. The changes in structure after annealing can be seen from the x-ray diffraction photographs as shown in figure 5.12. The crystalline orientation and crystallinity of all the copolymer filaments increased on annealing.

Figure 5.13 shows the SEM photographs of nonwoven samples at 0.3 g/hole/min of throughput for different primary air temperatures. Figure 5.13(a) is the fabric from filaments quenched by air at 50 ^{0}F (10 ^{0}C) which shows small and well defined bonding area. Because

Table 5.13 Change of Tensile Properties of PP+PE Spunbond Filaments after Free-Length Annealing at 115 ^{0}C for 30 sec.

PP+PE Spunbond Filament	Change* of Strength (%)	Change** of Breaking Elongation(%)	Change of Initial Modulus
C_1	+11.95	-6.45	+12.24
C_2	+26.77	-19.63	+18.95
C_3	+18.58	-17.72	+16.36
C_4	+24.52	-27.32	+23.34
C_5	+37.50	-30.94	+27.68
C_6	+16.95	-8.42	+12.68
C_7	+35.29	-11.30	+25.55

Table 5.14 Change of Tensile Properties of PP+PE Spunbond Filaments after Free-Length Annealing at 125 ^{0}C for 30 sec.

PP+PE Spunbond Filament	Change* of Strength (%)	Change** of Breaking Elongation(%)	Change of Initial Modulus
C_1	+18.56	-7.53	+14.42
C_2	+29.87	-20.70	+21.95
C_3	+20.23	-21.56	+19.55
C_4	+31.25	-29.26	+25.42
C_5	+39.95	-38.84	+31.68
C_6	+19.96	-9.42	+15.85
C_7	+37.35	-23.23	+27.46

Table 5.15 Change of Tensile Properties of PP+PE Spunbond Filaments after Fixed-Length Annealing at 115 ^{0}C for 30 sec.

PP+PE Spunbond Filament	Change of Strength (%)	Change of Breaking Elongation(%)	Change of Initial Modulus
C_1	+15.95	-7.18	+13.86
C_2	+28.53	-20.18	+20.23
C_3	+21.32	-19.34	+17.95
C_4	+24.52	-27.32	+23.34
C_5	+38.64	-33.32	+29.18
C_6	+18.52	-9.12	+14.24
C_7	+35.89	-18.46	+26.34

Table 5.16 Change of Tensile Properties of PP+PE Spunbond Filaments after Fixed-Length Annealing at 125 ^{0}C for 30 sec.

PP+PE Spunbond Filament	Change of Strength (%)	Change of Breaking Elongation(%)	Change of Initial Modulus
C_1	+23.14	-8.92	+18.24
C_2	+32.45	-29.87	+28.59
C_3	+25.32	-23.16	+21.45
C_4	+38.75	-32.56	+29.22
C_5	+45.75	-43.48	+41.88
C_6	+24.68	-11.32	+17.58
C_7	+41.52	-33.23	+31.56

(a)

(b)

(c)

Figure 5.12 Effect of Annealing on X-ray Diffraction Photographs for Filament Samples Produced from Different Cooling Air Temperature (a) 50 ^{0}F (10 ^{0}C), (b) 65 ^{0}F (18.33 ^{0}C), (c) 80 ^{0}F (26.67 ^{0}C).

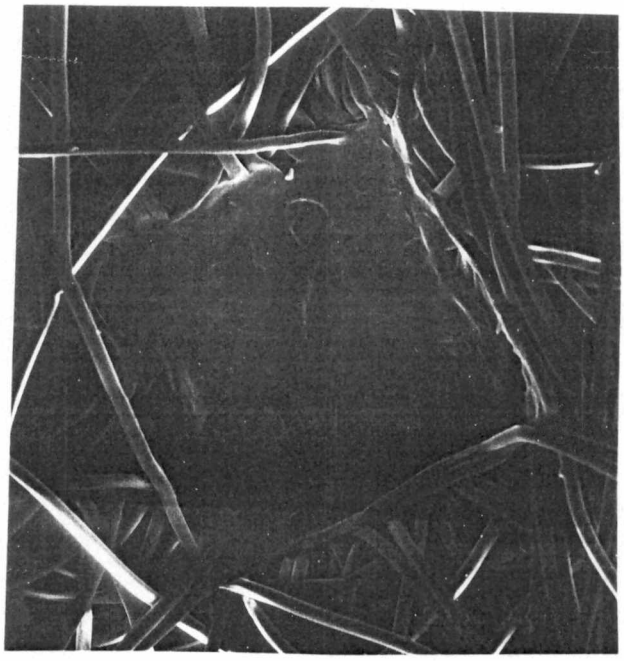

(a)

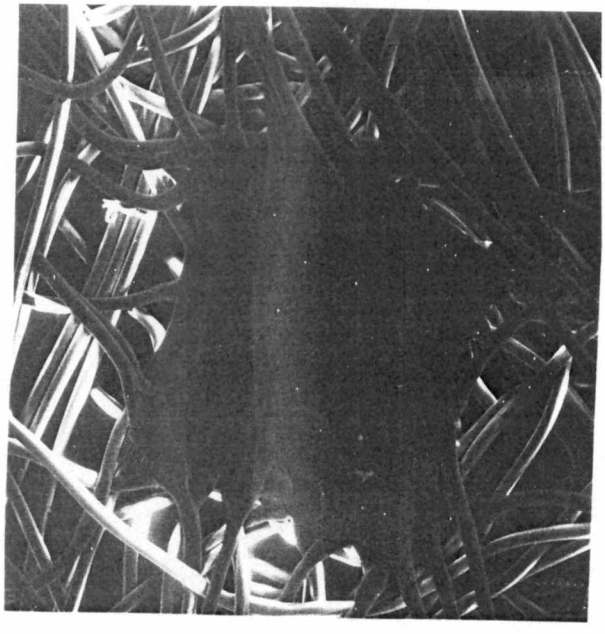

(b)

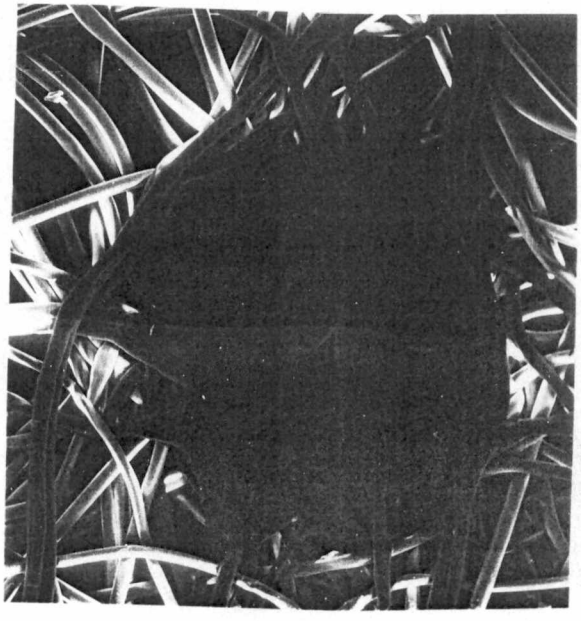

(c)

Figure 5.13 SEM Photographs for Nonwoven Samples produced from Different Cooling Air Temperatures (a) 50 ^{0}F (10 ^{0}C), (b) 65 ^{0}F (18.33 ^{0}C), (c) 80 ^{0}F (26.67 ^{0}C).

the filaments had high orientation and crystallinity, they are not easily deformed. Figure 5.13(b) and (c) are for quench air temperatures of 65 and 80 ^{0}F (18.33 and 26.67 ^{0}C) , respectively. In both the cases, the filaments were relatively easily deformable and the bonding area increased compared to samples from low primary air temperatures. The bond patterns showed a similar trend for samples with 0.2 and 0.4 g/hole min throughputs.

Since the nonwovens consist of filaments, the morphology and the properties of the filaments should influence the properties of the nonwovens as the filaments undergo the calendaring process. The relationship between the filament attributes and the corresponding nonwovens shows the same trends as observed with the homopolymer.

CHAPTER VI

Mathematical Model For Evaluation of Quality of Nonwoven Fabrics

6.1 Introduction

In this chapter, a mathematical model for evaluating the quality of nonwoven fabrics was established, based on mechanical properties of nonwoven fabrics, using factor analysis in multivariate analysis and comprehensive evaluation in fuzzy mathematics. Also a mathematical model for classification of nonwoven fabrics was developed, using non parameter method of fuzzy collection.

In 1926, Binns [59] studied evaluation of fabric quality by sensory organ. From that time, researchers and experts have been trying to find a method to evaluate the quality of textiles objectively and quantitatively in order to avoid the influence of different persons in subjective evaluation. In 1970's, a Japanese expert [60] established method for evaluating fabric quality. In their model, the measurement of mechanical factors was objective, but the model of comprehensive evaluation was partially subjective despite the quantitative evaluation of the method.

In 1980's, some researchers [61] studied the method, using mathematics, in order to find a way to evaluate quality of textiles objectively and quantitatively. However, up to date, there are no good reliable methods to evaluate the quality of textiles objectively and quantitatively. In this research, a mathematical model for evaluating quality of nonwovens was established based on mechanical factors of fabrics, using factor analysis in multivariate

analysis and comprehensive evaluation of fuzzy mathematics. Also a mathematical model for classification of nonwoven fabrics was set up, using non parameter method of fuzzy collection.

6.2 Mathematical Model for Classification of Nonwoven Fabrics

1. In this method the ith sample designated as S_i, and the corresponding mechanical quantities of S_i will be denoted by $a_{i1}, a_{i2}, ..., a_{iq}$ where i is the number of samples, i=1, 2, ..., p, and q is the number of mechanical quantities that determine fabric quality. The set of data results in the information matrix $A=(a_{ij})_{p*q}$. The mechanical quantities were obtained using Kawabata Testing. The matrix $X= (x_{ij})_{p*q}$ is obtained by applying a function transformation to A [62].

2. By non parameter method of fuzzy classification analysis [62], we let $x'_{ik}=x_{ik} - x_i$, where

$x_i= (1/q) \sum_{k=1}^{q} x_{ik}$.

n^+= the number of positive numbers in $\{x'_{i1}x'_{j1}, x'_{i2}x'_{j2}, ..., x'_{q1}x'_{q2}\}$,

n-= the number of negative numbers in $\{x'_{i1}x'_{j1}, x'_{i2}x'_{j2}, ..., x'_{q1}x'_{q2}\}$,

and $r_{ij}=|(n^+-n^-)/(n^++n^-)|$.

3. The establishment of the equivalent matrix R*.

First, set up similar relation $R= (r_{ij})_{p*p}$ on $S= \{s_1, s_2, ..., s_p\}$. Generally, R is only a similar matrix, but not a fuzzy similar relation [62]. Thus, the following operation on R will be done:

Consider $R^2, R^4, ..., R^{2k}$. There must be an integer K_o [62] such that $R^{2ko}=R^{2(ko+1)}$. Let

$R^*=R^{2ko}$ then R^* is a equivalent matrix [62]. Note that all the evolved matrix operations are fuzzy.

4. The classification diagram from R*.

For given βo [62], we can determine a fuzzy classification, using classification diagram. Furthermore, the relative order can be obtained from the diagram and which group is nearer to another can be determined.

6.3 Mathematical Model for Evaluation of Fabric Quality

The quality of fabrics is based on mechanical factors. According to these factors, give a nonnegative real number for each sample. By comparing these numbers, it is possible to order the samples. The higher the number, the better quality of the sample. It is the mathematical model that will be established for the objective evaluation of fabric quality.

1. The sample set is $S=\{s_1, s_2, ..., s_p\}$, s_i is ith sample. (i= 1, 2, ..., p).

2. The factor set is $M_i=\{m_{i1}, m_{i2}, ..., m_{iq}\}$, m_{ij} is the jth mechanical factor of ith sample. (j=1, 2, ..., q).

3. Evaluating matrix is $E=(e_{ij})_{p*q}$, E: S*M ~ [0, 1], e_{ij} is characteristic factor of mechanical property m_{ij} of sample s_i.

(1). By measuring the q mechanical factors of p samples, we get an information matrix $A=(a_{ij})_{p*q}$.

(2). We order the information matrix A in order to make these factors increasing, that is the value of fabric quality increases as the characteristic factors increase. The higher the value of fabric quality, the better fabric quality.

Table 6.1 Basic Mechanical Factors of Fabrics

FACTNAM	SAMPLE1	SAMPLE2	SAMPLE3	SAMPLE4	SAMPLE5	SAMPLE6	SAMPLE7
MIU	0.3791	0.4511	0.4631	0.4784	0.5505	0.4460	0.4755
MMD	0.0263	0.0338	0.0335	0.0351	0.0336	0.0356	0.0332
SMD	5.4650	5.8510	6.8090	6.5100	6.3950	7.0930	5.9310
B	1.3350	0.6950	0.6510	0.6390	0.6240	0.7090	0.4920
2HB	0.9130	0.4920	0.4610	0.4800	0.4470	0.5180	0.4220
LC	0.0274	0.0282	0.0299	0.0290	0.0301	0.0294	0.0306
WC	0.1500	0.1500	0.1500	0.1600	0.1600	0.1600	0.1700
RC%	67.2300	67.7500	63.3700	69.3500	71.1900	70.2700	70.1800
TO	0.4100	0.3800	0.4000	0.3900	0.4000	0.4300	0.4300
LT	2.2700	2.3100	2.3200	2.3300	2.6400	2.0400	2.7400
WT	41.0800	39.4500	49.1500	66.2300	103.8300	43.5900	80.5100
RT	0.4200	0.4500	0.4200	0.3400	0.2800	0.4000	0.3100
ET	14.8100	15.3100	17.1300	23.6900	31.5600	16.7500	23.9600
G	5.4400	5.7800	5.5600	4.8700	4.4000	5.8000	4.9900
2HG	6.7500	7.8300	7.7400	7.1300	8.3700	8.4300	7.9500
2HG5	7.5000	7.3600	7.6800	6.6900	6.8300	8.2000	6.8800
EMC%	26.9300	27.2100	25.4500	27.4900	27.4200	26.4100	26.6300

FACTNAM	SAMPLE1	SAMPLE2	SAMPLE3	SAMPLE4	SAMPLE5	SAMPLE6	SAMPLE7
MIU	0.3862	0.3865	0.4038	0.4224	0.4035	0.3904	0.4045
MMD	0.0310	0.0314	0.0330	0.0335	0.0302	0.0377	0.0347
SMD	5.6600	4.6090	6.5290	7.1690	6.4940	5.7590	6.0930
B	1.1270	1.2520	1.1700	1.1520	0.9750	1.1550	1.0960
2HB	0.6820	0.9390	0.8550	1.3900	0.7140	0.7630	0.8570
LC	0.0266	0.0271	0.0276	0.0270	0.0286	0.0277	0.0257
WC	0.1400	0.1400	0.1300	0.1300	0.1500	0.1300	0.1300
RC%	68.6900	67.2700	69.6100	68.7500	66.9500	69.5300	69.0400
TO	0.4300	0.4100	0.4100	0.4100	0.4500	0.4100	0.4200
LT	2.6000	2.1300	2.3200	1.7400	2.5000	2.5000	2.4900
WT	37.8600	36.8300	38.0400	42.3600	85.3400	45.3800	33.9900
RT	0.4300	0.4700	0.4200	0.4300	0.3400	0.3700	0.4200
ET	11.5800	12.7500	13.7500	22.6900	26.7500	13.6300	10.7500
G	7.2200	7.1600	7.2100	6.9700	5.3000	7.8700	7.5300
2HG	7.9000	7.5700	8.2300	7.8100	7.5600	8.6200	7.7200
2HG5	11.2000	10.2900	10.9800	10.1100	7.0100	11.2900	10.6300
EMC%	24.9100	24.8800	22.5300	23.2700	23.8700	22.7900	24.8600

(a).If m_{ij} increases, value of fabric quality increases, let $m'_{ij}=a_{ij}$

(b). If m_{ij} increases, value of fabric quality decreases, let $m'_{ij}=2\max a_{ij}-a_{ij}$

(c). If $m_{ij}=m_{ijo}$, fabric quality is best, let $m'_{ij}= 2\max |a_{ij}-a_{ijo}| - |a_{ij}-a_{ijo}|$

we get $M'=(m'_{ij})_{p*q}$

(3). Change M' to E and E is evaluating matrix. Let $e_{ij}=m'_{ij} / \max m_{ij}$ (i=1,2,...,p), which gives $E=(e_{ij})_{p*q}$.

4. Selection of Weight Vectors

Q mechanical quantums of fabric quality will be induced to r mechanical factors (r<q), basic quality. Factor load expresses relative coefficient which shows the relative degree between mechanical quantum and mechanical factors. The more the β value, the more important the relative mechanical factor. Therefore, the weight vectors can be determined based on factor load and characteristic value of β [63,64].

(1). Factor Analysis.

(a). Calculate the matrix R from information matrix A.

(b). Spectroanalysis for relative matrix R. $R=\sum_{i=1}^{p} \beta_i \emptyset_i \emptyset_i^T$

Note: $\beta_1>\beta_2>...>\beta_p$ are characteristic roots of R, $\emptyset_i$ is characteristic matrix of β_i, $\emptyset_i^T=(\emptyset_{i1}, \emptyset_{i2},...,\emptyset_{iq})^T$. It is a p dimensional vector.

(c). Take characteristic vector based on characteristic roots of 1, 2, ..., N. Let

$\sum_{i=1}^{N} \beta i > Co$, $Co@[0,1]$

(d). Make original factor model matrix B from taken characteristic roots and vector.

The number of factors is n.

$$B_{q*n} = (\emptyset_1, \emptyset_2, \ldots, \emptyset_n) \begin{matrix} \beta_1^{1/2} & & 0 \\ & \beta_2^{1/2} & \\ & \ldots & \\ 0 & & \beta_n^{1/2} \end{matrix} = \begin{matrix} b_{11}\ b_{12} \ldots b_{1n} \\ b_{21}\ b_{22} \ldots b_{2n} \\ \ldots\ldots\ldots\ldots \\ b_{q1}\ b_{q2} \ldots b_{qn} \end{matrix}$$

(e). In order to make physical meaning of factor model more clear, the matrix B will be transformed by rotating [65] and we get factor load matrix C. Note, cij is the contribution of ith mechanical quantum to jth mechanical factor. β_i shows the importance of jth factor.

$$C = \begin{matrix} c_{11}\ c_{12} \ldots c_{1n} \\ c_{21}\ c_{22} \ldots c_{2n} \\ \ldots\ldots\ldots\ldots \\ c_{q1}\ c_{q2} \ldots c_{qn} \\ \beta_1\ \beta_2 \ldots \beta_n \end{matrix}$$

(2). Choose the weight vectors.

(a). The weight vector of basic quality value from mechanical quantums, $H = (h_{ij})_{q*n}$

$$h_{ij} = \frac{c_{ij}}{\sum_{i=1}^{q} c_{ij}}, \qquad \sum_{i=1}^{q} h_{ij} = \sum_{i=1}^{q} \frac{c_{ij}}{\sum_{i=1}^{q} c_{ij}} = 1$$

(b). Calculate the weight vector of total quality value from basic value, $G = (g_j)_{n*1}$

$$g_j = \frac{\beta_j}{\sum_{j=1}^{n} \beta_j}, \qquad \sum_{j=1}^{n} g_j = \sum_{j=1}^{n} \frac{\beta_j}{\sum_{j=1}^{n} \beta_j} = 1$$

(c) The weight vector of total quality value from mechanical quantums. $D = (d_i)_{q*1}$,

$$d_i = \frac{\sum_{j=1}^{n} c_{ij}\ \beta_j / \sum_{j=1}^{n} \beta_j}{\sum_{i=1}^{q} \sum_{j=1}^{n} c_{ij}\ \beta_j / \sum_{j=1}^{n} \beta_j}, \qquad \text{thus } \sum_{i=1}^{q} d_i = 1$$

5. Calculation of Quality Value

(1). Calculate the basic quality value from mechanical quantums, $F= (f_{ij})_{p*n}$ Note f_{ij} is jth basic quality value of ith sample. $F=E_{p*q} H_{q*n}$.

(2) Calculate the total value of quality from basic value of quality, $T= (t_i)_{p*1}$, t_i is the total quality value of ith sample. $T= F_{p*n} G_{n*1}$.

(3) Calculate the total quality value from mechanical quantums, $T=(t_i)p*1 = E_{p*q} D_{q*1}$.

6. Example.

(1). From the factor analysis, get table of factor analysis.

(2). Establish evaluating matrix E.

(3). Set up weight vectors (H, G, D) from factor load and β value.

(4) Calculate the basic quality value of samples by F=EH.

(5) Calculate the total quality value of samples by T=FG.

7. Conclusions.

1. The value of fabric quality are consistent with structure and property analysis in Chapter VI and V. That means this mathematical model is practical and objective for evaluating quality of nonwovens which are commonly evaluated by subjective methods or practically objective methods.

2. This mathematical model can be applied to other areas for evaluating of samples objectively, which are based on lots of quantums and control the quality of the nonwoven fabrics by optimizing the processing conditions.

Table 6.2 Total Quality Value of Nonwoven Fabrics

SAMPLE	VALUE
S1	0.912
S2	0.892
S3	0.901
S4	0.873
S5	0.851
S6	0.896
S7	0.865
C1	0.887
C2	0.853
C3	0.874
C4	0.857
C5	0.792
C6	0.861
C7	0.832

CHAPTER VII

CONCLUSIONS

An in-depth investigation of the spunbonding process was conducted to study the relation between the structure and properties of the filaments and the nonwoven samples of a polypropylene homopolymer and a copolymer of PP. The study showed that the primary air temperature and throughput have a strong influence on the structure and properties of both the filaments (before bonding) and the nonwovens (after bonding). As the primary air temperature and throughput decreased, there was a tendency for decrease in filament diameter. The decrease in filament diameter was accompanied by a simultaneous increase in their crystallinity, birefringence, tensile strength, initial modulus, thermal stability and density.

The larger diameter fibers also had higher breaking elongation and thermal elongation, which indicated the drawability of the fibers. Lower primary air temperature and throughput produced the filaments with well developed structure and properties. Diameter increase with the increasing primary air temperature may be due to the lower level of spinline stress under those conditions. Higher stress in the threadline leads to a greater reduction in fiber diameter and increase in birefringence. X-ray diffraction studies showed that crystal orientation and crystallinity increased as primary air temperature decreased. Also crystal forms of polypropylene fibers changed on varying primary air temperatures.

Statistical analysis showed that the effect of primary air temperatures, throughput,

and their interaction on structure and properties of the filament samples are significant. Both the primary air temperature and throughput are critical variables in determining the structure and properties of the filaments and corresponding nonwovens.

Thermomechanical analysis of the filaments and nonwoven samples showed that filaments from low primary air temperature had better mechanical properties as well as thermal stability. With well developed morphology, the deformability of the filaments decreased during subsequent thermomechanical operation. This was clearly evident in the bond patters of the calendared fabrics. SEM studies of nonwoven samples showed that the filaments formed at higher primary air temperatures were easily deformed and the bonding area increased due to melting and flow. DSC scans did not show any difference in melting point for the filaments or nonwoven samples, but the melting enthalpy increased as the primary air temperature decreased. TMA studies indicated that there was a large difference in the observed response for the filaments, especially in the temperature range of 90 to 120 ^{0}C.

This investigation showed that there exists a strong relationship of structure and properties between the filaments and nonwoven samples. The nonwovens from filaments of low primary air temperature have better mechanical properties indicating that the morphology of the filaments are important and critical to the properties of nonwovens. Smaller diameter fibers with higher birefringence resulted in better tensile properties of calendared webs. However, difference in tensile properties for fabrics was not as large as for the filaments. This was due to changes taking place in the filament structure during calendaring. Thermal effect studied by free and fixed length annealing clearly indicated that

the structure and properties of the filaments change significantly during calendaring operation and the changes depend on the morphology of the filaments. The changes of structure and properties from fixed length annealing were more significant than those of free length annealing. Increasing the annealing temperature from 115 ^{0}C to 125 ^{0}C had a significant effect on the changes of structure and properties.

The properties of the nonwoven samples from the copolymer showed close relationships with processing conditions. Increase in primary air temperature resulted in increase air permeability and breaking elongation, and decrease in tensile strength, tear strength, burst strength and modulus. The homopolymer nonwovens showed the higher strength, elongation, and teas strength, and lower burst and stiffness compared to those of the copolymer nonwovens. That indicated that a higher level of bonding took place in the case of copolymer. Poorer mechanical properties in the case of copolymer filaments and nonwovens was due to the morphological differences such as lower crystallinity and orientation.

A mathematical model was developed to objectively evaluate the quality of nonwovens with regards to their perception of mechanical hand, drape, etc. Data obtained from the Kawabata Evaluation System were used to calculate the total hand quality of the fabrics.

CHAPTER VIII

RECOMMENDATION FOR FUTURE RESEARCH

The research done so far has indicated that the inherent properties of the filaments are important in the spunbonded webs. It is important to understand the impact of the process of transforming the collected web to bonded fabric by thermal calendaring. Effect of annealing on the morphology of the filaments were investigated and related to the structure and the properties of calendared webs.

Research should be continued to study the processing conditions which influence the crystal structures of the filaments using small angle x-ray diffraction technique and calculate the ratio of alpha, beta and gama crystals of PP and PP+PE from the spectra of x-ray diffraction. Also the influence of PE block in the copolymer to the crystal structure of the filaments should be researched to understand how the structure and properties of copolymer differ from those of the homopolymer. Crystallization kenatics of PP homopolymer and PP+PE copolymer should be studied.

The structure and properties of bonded area and interphase between the bonding and unbonding area of nonwovens should be analyzed by polarized IR technique. Birefringence measurement in bonding area and interphase should help to understand how the bonding temperature and pressure influence the structure and properties of the bond and the interphase between the bond and unbonded area.

The structure and properties of the filaments change with other processing

conditions, polymers, and new spunbonding techniques. Detailed investigations should be conducted with other systems and compared with the observations of this research. Mathematical model for evaluation of nonwovens should be improved and used to optimize the processing conditions and to control the quality and properties of the nonwovens.

REFERENCES

REFERENCES

[1]. Ronald L. Smorada, **INDA Journal of Nonwovens Research**, p-26, Vol.3, No.4, 1991

[2]. S. Damodara, G. Bhat, etc., **AICHE 2nd Topical Conference on Emerging Technologies in Materials**, San Francisco, CA, USA, Nov. 6-8, 1989

[3]. Roland Beyreuther, **Translation of Melliand Textilberichte**, p287, 74, 1999

[4]. Slator G, Thomas J H, **US Patent** No. 2206058, 1940

[5]. Callander M.E., **US Patent** No. 2382290, 1945

[6]. R.G.Hill, **Book of Papers,** Fiber Production Conference, Greenville, S.C., USA, April, 1990

[7]. L. Bradhe, **TA**, 4 (1973), 10, 32-37

[8]. Till D.E., Smallman C.R., **US Patent** No. 2810426, 1957

[9]. Dobo E. J., Dong W.K., Mallonee W.C., **US Patent** No. 3542615, 1967

[10]. **Textile Progress** issues devoted to Spunbonding, Sept. 1970, Sept. 1973

[11]. Malkan and Wadsworth, A Review on Spunbond Technology, **International Nonwovens Bulletin**, p-4, 3'1992

[12]. L. Hartman, **TM**, 101 (1974), 9, 26, 29, 30

[13]. B. Kunze, The Improvement of the State of Art Spunbonding Technology, **Proceeding of 4th Annual Conference of TANDEC**, Knoxville, TN, November 14-16, 1994

[14]. J.W.S. Hearle, M.I. Sultan, and S. Govender, The form taken by threads laid on a moving belt. 1. Experimental study, **Journal of Textile Institute**, 67, 373-6, 1976

[15]. J.W.S. Hearle, M.I. Sultan, and S. Govender, The form taken by threads laid on a moving belt. 1. Mechanism and theory, **Journal of Textile Institute**, 67, 377, 1976

[16]. J. Gould and F.S. Smith, Air drag on synthetic-fiber textile monofilamants and yarns in axial flow at speeds of up to 100 meter per second, **J. Text. Inst**. 71, 38-49, 1980

[17]. S. Misra, J.E. Spruiell and G.C. Richeson, Investigation of The Spunbonding Process Via Mathematical Modeling, **INDA Journal of Nonwoven Research**, Vol.5, No.2, p13, 1993

[18]. S.R. Malkan, L.C. Wadsworth, and C. Davey, Parameter Studies of the Reicofil Spunbonding Process, **International Nonwoven Journal,** 6, No. 2, pp 42-70, 1994

[19]. L. P. B. M. Janssen, **Twin Screw Extrusion**, Eslevier, New York (1978)

[20]. H. Kassig, **J. Polym. Sci.**, Macromolecular Rev., 12, 321, (1977)

[21]. M. T. Gillies, **Nonwoven Materials** (Recent Developments). Noyes Date Corporation, Park Ridge, New Jersey (1979)

[22]. Mark S. M. Alger, **Polymer Science Directionary**, Elsevier Science Publishers LTD. England, 1989

[23]. S. R. Malkan, L. C. Wadsworth, A Review on Spunbond Technology, in **International Nonwovens Bulletin**, Vol.3 pp24-33, 1992

[24]. G. Natta and P. Corradini, Nuovo Cimento, **Suppl**. 15, 40 (1960)

[25]. J. A. Gailey and R. H. Ralston, **SPE Transactions**, 29, 1964

[26]. A. Weidinger and P. H. Hernians, **Makromol. Chem**. 50, 98 (1961)

[27]. S.G. Turley and H. Keskkula, **J. Appl. Polymer Sci**. 9, 2693 (1965)

[28]. M. P Groenwege, J Schuyer, J. Smidt and C. a. F. Tuilinman, 'Absorption and Relaxation Spectra of Polyolefins,' in R. Raff and K. W. Doak, eds, **Crystalline olefin polymers**, Interscience, New York, 1965. Chapter 1/14

[29]. J. P. Luongo, **J. Appl. Polymer Sci**., 3, 302 (1960)

[30]. R. H. Hughes, **Am. Chem. Soc**., meeting, Polymer div. (Sept. 1963), 4/2, 697

[31]. R. L. Miller, **Polymer**, 1, 135 (1960)

[32]. J. Mejer, **Kunstst**., 54, 578 (1964)

[33]. M. P Groenwege, J Schuyer, J. Smidt and C. a. F. Tuilinman, 'Absorption and Relaxation Spectra of Polyolefins,' in R. Raff and K. W. Doak, eds, **Crystalline olefin polymers**, Interscience, New York, 1965. Chapter 1/14

[34]. P. Corrdini, **Angew. Chemie**., 70, 598 (1958)

[35]. M. Ahmed, **Polypropylene Fibers-Science and Technology**, Elsevier, The Netherlands, 1982

[36]. N. Haiji, J.E. Spruiell, F.M. Lu, S. Malkan & G.C. Richeson, Modeling of the Reicofil Spunbonding Process, **INDA Journal of Nonwovens Research**, 4, 16, 1991

[37]. J. Mejer, **Kunstst**., 54, 578 (1964)

[38]. G. E. Hagler, Polym. Eng. Sci. 21, 121 (1981).

[39]. H. M. Henson and J. E Spruiell, Paper Presented at Division of Cellulose, **Paper and Textile Chemistry**, American Chemical Society, Philadelphia, April, 1975.

[40]. J. R. Dees and J. E. Spruiell, **J. Appl. Polym. Sci**. 18, 1053 (1974).

[41]. P. Y. F. Fung, E. Orlando, and S. H. Carr, **Polym. Eng. Sci.** 13, 295 91973).

[42]. R. J. Samuels, **Polym. Eng. Sci.** 16, 327 (1976).

[43]. A. Peterlin, **J. Mater. Sci.** 17, 183 (1977).

[44]. A. Peterlin, **Polym. Eng. Sci**. 17, 183 (1977).

[45]. A. Peterlin, in **Polymeric Materials**. American Society for Metals, Metals Park, Ohio (1975).

[46]. F. J. Balta-Calleja and A. Peterlin, **Macromol. Chem**. 141, 91 (1971).

[47]. C. A. Lukach and H.M. Spurlin, **'Copolymers of a-olefins**, in G. E. Ham, ed., Copolymerization, Interscience, New York, 1964. Chapter IV A

[48]. G. Beckmann and E. F. Engle, **Chem. Ing Technik**, 38, 1026 (1966)

[49]. G. Natta, **Gelg.Pat.** 549638, July 18, 1966.

[50]. H. G. Kirschner, A. G. M. Gumboldt and G. Bier, **US Pat**. 3002961, Oct. 3, 1961.

[51]. P. Parrini, F. Sebastiano, and G. Messina, **Makromol. Chem**., 38, 27 (1960)

[52]. Roberta A. Storer, **ASTM**, Easton, MD, USA, 1986

[53]. W. N. Taylor, Jr. and E. S. Clark, **Polymer Engineering and Science**, 18, 518 (1978).

[54]. **INDA Standard Test** 1980

[55]. Lyman Ott, **An Introduction to Statistical Methods and Data Analysis**, 3rd. Ed. 1988, PVS Publisher, Boston, MA

[56]. S. D. Schlotzhauer and R. C. Littell, **SAS System for Elementary Statistical Analysis**, 1987, SAS Institute, Inc., Cary, NC

[57]. S. R. Malkan, L. C. Wadsworth, and C. Davey, Parametric Studies of the Reicofil Spunbonding Process **in Proceedings of Third Annual TANDEC Conference**, Knoxville, Tennessee, Nov. 1993

[58]. S. Misra, F-M. Lu, J. E. Spruiell, and G. C. Richeson, **Influence of Molecular Weight Distribution on the Structure and Properties of Melt Spun Polypropylene Filaments,** Report to Exxon Chemical Company, 1993

[59]. H.Binns, Brit J. **Psychol**. 16, p237 (1926).

[60]. **Instrument for Fabric Style**, Translated by Beijing Institute of Textile Science.

[61]. Pan Ning, Quantitative Evaluation of Textile Fabrics, **Journal of Textile Engineering**, 1984

[62]. Wang Peizhuang, **Theory and Application of Fuzzy Set**, 1980, Shanghai.

[63]. Dong Zhang, Study of Physical and Mechanical Properties of Knitted Fabrics Knitting from Textured Polyester Yarn, **Master Thesis** in Tianjin Textile Institute of Science and Technology, 1986.

[64]. Zhang Xiaoting, **Introduction to Multistatistics**, China, 1982.

[65]. Zheng Peiyuan, **Fussy Mathematics**, Huazhong Engineering Institute, China, 1984

APPENDICES

Appendix A. SAS Program and Output from Birefringence of Filament Samples.

```
NOTE: Copyright(c) 1989 by SAS Institute Inc., Cary, NC USA.
NOTE: SAS (r) Proprietary Software Release 6.08  TS404
      Licensed to UNIVERSITY OF TENNESSEE, Site 0001395003.

NOTE: Running on VAX Model 6000-460 Serial Number 0B000006.


NOTE: AUTOEXEC processing beginning; file is SAS$ROOT:[000000]AUTOEXEC.SAS;6.


NOTE: AUTOEXEC processing completed.

1     OPTIONS LS=72 PS=54;
2     DATA BIRE;
3     INPUT Through     Temp      Birefr ;
4     CARDS;

NOTE: The data set WORK.BIRE has 70 observations and 3 variables.

75    ;
76    PROC PRINT;
77      title '1=0.2, 2=0.3, 3=0.4 for throughput  and 1=50F, 2=65F,
3=80F for Temperture';


78    PROC GLM;
79    CLASS through temp;
80    MODEL birefr= through temp through*temp/ss1 ss2 ss3 ss4 solution;
81    means through  temp  through*temp;
82    means through  temp/lsd cldiff;
83    LSMEANs through temp/stderr pdiff;
84    OUTPUT P=YBAR;

NOTE: Means from the MEANS statement are not adjusted for other terms
      in the model.  For adjusted means, use the LSMEANS statement.
NOTE: Means from the MEANS statement are not adjusted for other terms
      in the model.  For adjusted means, use the LSMEANS statement.
NOTE: The data set WORK.DATA1 has 70 observations and 4 variables.

85    PROC PLOT;
86    PLOT YBAR*through=temp;
87    PLOT YBAR*temp=through;


88    DATA C; SET BIRE;
89    C=10*through + temp;

NOTE: The data set WORK.C has 70 observations and 4 variables.

90    PROC PRINT;


91    PROC GLM;
92    CLASS C;
93    MODEL BIREfr = c;
94    ESTIMATE '50Fvs60F' c 1  -1  1  -1  0  1  -1 ;
95    ESTIMATE '0.2vs0.3' c 1  1  -1  -1  0  0  0  ;
96    ESTIMATE '0.2&0.3 vs 0.4' c 1  1  1  1  0  -2  -2;
97    ESTIMATE '(21-22)vs(22-23)' c 0 0  1  -2  1  0  0;
98    RUN;
```

1=0.2, 2=0.3, 3=0.4 for throughput and 1=50F, 2=65F, 3=80F for Temper 1
10:33 Thursday, December 9, 1993

OBS	THROUGH	TEMP	BIREFR
1	1	1	2.497
2	1	1	2.463
3	1	1	2.564
4	1	1	2.564
5	1	1	2.564
6	1	1	2.387
7	1	1	2.252
8	1	1	2.547
9	1	1	2.235
10	1	1	2.404
11	1	2	2.164
12	1	2	2.317
13	1	2	2.116
14	1	2	2.124
15	1	2	2.132
16	1	2	2.027
17	1	2	2.099
18	1	2	2.116
19	1	2	2.166
20	1	2	2.099
21	2	1	2.195
22	2	1	2.191
23	2	1	2.186
24	2	1	2.366
25	2	1	2.266
26	2	1	2.391
27	2	1	2.249
28	2	1	2.199
29	2	1	2.182
30	2	1	2.187
31	2	2	1.955
32	2	2	1.970
33	2	2	2.046
34	2	2	2.038
35	2	2	2.031
36	2	2	2.121
37	2	2	1.993
38	2	2	2.114
39	2	2	1.925
40	2	2	2.099
41	2	3	1.123
42	2	3	1.113
43	2	3	1.149
44	2	3	1.118
45	2	3	1.442
46	2	3	1.139
47	2	3	1.217
48	2	3	1.191
49	2	3	1.105

1=0.2, 2=0.3, 3=0.4 for throughput and 1=50F, 2=65F, 3=80F for Temper 2
10:33 Thursday, December 9, 1993

OBS	THROUGH	TEMP	BIREFR
50	2	3	1.107
51	3	1	2.085
52	3	1	2.078
53	3	1	2.070
54	3	1	2.112
55	3	1	1.917
56	3	1	2.055
57	3	1	2.093
58	3	1	2.078
59	3	1	2.000
60	3	1	1.852
61	3	2	1.904
62	3	2	2.077
63	3	2	2.036
64	3	2	1.944
65	3	2	2.025
66	3	2	1.948
67	3	2	1.963
68	3	2	1.727
69	3	2	1.999
70	3	2	1.933

1=0.2, 2=0.3, 3=0.4 for throughput and 1=50F, 2=65F, 3=80F for Temper 3
10:33 Thursday, December 9, 1993

General Linear Models Procedure
Class Level Information

Class	Levels	Values
THROUGH	3	1 2 3
TEMP	3	1 2 3

Number of observations in data set = 70

1=0.2, 2=0.3, 3=0.4 for throughput and 1=50F, 2=65F, 3=80F for Temper 4
10:33 Thursday, December 9, 1993

General Linear Models Procedure

Dependent Variable: BIREFR

Source	DF	Sum of Squares	Mean Square	F Value	Pr > F
Model	6	9.6929649	1.6154941	191.09	0.0001
Error	63	0.5326221	0.0084543		
Corrected Total	69	10.2255870			

R-Square	C.V.	Root MSE	BIREFR Mean
0.947913	4.592743	0.0919	2.0020

Source	DF	Type I SS	Mean Square	F Value	Pr > F
THROUGH	2	2.7461340	1.3730670	162.41	0.0001
TEMP	2	6.8098010	3.4049005	402.74	0.0001
THROUGH*TEMP	2	0.1370299	0.0685149	8.10	0.0007

Source	DF	Type II SS	Mean Square	F Value	Pr > F
THROUGH	2	0.8832672	0.4416336	52.24	0.0001
TEMP	2	6.8098010	3.4049005	402.74	0.0001
THROUGH*TEMP	2	0.1370299	0.0685149	8.10	0.0007

Source	DF	Type III SS	Mean Square	F Value	Pr > F
THROUGH	2	0.8832672	0.4416336	52.24	0.0001
TEMP	2	6.8098010	3.4049005	402.74	0.0001
THROUGH*TEMP	2	0.1370299	0.0685149	8.10	0.0007

Source	DF	Type IV SS	Mean Square	F Value	Pr > F
THROUGH	2*	0.8832672	0.4416336	52.24	0.0001
TEMP	2*	6.4303136	3.2151568	380.30	0.0001
THROUGH*TEMP	2	0.1370299	0.0685149	8.10	0.0007

* NOTE: Other Type IV Testable Hypotheses exist which may yield different SS.

Parameter	Estimate	T for H0: Parameter=0	Pr > |T|	Std Error of Estimate
INTERCEPT	1.096800000 B	21.78	0.0001	0.05036165

1=0.2, 2=0.3, 3=0.4 for throughput and 1=50F, 2=65F, 3=80F for Temper 5
10:33 Thursday, December 9, 1993

General Linear Models Procedure

Dependent Variable: BIREFR

Parameter			Estimate	T for H0: Parameter=0	Pr > |T|	Std Error of Estimate
THROUGH	1		0.180400000 B	4.39	0.0001	0.04112011
	2		0.073600000 B	1.79	0.0783	0.04112011
	3		0.000000000 B	.	.	.
TEMP	1		0.937200000 B	16.12	0.0001	0.05815262
	2		0.858800000 B	20.89	0.0001	0.04112011
	3		0.000000000 B	.	.	.
THROUGH*TEMP	1	1	0.233300000 B	4.01	0.0002	0.05815262
	1	2	0.000000000 B	.	.	.
	2	1	0.133600000 B	2.30	0.0249	0.05815262
	2	2	0.000000000 B	.	.	.
	2	3	0.000000000 B	.	.	.
	3	1	0.000000000 B	.	.	.
	3	2	0.000000000 B	.	.	.

NOTE: The X'X matrix has been found to be singular and a generalized inverse was used to solve the normal equations. Estimates followed by the letter 'B' are biased, and are not unique estimators of the parameters.

1=0.2, 2=0.3, 3=0.4 for throughput and 1=50F, 2=65F, 3=80F for Temper 6
10:33 Thursday, December 9, 1993

General Linear Models Procedure

Level of THROUGH	N	BIREFR Mean	BIREFR SD
1	20	2.29185000	0.18890885
2	30	1.81360000	0.47783099
3	20	1.99480000	0.09734832

Level of TEMP	N	BIREFR Mean	BIREFR SD
1	30	2.24096667	0.19637534
2	30	2.04026667	0.10830892
3	10	1.17040000	0.10241007

Level of THROUGH	Level of TEMP	N	BIREFR Mean	BIREFR SD
1	1	10	2.44770000	0.12571401
1	2	10	2.13600000	0.07455349
2	1	10	2.24120000	0.07789994
2	2	10	2.02920000	0.06833870
2	3	10	1.17040000	0.10241007
3	1	10	2.03400000	0.08546864
3	2	10	1.95560000	0.09636758

1=0.2, 2=0.3, 3=0.4 for throughput and 1=50F, 2=65F, 3=80F for Temper 7
10:33 Thursday, December 9, 1993

General Linear Models Procedure

T tests (LSD) for variable: BIREFR

NOTE: This test controls the type I comparisonwise error rate not the experimentwise error rate.

Alpha= 0.05 Confidence= 0.95 df= 63 MSE= 0.008454
Critical Value of T= 1.99834

Comparisons significant at the 0.05 level are indicated by '***'.

THROUGH Comparison		Lower Confidence Limit	Difference Between Means	Upper Confidence Limit	
1	- 3	0.23895	0.29705	0.35515	***
1	- 2	0.42521	0.47825	0.53129	***
3	- 1	-0.35515	-0.29705	-0.23895	***
3	- 2	0.12816	0.18120	0.23424	***
2	- 1	-0.53129	-0.47825	-0.42521	***
2	- 3	-0.23424	-0.18120	-0.12816	***

1=0.2, 2=0.3, 3=0.4 for throughput and 1=50F, 2=65F, 3=80F for Temper 8
10:33 Thursday, December 9, 1993

General Linear Models Procedure

T tests (LSD) for variable: BIREFR

NOTE: This test controls the type I comparisonwise error rate not the experimentwise error rate.

Alpha= 0.05 Confidence= 0.95 df= 63 MSE= 0.008454
Critical Value of T= 1.99834

Comparisons significant at the 0.05 level are indicated by '***'.

TEMP Comparison		Lower Confidence Limit	Difference Between Means	Upper Confidence Limit	
1	- 2	0.15326	0.20070	0.24814	***
1	- 3	1.00347	1.07057	1.13766	***
2	- 1	-0.24814	-0.20070	-0.15326	***
2	- 3	0.80277	0.86987	0.93696	***
3	- 1	-1.13766	-1.07057	-1.00347	***
3	- 2	-0.93696	-0.86987	-0.80277	***

1=0.2, 2=0.3, 3=0.4 for throughput and 1=50F, 2=65F, 3=80F for Temper 9
10:33 Thursday, December 9, 1993

General Linear Models Procedure
Least Squares Means

THROUGH	BIREFR LSMEAN	Std Err LSMEAN	Pr > |T| HO:LSMEAN=0
1	Non-est	.	.
2	1.81360000	0.01678722	0.0001
3	Non-est	.	.

TEMP	BIREFR LSMEAN	Std Err LSMEAN	Pr > |T| HO:LSMEAN=0	LSMEAN Number
1	2.24096667	0.01678722	0.0001	1
2	2.04026667	0.01678722	0.0001	2
3	Non-est	.	.	3

Pr > |T| HO: LSMEAN(i)=LSMEAN(j)

i/j	1	2	3
1	.	0.0001	.
2	0.0001	.	.
3	.	.	.

NOTE: To ensure overall protection level, only probabilities associated with pre-planned comparisons should be used.

1=0.2, 2=0.3, 3=0.4 for throughput and 1=50F, 2=65F, 3=80F for Tempe 10
10:33 Thursday, December 9, 1993

Plot of YBAR*THROUGH. Symbol is value of TEMP.

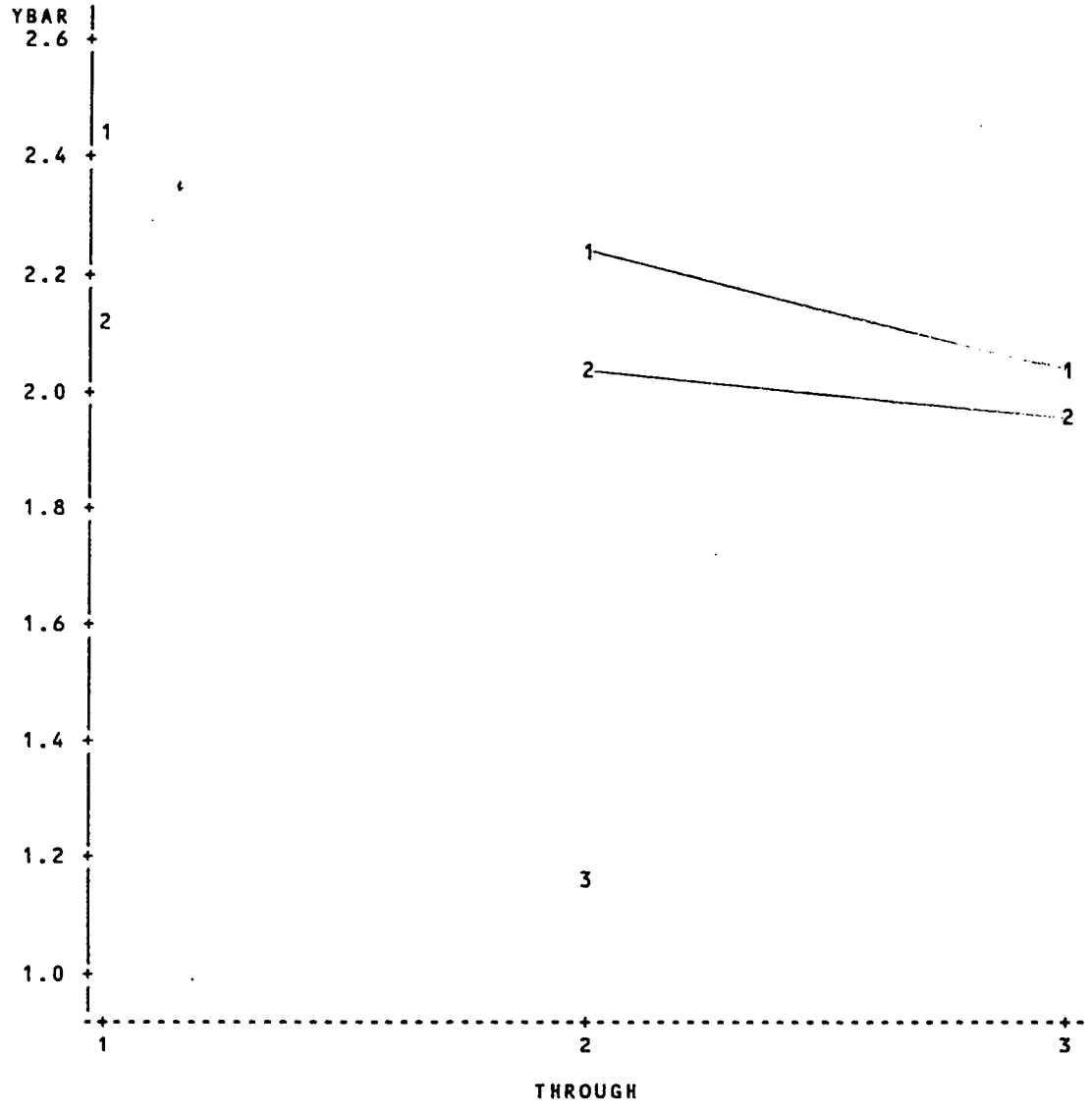

NOTE: 63 obs hidden.

1=0.2, 2=0.3, 3=0.4 for throughput and 1=50F, 2=65F, 3=80F for Tempe 11
10:33 Thursday, December 9, 1993

Plot of YBAR*TEMP. Symbol is value of THROUGH.

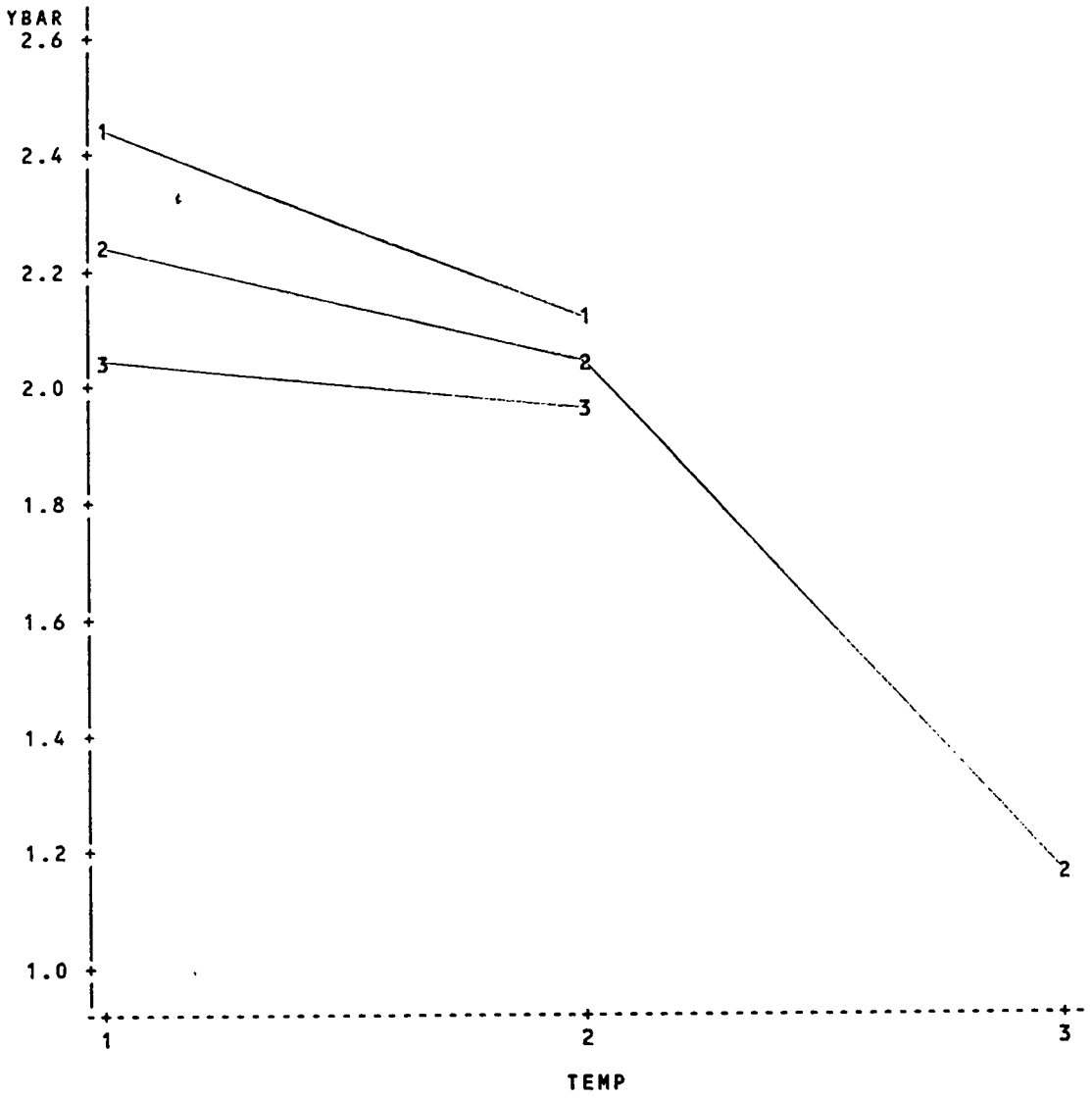

NOTE: 63 obs hidden.

1=0.2, 2=0.3, 3=0.4 for throughput and 1=50F, 2=65F, 3=80F for Tempe 12
10:33 Thursday, December 9, 1993

OBS	THROUGH	TEMP	BIREFR	C
1	1	1	2.497	11
2	1	1	2.463	11
3	1	1	2.564	11
4	1	1	2.564	11
5	1	1	2.564	11
6	1	1	2.387	11
7	1	1	2.252	11
8	1	1	2.547	11
9	1	1	2.235	11
10	1	1	2.404	11
11	1	2	2.164	12
12	1	2	2.317	12
13	1	2	2.116	12
14	1	2	2.124	12
15	1	2	2.132	12
16	1	2	2.027	12
17	1	2	2.099	12
18	1	2	2.116	12
19	1	2	2.166	12
20	1	2	2.099	12
21	2	1	2.195	21
22	2	1	2.191	21
23	2	1	2.186	21
24	2	1	2.366	21
25	2	1	2.266	21
26	2	1	2.391	21
27	2	1	2.249	21
28	2	1	2.199	21
29	2	1	2.182	21
30	2	1	2.187	21
31	2	2	1.955	22
32	2	2	1.970	22
33	2	2	2.046	22
34	2	2	2.038	22
35	2	2	2.031	22
36	2	2	2.121	22
37	2	2	1.993	22
38	2	2	2.114	22
39	2	2	1.925	22
40	2	2	2.099	22
41	2	3	1.123	23
42	2	3	1.113	23
43	2	3	1.149	23
44	2	3	1.118	23
45	2	3	1.442	23
46	2	3	1.139	23
47	2	3	1.217	23
48	2	3	1.191	23
49	2	3	1.105	23

1=0.2, 2=0.3, 3=0.4 for throughput and 1=50F, 2=65F, 3=80F for Tempe 13
10:33 Thursday, December 9, 1993

OBS	THROUGH	TEMP	BIREFR	C
50	2	3	1.107	23
51	3	1	2.085	31
52	3	1	2.078	31
53	3	1	2.070	31
54	3	1	2.112	31
55	3	1	1.917	31
56	3	1	2.055	31
57	3	1	2.093	31
58	3	1	2.078	31
59	3	1	2.000	31
60	3	1	1.852	31
61	3	2	1.904	32
62	3	2	2.077	32
63	3	2	2.036	32
64	3	2	1.944	32
65	3	2	2.025	32
66	3	2	1.948	32
67	3	2	1.963	32
68	3	2	1.727	32
69	3	2	1.999	32
70	3	2	1.933	32

1=0.2, 2=0.3, 3=0.4 for throughput and 1=50F, 2=65F, 3=80F for Tempe 14
10:33 Thursday, December 9, 1993

General Linear Models Procedure
Class Level Information

Class	Levels	Values
C	7	11 12 21 22 23 31 32

Number of observations in data set = 70

1=0.2, 2=0.3, 3=0.4 for throughput and 1=50F, 2=65F, 3=80F for Tempe 15
10:33 Thursday, December 9, 1993

General Linear Models Procedure

Dependent Variable: BIREFR

Source	DF	Sum of Squares	Mean Square	F Value	Pr > F
Model	6	9.6929649	1.6154941	191.09	0.0001
Error	63	0.5326221	0.0084543		
Corrected Total	69	10.2255870			

R-Square	C.V.	Root MSE	BIREFR Mean
0.947913	4.592743	0.0919	2.0020

Source	DF	Type I SS	Mean Square	F Value	Pr > F
C	6	9.6929649	1.6154941	191.09	0.0001

Source	DF	Type III SS	Mean Square	F Value	Pr > F
C	6	9.6929649	1.6154941	191.09	0.0001

Parameter	Estimate	T for H0: Parameter=0	Pr > |T|	Std Error of Estimate
50Fvs60F	0.60210000	8.45	0.0001	0.07122213
0.2vs0.3	0.31330000	5.39	0.0001	0.05815262
0.2&0.3 vs 0.4	0.87490000	8.69	0.0001	0.10072330
(21-22)vs(22-23	-0.64680000	-9.08	0.0001	0.07122213

Appendix B. SAS Program and Output from Tensile Strength of Filament Samples.

```
NOTE: Copyright(c) 1989 by SAS Institute Inc., Cary, NC USA.
NOTE: SAS (r) Proprietary Software Release 6.08  TS404
      Licensed to UNIVERSITY OF TENNESSEE, Site 0001395003.

NOTE: Running on VAX Model 6000-420 Serial Number 0B000006.


NOTE: AUTOEXEC processing beginning; file is SAS$ROOT:[000000]AUTOEXEC.SAS;6.


NOTE: AUTOEXEC processing completed.

1     OPTIONS LS=72 PS=54;
2     DATA Str;
3     INPUT Through  Temp  Str1  Str2  Str3;
4     CARDS;

NOTE: The data set WORK.STR has 70 observations and 5 variables.

75    ;
76    PROC PRINT;
77      title '1=0.2, 2=0.3, 3=0.4 for throughput  and 1=50F, 2=65F,
3=80F for Tempert
78    ure';


79    PROC GLM;
80    CLASS through temp;
81    MODEL Str1 =  through temp through*temp/ss1 ss2 ss3 ss4 solution;
82    means through  temp  through*temp;
83    OUTPUT P=YBAR;

NOTE: Means from the MEANS statement are not adjusted for other terms
      in the model.  For adjusted means, use the LSMEANS statement.
NOTE: The data set WORK.DATA1 has 70 observations and 6 variables.

84    PROC PLOT;
85    PLOT YBAR*through=temp;
86    PLOT YBAR*temp=through;


87    DATA C; SET Str;
88    C=10*through + temp;

NOTE: The data set WORK.C has 70 observations and 6 variables.

89    PROC GLM;
90    CLASS C;
91    MODEL Str1 = c;
92    ESTIMATE '50Fvs60F' c 1  -1  1  -1  0  1  -1 ;
93    ESTIMATE '0.2vs0.3' c 1  1  -1  -1  0  0  0  ;
94    ESTIMATE '0.2&0.3 vs 0.4' c 1  1  1  1  0  -2  -2;
95    ESTIMATE '(21-22)vs(22-23)' c 0 0  1  -2  1  0  0;
96    RUN;
```

1=0.2, 2=0.3, 3=0.4 for throughput and 1=50F, 2=65F, 3=80F for Temper 1
10:39 Tuesday, January 11, 1994

OBS	THROUGH	TEMP	STR1	STR2	STR3
1	1	1	403.20	357.22	256.600
2	1	1	391.90	373.24	130.630
3	1	1	466.50	410.56	144.630
4	1	1	455.10	417.17	151.320
5	1	1	473.80	385.21	144.630
6	1	1	414.00	357.22	177.380
7	1	1	470.14	289.12	222.800
8	1	1	470.47	320.53	151.410
9	1	1	334.91	334.17	170.080
10	1	1	363.14	348.90	166.820
11	1	2	263.78	123.60	131.570
12	1	2	213.32	103.66	163.470
13	1	2	186.92	95.69	207.320
14	1	2	145.56	71.77	162.590
15	1	2	235.41	105.24	239.220
16	1	2	197.22	62.26	287.070
17	1	2	211.87	86.83	212.790
18	1	2	280.12	99.79	205.140
19	1	2	275.79	73.57	160.960
20	1	2	165.34	63.14	227.350
21	2	1	202.96	115.98	91.120
22	2	1	149.11	74.56	66.270
23	2	1	136.69	95.27	136.690
24	2	1	123.55	95.27	161.540
25	2	1	133.14	161.54	169.820
26	2	1	212.98	98.83	102.970
27	2	1	159.12	92.91	143.390
28	2	1	146.69	113.04	115.990
29	2	1	123.54	63.86	91.410
30	2	1	143.14	66.29	123.090
31	2	2	115.51	122.31	84.942
32	2	2	101.92	112.12	112.120
33	2	2	98.63	88.33	118.910
34	2	2	85.17	132.50	81.540
35	2	2	84.18	166.47	163.080
36	2	2	121.17	122.44	114.860
37	2	2	111.93	116.61	107.060
38	2	2	108.54	132.12	96.490
39	2	2	94.12	116.61	131.300
40	2	2	87.32	124.54	110.390
41	2	3	38.74	56.20	38.730
42	2	3	52.53	79.62	61.630
43	2	3	80.63	54.87	41.820
44	2	3	82.98	88.98	77.020
45	2	3	55.76	79.62	40.430
46	2	3	47.84	55.13	50.880
47	2	3	81.68	61.47	35.750
48	2	3	58.32	57.21	49.920
49	2	3	72.16	91.72	59.730

1=0.2, 2=0.3, 3=0.4 for throughput and 1=50F, 2=65F, 3=80F for Temper 2
10:39 Tuesday, January 11, 1994

OBS	THROUGH	TEMP	STR1	STR2	STR3
50	2	3	65.23	98.80	32.03
51	3	1	186.94	82.42	120.23
52	3	1	188.85	144.98	91.94
53	3	1	204.45	139.99	99.01
54	3	1	221.12	95.73	102.55
55	3	1	190.74	122.42	106.09
56	3	1	182.82	101.53	98.86
57	3	1	232.12	74.75	107.99
58	3	1	199.94	65.73	115.38
59	3	1	224.56	64.74	118.03
60	3	1	191.21	131.10	93.78
61	3	2	108.39	141.23	91.97
62	3	2	52.55	82.11	75.54
63	3	2	91.97	111.67	63.04
64	3	2	124.81	124.81	101.82
65	3	2	128.10	141.23	61.22
66	3	2	82.26	127.43	122.22
67	3	2	99.40	117.96	137.08
68	3	2	87.50	118.78	99.17
69	3	2	120.80	125.40	136.94
70	3	2	116.26	120.60	85.46

1=0.2, 2=0.3, 3=0.4 for throughput and 1=50F, 2=65F, 3=80F for Temper 3
10:39 Tuesday, January 11, 1994

General Linear Models Procedure
Class Level Information

Class	Levels	Values
THROUGH	3	1 2 3
TEMP	3	1 2 3

Number of observations in data set = 70

1=0.2, 2=0.3, 3=0.4 for throughput and 1=50F, 2=65F, 3=80F for Temper 4
10:39 Tuesday, January 11, 1994

General Linear Models Procedure

Dependent Variable: STR1

Source	DF	Sum of Squares	Mean Square	F Value	Pr > F
Model	6	883437.62	147239.60	149.71	0.0001
Error	63	61958.87	983.47		
Corrected Total	69	945396.48			

R-Square	C.V.	Root MSE	STR1 Mean
0.934463	17.38304	31.360	180.41

Source	DF	Type I SS	Mean Square	F Value	Pr > F
THROUGH	2	578135.06	289067.53	293.92	0.0001
TEMP	2	242899.54	121449.77	123.49	0.0001
THROUGH*TEMP	2	62403.02	31201.51	31.73	0.0001

Source	DF	Type II SS	Mean Square	F Value	Pr > F
THROUGH	2	445701.48	222850.74	226.60	0.0001
TEMP	2	242899.54	121449.77	123.49	0.0001
THROUGH*TEMP	2	62403.02	31201.51	31.73	0.0001

Source	DF	Type III SS	Mean Square	F Value	Pr > F
THROUGH	2	445701.48	222850.74	226.60	0.0001
TEMP	2	242899.54	121449.77	123.49	0.0001
THROUGH*TEMP	2	62403.02	31201.51	31.73	0.0001

Source	DF	Type IV SS	Mean Square	F Value	Pr > F
THROUGH	2*	445701.48	222850.74	226.60	0.0001
TEMP	2*	40429.78	20214.89	20.55	0.0001
THROUGH*TEMP	2	62403.02	31201.51	31.73	0.0001

* NOTE: Other Type IV Testable Hypotheses exist which may yield different SS.

Parameter	Estimate	T for H0: Parameter=0	Pr > |T|	Std Error of Estimate
INTERCEPT	63.9420000 B	3.72	0.0004	17.17679290

1=0.2, 2=0.3, 3=0.4 for throughput and 1=50F, 2=65F, 3=80F for Temper 5
10:39 Tuesday, January 11, 1994

General Linear Models Procedure

Dependent Variable: STR1

Parameter			Estimate	T for H0: Parameter=0	Pr > |T|	Std Error of Estimate
THROUGH	1		116.3290000 B	8.29	0.0001	14.02479267
	2		-0.3550000 B	-0.03	0.9799	14.02479267
	3		0.0000000 B	.	.	.
TEMP	1		138.3330000 B	6.97	0.0001	19.83405201
	2		37.2620000 B	2.66	0.0100	14.02479267
	3		0.0000000 B	.	.	.
THROUGH*TEMP	1	1	105.7120000 B	5.33	0.0001	19.83405201
	1	2	0.0000000 B	.	.	.
	2	1	-48.8280000 B	-2.46	0.0166	19.83405201
	2	2	0.0000000 B	.	.	.
	2	3	0.0000000 B	.	.	.
	3	1	0.0000000 B	.	.	.
	3	2	0.0000000 B	.	.	.

NOTE: The X'X matrix has been found to be singular and a generalized inverse was used to solve the normal equations. Estimates followed by the letter 'B' are biased, and are not unique estimators of the parameters.

1=0.2, 2=0.3, 3=0.4 for throughput and 1=50F, 2=65F, 3=80F for Temper 6
10:39 Tuesday, January 11, 1994

General Linear Models Procedure

Level of THROUGH	N	STR1 Mean	STR1 SD
1	20	320.924500	115.988684
2	30	105.842667	42.678894
3	20	151.739500	55.641781

Level of TEMP	N	STR1 Mean	STR1 SD
1	30	259.894333	124.822328
2	30	139.862000	63.267048
3	10	63.587000	15.444188

Level of THROUGH	Level of TEMP	N	STR1 Mean	STR1 SD
1	1	10	424.316000	50.2713522
1	2	10	217.533000	46.0352491
2	1	10	153.092000	31.0533043
2	2	10	100.849000	13.1989010
2	3	10	63.587000	15.4441884
3	1	10	202.275000	17.6447740
3	2	10	101.204000	23.4411098

1=0.2, 2=0.3, 3=0.4 for throughput and 1=50F, 2=65F, 3=80F for Temper 7
10:39 Tuesday, January 11, 1994

Plot of YBAR*THROUGH. Symbol is value of TEMP.

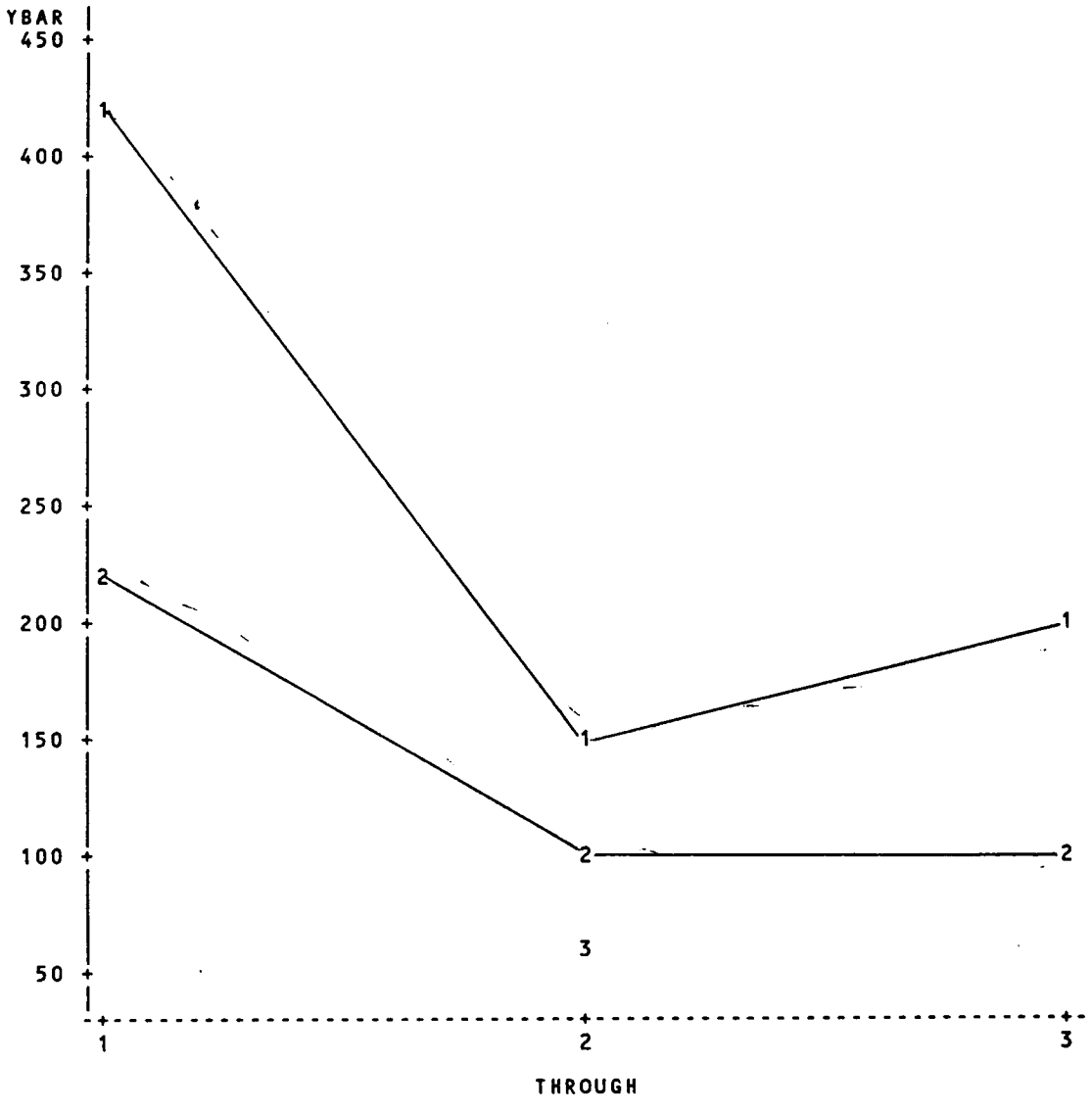

NOTE: 63 obs hidden.

1=0.2, 2=0.3, 3=0.4 for throughput and 1=50F, 2=65F, 3=80F for Temper 8
10:39 Tuesday, January 11, 1994

Plot of YBAR*TEMP. Symbol is value of THROUGH.

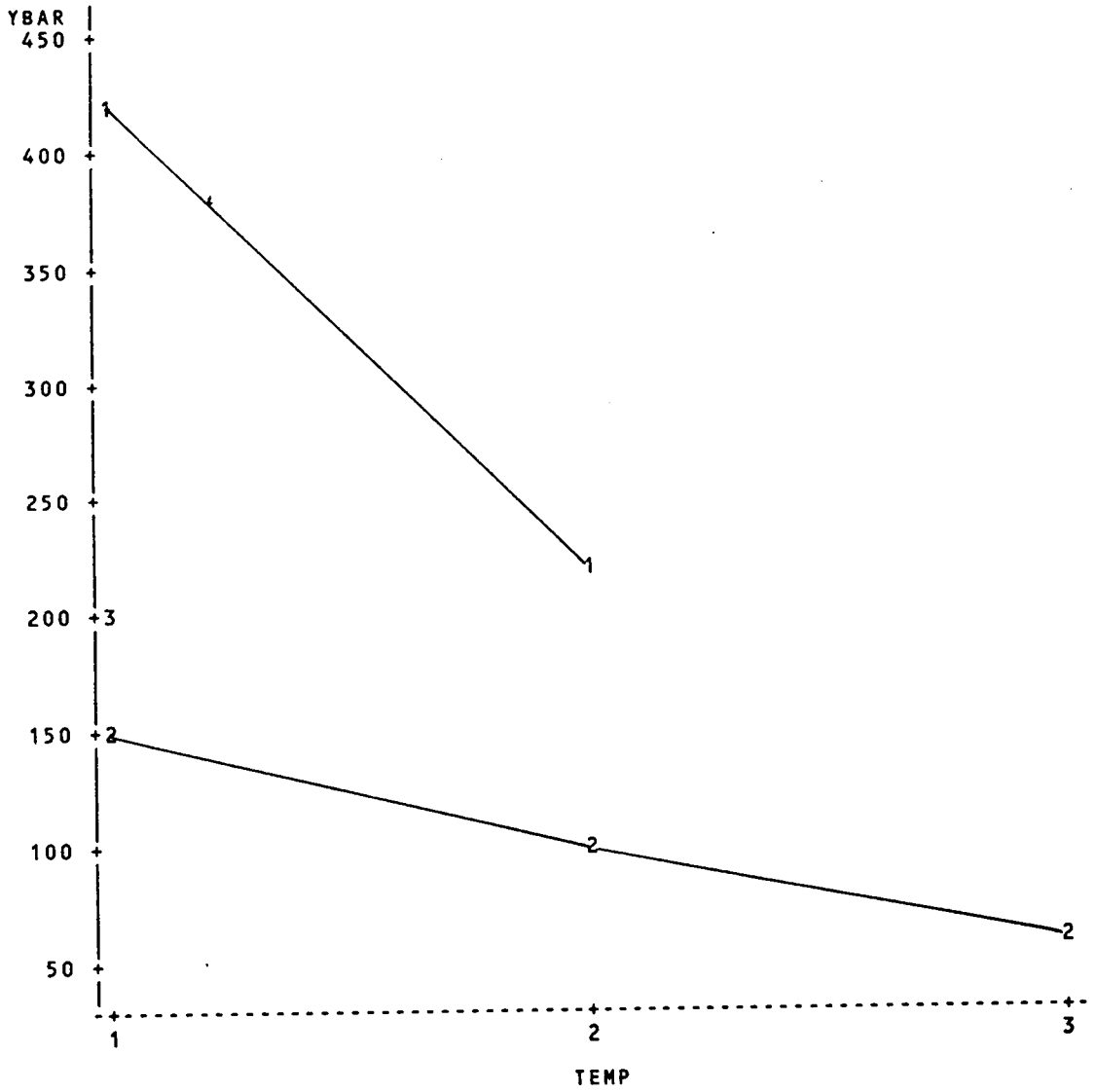

NOTE: 64 obs hidden.

General Linear Models Procedure
Class Level Information

Class	Levels	Values
C	7	11 12 21 22 23 31 32

Number of observations in data set = 70

1=0.2, 2=0.3, 3=0.4 for throughput and 1=50F, 2=65F, 3=80F for Tempe 10
10:39 Tuesday, January 11, 1994

General Linear Models Procedure

Dependent Variable: STR1

Source	DF	Sum of Squares	Mean Square	F Value	Pr > F
Model	6	883437.62	147239.60	149.71	0.0001
Error	63	61958.87	983.47		
Corrected Total	69	945396.48			

R-Square	C.V.	Root MSE	STR1 Mean
0.934463	17.38304	31.360	180.41

Source	DF	Type I SS	Mean Square	F Value	Pr > F
C	6	883437.62	147239.60	149.71	0.0001

Source	DF	Type III SS	Mean Square	F Value	Pr > F
C	6	883437.62	147239.60	149.71	0.0001

Parameter	Estimate	T for H0: Parameter=0	Pr > |T|	Std Error of Estimate
50Fvs60F	360.097000	14.82	0.0001	24.2916535
0.2vs0.3	387.908000	19.56	0.0001	19.8340520
0.2&0.3 vs 0.4	288.832000	8.41	0.0001	34.3535858
(21-22)vs(22-23	14.981000	0.62	0.5396	24.2916535

Appendix C. SAS Program and Output from Breaking Elongation of Filament Samples.

```
NOTE: Copyright(c) 1989 by SAS Institute Inc., Cary, NC USA.
NOTE: SAS (r) Proprietary Software Release 6.08  TS404
      Licensed to UNIVERSITY OF TENNESSEE, Site 0001395003.

NOTE: Running on VAX Model 6000-420 Serial Number 0B000006.


NOTE: AUTOEXEC processing beginning; file is SAS$ROOT:[000000]AUTOEXEC.SAS;6.


NOTE: AUTOEXEC processing completed.

1     OPTIONS LS=72 PS=54;
2     DATA Elngtn;
3     INPUT Through  Temp  Elng1 Elng2 Elng3;
4     CARDS;

NOTE: The data set WORK.ELNGTN has 70 observations and 5 variables.

75    ;
76    PROC PRINT;
77      title '1=0.2, 2=0.3, 3=0.4 for throughput  and 1=50F, 2=65F,
3=80F for Tempert
78    ure';


79    PROC GLM;
80    CLASS through temp;
81    MODEL elng1 = through temp through*temp/ss1 ss2 ss3 ss4 solution;
82    means through  temp  through*temp;
83    OUTPUT P=YBAR;

NOTE: Means from the MEANS statement are not adjusted for other terms
      in the model.  For adjusted means, use the LSMEANS statement.
NOTE: The data set WORK.DATA1 has 70 observations and 6 variables.

84    PROC PLOT;
85    PLOT YBAR*through=temp;
86    PLOT YBAR*temp=through;


87    DATA C; SET elngtn;
88    C=10*through + temp;

NOTE: The data set WORK.C has 70 observations and 6 variables.

89    PROC GLM;
90    CLASS C;
91    MODEL elng1 = c;
92    ESTIMATE '50Fvs60F' c 1  -1  1  -1  0  1  -1 ;
93    ESTIMATE '0.2vs0.3' c 1  1  -1  -1  0  0  0  ;
94    ESTIMATE '0.2&0.3 vs 0.4' c 1  1  1  1  0  -2  -2;
95    ESTIMATE '(21-22)vs(22-23)' c 0 0  1  -2  1  0  0;
96    RUN;
```

1=0.2, 2=0.3, 3=0.4 for throughput and 1=50F, 2=65F, 3=80F for Temper 1
10:48 Tuesday, January 11, 1994

OBS	THROUGH	TEMP	ELNG1	ELNG2	ELNG3
1	1	1	210.70	284.55	215.40
2	1	1	149.20	263.96	268.83
3	1	1	218.60	270.61	196.96
4	1	1	197.20	290.22	212.74
5	1	1	169.30	240.96	194.64
6	1	1	198.70	276.68	206.29
7	1	1	96.95	249.01	262.87
8	1	1	215.57	261.78	181.13
9	1	1	187.01	290.22	208.44
10	1	1	162.84	234.30	187.69
11	1	2	238.28	214.26	107.27
12	1	2	344.52	230.85	122.46
13	1	2	238.52	265.78	229.40
14	1	2	252.16	276.10	213.79
15	1	2	332.01	321.28	229.96
16	1	2	230.32	210.89	157.92
17	1	2	333.37	205.67	154.27
18	1	2	285.22	257.41	224.88
19	1	2	294.39	271.78	233.12
20	1	2	258.54	320.08	235.88
21	2	1	182.55	218.98	237.98
22	2	1	291.39	294.25	262.45
23	2	1	308.84	298.22	175.52
24	2	1	298.15	191.68	243.37
25	2	1	287.24	238.36	217.89
26	2	1	177.29	212.29	232.49
27	2	1	285.63	272.89	258.37
28	2	1	301.01	269.83	171.66
29	2	1	281.53	184.74	239.78
30	2	1	280.58	231.94	204.25
31	2	2	226.70	261.32	129.32
32	2	2	266.37	268.54	251.56
33	2	2	335.16	259.66	283.67
34	2	2	274.28	183.48	238.78
35	2	2	316.59	280.77	203.43
36	2	2	222.88	233.99	142.51
37	2	2	253.52	252.75	248.69
38	2	2	331.60	256.07	282.47
39	2	2	264.79	173.69	223.44
40	2	2	304.27	273.18	197.93
41	2	3	515.83	384.41	445.67
42	2	3	451.62	479.76	436.06
43	2	3	641.61	442.81	398.55
44	2	3	404.61	461.57	334.37
45	2	3	468.87	568.41	414.24
46	2	3	509.84	380.10	424.98
47	2	3	449.72	475.43	430.85
48	2	3	641.87	433.07	394.53
49	2	3	400.35	442.66	331.30

1=0.2, 2=0.3, 3=0.4 for throughput and 1=50F, 2=65F, 3=80F for Temper 2
10:48 Tuesday, January 11, 1994

OBS	THROUGH	TEMP	ELNG1	ELNG2	ELNG3
50	2	3	468.87	496.27	408.09
51	3	1	295.12	254.15	186.89
52	3	1	300.81	242.04	282.61
53	3	1	301.15	267.44	203.53
54	3	1	265.59	236.74	206.88
55	3	1	268.01	250.09	254.28
56	3	1	288.73	254.15	170.66
57	3	1	300.81	225.15	269.93
58	3	1	299.51	266.47	193.56
59	3	1	264.65	236.74	167.35
60	3	1	265.89	245.67	246.35
61	3	2	303.91	217.89	207.02
62	3	2	328.04	196.08	222.45
63	3	2	264.43	196.72	236.93
64	3	2	276.66	278.23	130.00
65	3	2	287.30	223.03	251.33
66	3	2	298.86	212.15	201.50
67	3	2	323.70	192.96	186.60
68	3	2	263.49	177.55	233.16
69	3	2	271.41	206.25	106.24
70	3	2	281.53	179.89	251.33

1=0.2, 2=0.3, 3=0.4 for throughput and 1=50F, 2=65F, 3=80F for Temper 3
10:48 Tuesday, January 11, 1994

General Linear Models Procedure
Class Level Information

Class	Levels	Values
THROUGH	3	1 2 3
TEMP	3	1 2 3

Number of observations in data set = 70

1=0.2, 2=0.3, 3=0.4 for throughput and 1=50F, 2=65F, 3=80F for Temper 4
10:48 Tuesday, January 11, 1994

General Linear Models Procedure

Dependent Variable: ELNG1

Source	DF	Sum of Squares	Mean Square	F Value	Pr > F
Model	6	543980.80	90663.47	41.13	0.0001
Error	63	138876.76	2204.39		
Corrected Total	69	682857.56			

R-Square	C.V.	Root MSE	ELNG1 Mean
0.796624	15.79582	46.951	297.24

Source	DF	Type I SS	Mean Square	F Value	Pr > F
THROUGH	2	168195.61	84097.81	38.15	0.0001
TEMP	2	347147.84	173573.92	78.74	0.0001
THROUGH*TEMP	2	28637.34	14318.67	6.50	0.0027

Source	DF	Type II SS	Mean Square	F Value	Pr > F
THROUGH	2	35453.78	17726.89	8.04	0.0008
TEMP	2	347147.84	173573.92	78.74	0.0001
THROUGH*TEMP	2	28637.34	14318.67	6.50	0.0027

Source	DF	Type III SS	Mean Square	F Value	Pr > F
THROUGH	2	35453.78	17726.89	8.04	0.0008
TEMP	2	347147.84	173573.92	78.74	0.0001
THROUGH*TEMP	2	28637.34	14318.67	6.50	0.0027

Source	DF	Type IV SS	Mean Square	F Value	Pr > F
THROUGH	2*	35453.78	17726.89	8.04	0.0008
TEMP	2*	325538.76	162769.38	73.84	0.0001
THROUGH*TEMP	2	28637.34	14318.67	6.50	0.0027

* NOTE: Other Type IV Testable Hypotheses exist which may yield different SS.

Parameter	Estimate	T for H0: Parameter=0	Pr > |T|	Std Error of Estimate
INTERCEPT	505.6360000 B	19.66	0.0001	25.71610235

1=0.2, 2=0.3, 3=0.4 for throughput and 1=50F, 2=65F, 3=80F for Temper 5
10:48 Tuesday, January 11, 1994

General Linear Models Procedure

Dependent Variable: ELNG1

Parameter			Estimate	T for H0: Parameter=0	Pr > |T|	Std Error of Estimate
THROUGH	1		-9.2000000 B	-0.44	0.6628	20.99710965
	2		-10.3170000 B	-0.49	0.6249	20.99710965
	3		0.0000000 B	.	.	.
TEMP	1		-220.6090000 B	-7.43	0.0001	29.69439723
	2		-215.7030000 B	-10.27	0.0001	20.99710965
	3		0.0000000 B	.	.	.
THROUGH*TEMP	1	1	-95.2200000 B	-3.21	0.0021	29.69439723
	1	2	0.0000000 B	.	.	.
	2	1	-5.2890000 B	-0.18	0.8592	29.69439723
	2	2	0.0000000 B	.	.	.
	2	3	0.0000000 B	.	.	.
	3	1	0.0000000 B	.	.	.
	3	2	0.0000000 B	.	.	.

NOTE: The X'X matrix has been found to be singular and a generalized inverse was used to solve the normal equations. Estimates followed by the letter 'B' are biased, and are not unique estimators of the parameters.

1=0.2, 2=0.3, 3=0.4 for throughput and 1=50F, 2=65F, 3=80F for Temper 6

10:48 Tuesday, January 11, 1994

General Linear Models Procedure

Level of THROUGH	N	ELNG1 Mean	ELNG1 SD
1	20	230.670000	64.839746
2	30	348.118667	121.387918
3	20	287.480000	19.823585

Level of TEMP	N	ELNG1 Mean	ELNG1 SD
1	30	245.018333	58.5372609
2	30	283.427333	35.9363218
3	10	495.319000	85.7289119

Level of THROUGH	Level of TEMP	N	ELNG1 Mean	ELNG1 SD
1	1	10	180.607000	37.4811932
1	2	10	280.733000	43.6017627
2	1	10	269.421000	48.0113485
2	2	10	279.616000	40.6696532
2	3	10	495.319000	85.7289119
3	1	10	285.027000	16.7740461
3	2	10	289.933000	23.1273143

1=0.2, 2=0.3, 3=0.4 for throughput and 1=50F, 2=65F, 3=80F for Temper 7
10:48 Tuesday, January 11, 1994

Plot of YBAR*THROUGH. Symbol is value of TEMP.

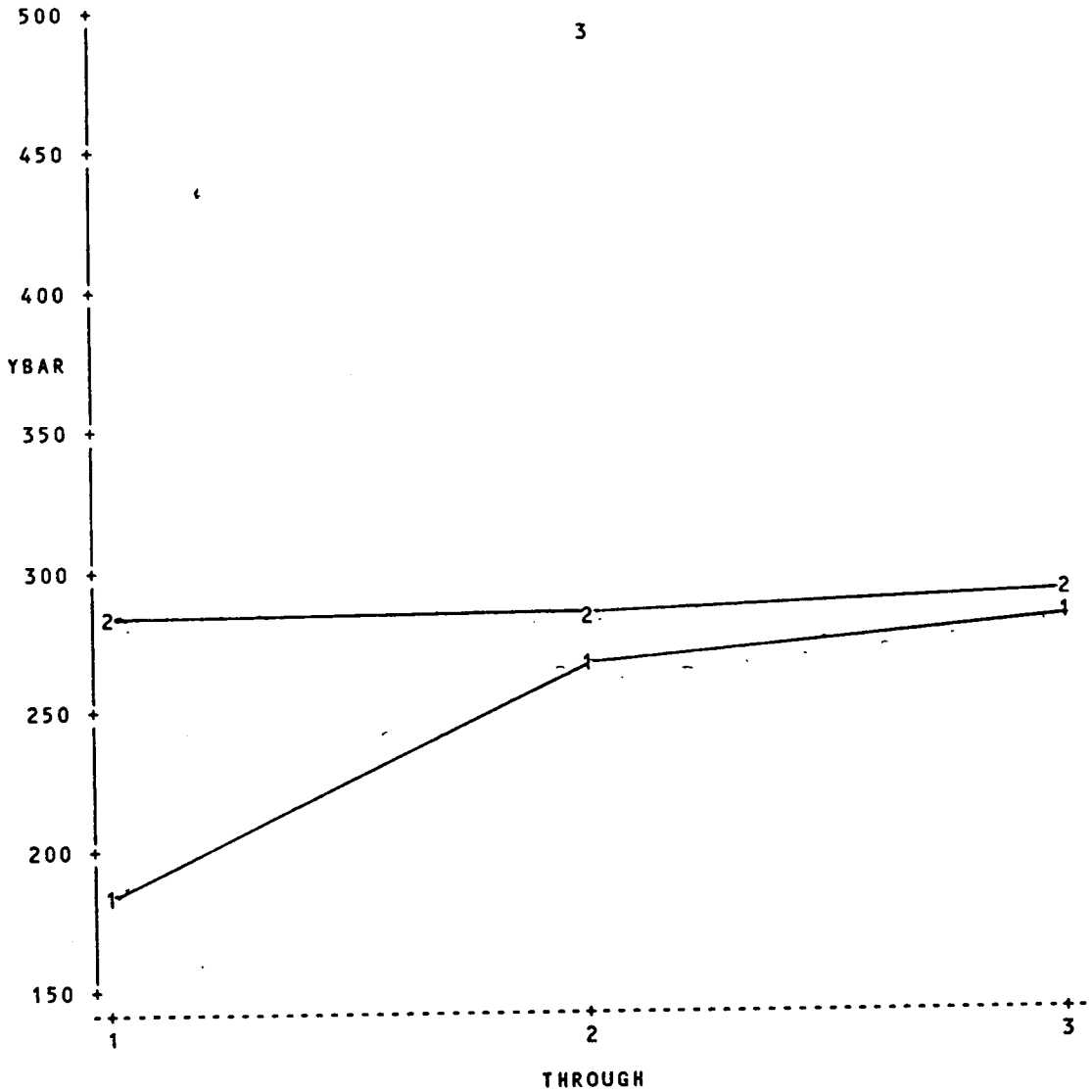

NOTE: 63 obs hidden.

1=0.2, 2=0.3, 3=0.4 for throughput and 1=50F, 2=65F, 3=80F for Temper 8
10:48 Tuesday, January 11, 1994

Plot of YBAR*TEMP. Symbol is value of THROUGH.

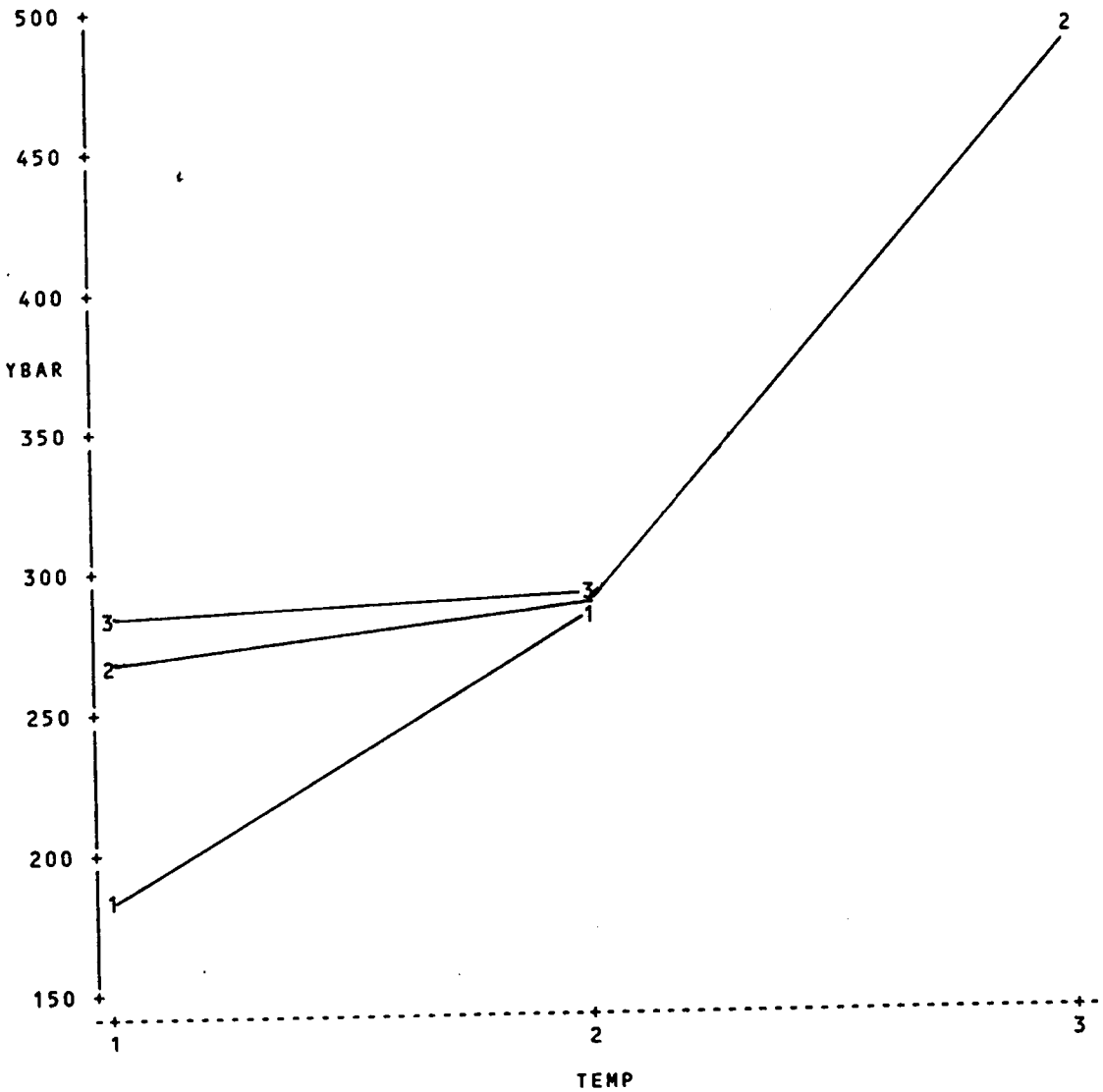

NOTE: 64 obs hidden.

1=0.2, 2=0.3, 3=0.4 for throughput and 1=50F, 2=65F, 3=80F for Temper 9
10:48 Tuesday, January 11, 1994

General Linear Models Procedure
Class Level Information

Class	Levels	Values
C	7	11 12 21 22 23 31 32

Number of observations in data set = 70

1=0.2, 2=0.3, 3=0.4 for throughput and 1=50F, 2=65F, 3=80F for Tempe 10
10:48 Tuesday, January 11, 1994

General Linear Models Procedure

Dependent Variable: ELNG1

Source	DF	Sum of Squares	Mean Square	F Value	Pr > F
Model	6	543980.80	90663.47	41.13	0.0001
Error	63	138876.76	2204.39		
Corrected Total	69	682857.56			

R-Square	C.V.	Root MSE	ELNG1 Mean
0.796624	15.79582	46.951	297.24

Source	DF	Type I SS	Mean Square	F Value	Pr > F
C	6	543980.80	90663.47	41.13	0.0001

Source	DF	Type III SS	Mean Square	F Value	Pr > F
C	6	543980.80	90663.47	41.13	0.0001

Parameter	Estimate	T for H0: Parameter=0	Pr > |T|	Std Error of Estimate
50Fvs60F	-115.227000	-3.17	0.0024	36.3680607
0.2vs0.3	-87.697000	-2.95	0.0044	29.6943972
0.2&0.3 vs 0.4	-139.543000	-2.71	0.0086	51.4322047
(21-22)vs(22-23	205.508000	5.65	0.0001	36.3680607

VITA

DONG ZHANG

Dong Zhang was born in Tianjin, China, on May 20, 1960, to Mr. and Mrs. Binyue Zhang as their first son of twin. He graduated from Tianjin Textile Institute of Science and Technology, Tianjin, China, and got his Bachelor of Science degree in Textile Science in 1983. At the same year, he attended the Institute from 1983 to 1986. In January, 1986, he received a Master of Science degree in Textile Material Science in Tianjin Textile Institute of Science and Technology, Tianjin, China. He had been doing teaching and research work in the institute from 1986 to 1991. In August, 1991, he enter the Graduate School at The University of Tennessee, and awarded a Graduate Research Assistantship. In August, 1992, he was awarded a Graduate Assistantship from the Department of Textiles, Retailing and Interior Design. In December, 1992, he received his second Master of Science degree in Textile Science from The University of Tennessee. He continued his graduate study for Ph.D. in Textile Science in The University of Tennessee and got several awards for recognizing his research, including Chancellor's Citation for Extraordinary Professional Promise in April 1994. He got his Ph.D. in May 1995.